INFORMATION TO USERS

University of Alberta

Geomechanics of CO_2 Sequestration in Coalbed Methane Reservoirs

by

Mohamad Al-hawaree   Ⓒ

A thesis submitted to the Faculty of Graduate Studies and Research in partial fulfillment

of the

requirements for the degree of Master of Science

in

Geotechnical Engineering

Department of Civil and Environmental Engineering

Edmonton, Alberta

Fall 1999

University of Alberta

Library Release Form

Name of Author: Mohamad Al-hawaree

Title of Thesis: Geomechanics of CO_2 Sequestration in Coalbed Methane Reservoirs

Degree: Master of Science

Year this Degree Granted: 1999

Permission is hereby granted to the University of Alberta Library to reproduce single copies of this thesis and to lend or sell such copies for private, scholarly, or scientific research purposes only.

The author reserves all other publication and other rights in association with the copyright in the thesis, and except as hereinbefore provided, neither the thesis nor any substantial portion thereof may be printed or otherwise reproduced in any material form whatever without the author's prior permission.

....
Apt 214   11012 82 Ave
Edmonton, Alberta
T6G 2P6, Canada

Date : September 29, 1999

University of Alberta

Faculty of Graduate Studies and Research
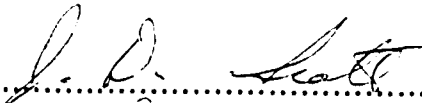
The undersigned certify that they have read, and recommended to the Faculty of Graduate Studies and Research for acceptance, a thesis entitled *Geomechanics of CO_2 Sequestration in Coalbed Methane Reservoirs* submitted by Mohamad Al-hawaree in partial fulfillment of the requirements for the degree of Master of Science in Geotechnical Engineering.
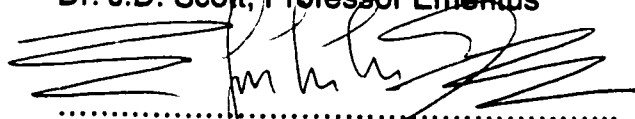
Dr. R. Chalaturnyk, Assistant Professor
Supervisor

Dr. D.C. Sego, Professor

Dr. J.D. Scott, Professor Emeritus

Dr. S. Frimpong, Associate Professor

Dr. W.D. Gunter, Scientist
Alberta Research Council

Date : September 29, 1999

To my homeland Palestine

ABSTRACT

Coalbeds in the Western Sedimentary Basin of Canada could potentially trap over 12 trillion cubic meters of carbon dioxide which is equal to decades of Canada's CO_2 production. The injection of CO_2 into deep coalbed methane reservoirs is appealing because of its offsetting benefit in the production of methane. Successful implementation of the CO_2 disposal/CH_4 recovery process will require a fundamental understanding of the geomechanical and hydraulic characteristics of the coal.

A special multiphase geomechanic testing facility, which included a high pressure, double wall triaxial cell, was developed to accommodate the testing conditions of this research. Fundamental experiments were carried out to study permeability variations in coal during the CO_2 sequestration process. Increasingly complex tests were conducted to gain an understanding of the coal response to variations in effective stress and gas pressure. At constant effective stress levels, a 75% reduction in intrinsic permeability was measured as CO_2 pressure increased from 3.5 and 12 MPa. Permeability reductions of 51% to 90% were measured over an isotropic effective stress range of 6 to 16 MPa. Coals of increasing rank show larger reduction in permeability. Permeability variation due to CO_2 pressure displayed a bi-linear relationship.

ACKNOWLEDGMENTS

TABLE OF CONTENTS

LIST OF TABLES

LIST OF FIGURES

CHAPTER 1

1.1 INTRODUCTION

Greenhouse gases are increasing dramatically due to anthropological activities and natural catastrophes causing global warming. CO_2 is one of the greenhouse gases which is mainly produced by burning coal in the power plants in order to provide an adequate supply of energy. The dichotomy is that energy supply is a major prerequisite to achieving socio-economic development in any country. The development of energy sources leads to an improvement in the quality of life, which includes access to employment opportunities, health services, education, housing and other amenities. Therefore, energy has been found to be the key to prosperity in the industrialized world and a prerequisite for sustainable development in countries with transition economies. However, development of energy systems must be accomplished without endangering the quality of life for present and future generations, without exceeding the capacity of supporting ecosystems and must be done in a safe and manner.

The CO_2 content of the air is presently about 360 part per million volume (ppmv) and increasing at the rate of approximately 1.5 ppmv per year (Houghton et al.,1996). At present about 22 Gigatonne (Gt) of CO_2 is emitted to the atmosphere annually. The increasing worldwide use of carbonaceous fuels is expected to increase the rate of CO_2 growth in the atmosphere to $\approx$ 2 ppmv per year by the year 2000 and $\approx$ 3 ppmv per year by 2025. Thus, the CO_2 concentration would then be $\approx$ 435 ppmv, causing increases in the temperature of the earth surface with consequent disturbing climatic effects. An expected global warming of 1-2 $^\circ$C in the atmosphere over the next fifty years will not be evenly distributed (Rotty et al., 1980). There will be less warming in the tropics and more in the moderate and arctic regions, the increase in the temperature being as much as 3-4 $^\circ$C. The additional warming will change the distribution

1

of heat and thus the flow of energy through the climate system. This will in turn alter the circulation patterns of the atmosphere and the oceans, and modify the hydrological cycle by which water is circulated between the earth's surface and the air. As a result, the position of many of the world's major storm tracks could shift significantly. To see what the effects of such a shift might be, one has only to look at what happens when circulation patterns are changed by an El Nino (Francis et al., 1998). Some areas would be exposed to more storms and heavier rainfalls, while others might see formerly reliable rainfalls give way to prolonged dry spells. Other areas might actually see improvements in their climates, but if the experience of the recent El Nino is a guide, most localities would encounter at least some weather difficulties that they were poorly prepared to deal with. Over time, communities could adapt to these new conditions, but the costs could be substantial.

Another and more compelling reason for suspecting a link between greenhouse warming and weather extremes is related to the potential effects of a warmer climate on the physical processes that generate different types of weather events. Consider the example of rainfall. Precipitation and flow to rivers is one half of the hydrological (or water) cycle. Evaporation (and transpiration from plants) is the other. A virtually certain outcome of a rise in global temperatures is a widespread increase in the amount of water that is moved through the cycle. That is because higher temperatures not only increase evaporation and transpiration but also raise the air's capacity to hold moisture. Consequently, more moisture will be available in the atmosphere to fall as rain and snow. Add to this a more unstable atmosphere due to increased convection over warmer land and sea surfaces, and the result is an increased potential for major precipitation events in many parts of the world. Because of changes in large-scale circulation patterns as well as regional differences in hydrological processes, the resulting increase in precipitation will not be spread uniformly around the world. In fact, some areas may receive less precipitation.

The US National Academy of Science stated: " A major climatic change will force economic and social adjustments on a world scale, because the global patterns of food production and population that have evolved are implicitly dependent on the climate of the present century. This dependence of the nation's welfare, as well as that of the international community as a whole, on the present climatic conditions, should serve as a warning signal that we simply cannot afford to be unprepared for either natural or man made catastrophe". Industrial nationals of the world, heeding this warning, made commitments to stabilize greenhouse gas emissions at 1990 levels by the year 2000 at the Rio convention on climate change in 1992.

Based on recommendations of the Intergovernmental Panel on Climate Change (IPCC), the UN Framework Convention on Climate Change was set up in 1992 and entered into force on March 21, 1994. By September 1996, the Framework had been signed and ratified by 159 states. According to Article 2 of the convention, "the ultimate objective of this convention is to achieve stabilization of greenhouse gas concentrations in the atmosphere". With regard to the level at which this stabilization should be achieved, the convention says that it should be a level "that would prevent dangerous anthropogenic interference with the climate system". With regard to the time-frame within which this level should be achieved, the convention says that this time-frame should be "sufficient to allow ecosystems to adapt naturally to climate change, to ensure that food production is not threatened and to enable economic development to proceed in a sustainable manner". Due to our limited knowledge about the climate system and the intrinsic impossibility to forecast climate behavior in relation to human activities it will not be easy to achieve international agreement about a translation of these preconditions into quantitative goals (Turkenburg et al., 1997).

According to Article 3.1 of the United Nations Framework Convention on Climate Change (UN-FCCC) "the Parties should protect the climate system in

accordance with their common but differentiated responsibilities and respective capabilities. Accordingly, the developed country parties should take the lead in combating climate change and the adverse effects thereof". Consequently, a global reduction of the annual CO_2 emissions with more than 50% probably implies a reduction in the industrialized countries with at least 80%, an average of approximately 1.5% per year between 1990 and 2100.

Carbon dioxide is the largest contributor to the greenhouse effect, Figure 1-1 shows the contribution to global warming from anthropogenic sources.
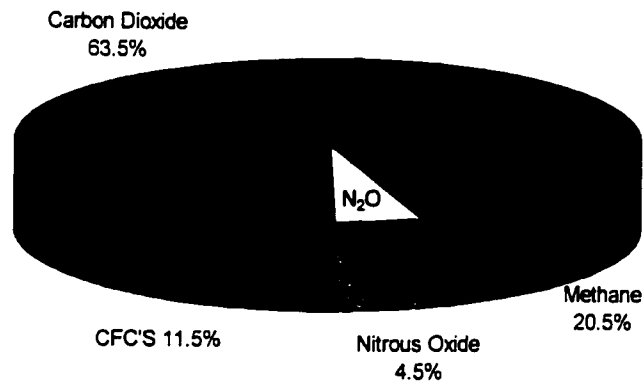
Figure 1-1 Contributions to global warming from anthropongenic sources (after Freund 1998)

Canada, through unique circumstances, has a relatively high greenhouse gas (GHG) emission rate per capita. These unique circumstances include a diverse and generally cold climate, high rate of immigration, a resource-based, energy-intensive, export oriented economy, and low population density. In 1990 Canada's production of CO_2 was 461 Megatonne (Mt). Alberta's contribution in the same year was 127 Megtonnes, 30% of which originated from coal-fired

thermal power stations (Gunter et al. 1997). Table 1-1 shows a comparison between Canada's greenhouse gas emissions for the years 1990 and 1995; Alberta comes in the second place after Ontario in equivalent CO_2 production.

Province or Region	1990	1995	Unit
Atlantic	44.8	45	Million metric tonnes of CO2 Equivlan
Quebec	78.8	80.1	Million metric tonnes of CO2 Equivlan
Ontario	175	179	Million metric tonnes of CO2 Equivlan
Alberta	160	190	Million metric tonnes of CO2 Equivlan
West (Excluding Alberta)	107.4	124.9	Million metric tonnes of CO2 Equivlan
Canada Total	566	619	Million metric tonnes of CO2 Equivlan

Table 1-1 Canada greenhouse gas emissions (after Webster 1998)

Canada's emissions are significant; equivalent to more than 16 tonnes of CO_2 per individual living in Canada. Projections of the release of greenhouse gases indicate that Canada, by the year 2000, will exceed its 1990 emissions of 461 Mt by 13% (Gunter et al., 1997). In order for Canada to meet its commitment to stabilize greenhouse gas emissions at 1990 levels by the year 2000, large sinks for CO_2 which are environmentally acceptable, have to be identified and the technology developed to utilize them.

Greenhouse gases (GHG) could be controlled by either reducing their production and release into the atmosphere, or by disposing produced GHG's (mainly CO_2) in a safe way. The disposal and reduction of carbon dioxide has been the subject of several previous investigations. The options include:

1- Injection in the deep ocean.

2- Absorption by photosynthesis in plants and trees.

3- Conversion of CO_2 into useful products.

4- Extraterrestrial disposal.

5- Disposal in Geological media:

       - Using it in enhanced oil recover (EOR) operations

- Storing it in depleted oil, gas and bitumen reservoirs
- Injecting it in coalbeds for enhanced gas recovery (EGR).
- Injecting it in deep saline aquifers (hydrodynamic trapping).

6- There is always the option of converting to a non-fossil energy sources (nuclear, wind or solar) thus eliminating the formation of CO_2.

7- Conserving the use of energy or minimizing the lost of energy during the production.

However, most CO_2 reduction methods have their own environmental and economic problems such as radiation from nuclear energy and the limitation in land and resources for wind or solar energy.

Injection into the ocean at different depths (shallow, intermediate and deep release) is feasible mainly for near shoreline power plants. Adams et al., (1995) recommended CO_2 release at intermediate ocean depths. However, the economic penalty for removal, recovery and disposal is severe. Shore pumping stations and long pipelines would be required. There are also some concerns of the unknown ecological effects and permanence of deep ocean disposal of CO_2.

The proposal of terrestrial burial by injection under pressure into abandoned and depleted oil or gas wells or solution-mined salt domes has been studied by Horn and Steinberg (1981). CO_2 pumped into these wells must be maintained under pressure, and remain sealed. There is a big risk if these wells release the stored gas suddenly due to unexpected tectonic movement.

Storage by trees and plants appears feasible. A 1000 MW coal-burning plant requires on the average $\approx$ 1000 Km^2 of forest land to photosynthesize the effluent CO_2. There appears to be little benefit of locating this area adjacent to the plant. There is, however, some concern about other environmental side effects due to a change in the Earth's albedo caused by extensive forestation.

Conversion of CO_2 into useful marketable products is extremely limited compared to the large quantities of CO_2 being produced from power production. Some of these products include methanol, formaldehyde, methane and other organic compounds widely used in commerce. These products, however, eventually return CO_2 into the atmosphere.

Extraterrestrial disposal is considered impractical because of the large payload to be lifted clear of the earth (816 Mgh^{-1} of CO_2 for a 1000 MW plant). The large fuel to payload ratio in conventional fueled rockets would generate much more CO_2 in the atmosphere than would be disposed of.

Injecting CO_2 in aquifers was studied by Gunter et al., (1997). The experiments and modelling indicated that geochemical trapping reactions of CO_2 are slow- at least on the order of tens of hundreds of years. The capacity of these traps is large, in order of million of metric tons. On the other hand, this method of CO_2 disposal is expensive, of the order of \$50/tonne if flue gas separation costs are included (Perkins et al., 1995).

A synergy is needed between the production of the fossil fuels and the disposal of their gaseous emissions created during the energy conversion process. One such synergy is the use of CO_2 for enhanced oil recovery, which is done regularly and considered a mature technology (Bailey and McDonald, 1993). In contrast, production of coalbed methane (CBM) by enhanced recovery techniques utilizing injection of CO_2 is still in the research stage.

1.2 OBJECTIVE

The objectives of this thesis are based on the need to better understand the geomechanical phenomena associated with CO_2 injection into coalbed methane reservoirs. While this encompasses the constitutive behavior of coal under CO_2

injection conditions and the ability to numerically model the CBM-EOR process, the objectives of this thesis are proved experimentally.

The first objective of this research was to design and construct a triaxial testing system capable of providing the required testing conditions such as high stresses and controlled temperature, as well as being suitable for testing with greenhouse gases, mainly carbon dioxide and methane.

The experimental program in this work aims to understand the role of CO_2 sequestration on the permeability and compressibility of different types of coal. The second objective was to measure the intrinsic permeability of intact coal specimens and its variation with effective stress and gas pressures.

1.3 SCOPE

The complexity of the CO_2 sequestration process combined with CH_4 desorption creates an equally complex geomechanical response in coal. Consequently, the scope of this thesis was developed around understanding individual components of the process and not attempting to recreate the sequestration-desorption stress path.

The experimental program was performed with intact coal specimens only. The geomechanical and geochemical response of a coalbed methane reservoir will be influenced to a great extent by the cleat or fracture system than the intact matrix. While this is true, the intact matrix response must still be characterized in order to fully understand the reservoir response to CO_2 injection and CH_4 production.

This research has considered the permeability and compressibility response of intact coal under isotropic stress conditions only. It is recognized that shear

stresses will also play an important role in permeability enhancement or reduction which will have to be characterized in subsequent research studies.

As a consequence of the isotropic stress conditions, the coal specimens are not subjected to triaxial shear conditions which prohibits the development of the constitutive behavior of the coal. Again, the focus of the research is the variation in permeability and compressibility that occurs at various effective stress levels under CO_2 and CH_4 injection conditions.

1.4 OUTLINE OF THESIS CONTENT

Chapter 1 provides an introduction to the global issues surrounding greenhouse gases. The environmental and political background, in particular, is discussed and concluded with summarizing the technical challenges Canada faces in meeting its greenhouse gas reduction targets.

Chapter 2 is a technical review of the structure and flow behavior of coal and other coal properties as well as gases in coal and their properties. The process of adsorption and desorption are reviewed.

Chapter 3 describes coal sampling, characterization tests and their results. These tests include specific gravity, bulk density, porosity, moisture content, reflectance index, maceral content, ultimate and proximate analysis.

Chapter 4 describes the multiphase geomechanical testing facility that was developed for high stresses and volumetric strain measurements. The apparatus design and design conditions are described in this chapter. The triaxial permeability test system used in this research is discussed and explained. Calibration of all the measurement systems is also discussed in this chapter.

Chapter 5 explains the experimental procedure of adsorption, compressibility and permeability tests. It describes the set up procedure and the application of isotropic stresses on the coal samples.

Chapters 6 presents the experimental results of the adsorption and triaxial permeability's tests. These test results describe the permeability changes of the coal at various gas pressures and effective stresses.

Chapter 7 summarizes the findings in the thesis and provides conclusions on the geomechanical behavior of the coalbed formation under different isotropic stress conditions and different gas pressures. These include the issues of absolute permeability changes under different gases. Topics of further research are identified and discussed.

CHAPTER 2 TECHNICAL REVIEW

2.1 INTRODUCTION

This chapter provides a technical review on coalbed formation and the different physical and mechanical properties of coal. It also introduces selected aspects and concepts of CO_2 disposal methods as well as coalbed methane resources and CO_2 properties.

2.2 COAL BEHAVIOR

Coal forms by the subjection to diagenetic alteration of plant material that accumulated in swamps, generally under tropical or semi-tropical conditions. The organic sedimentary material transforms to coal by a coalification process, which is the action of both pressure and temperature as the coal swamp is buried under younger sediments as illustrated in Figure 2-1.
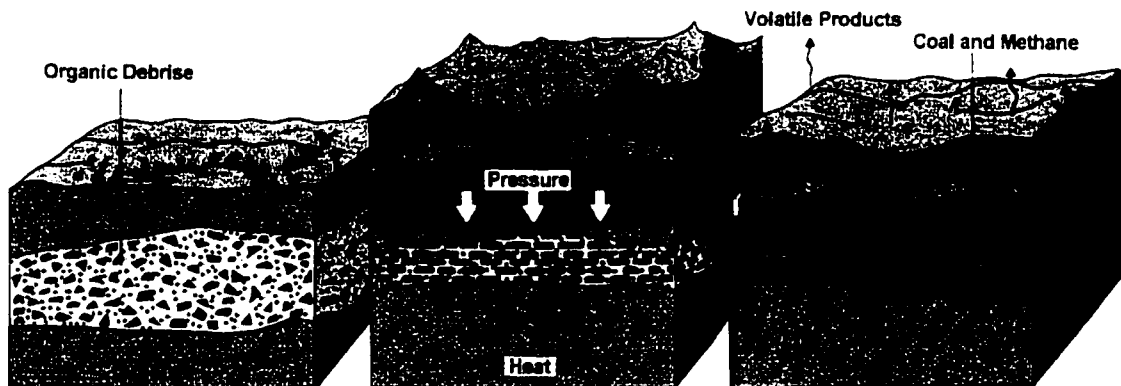
Figure 2-1 Coalification process

Coals are classified according to the proportion of carbon they contain, which increases as the degree of maturation increases. Lignite has 70% carbon, bituminous coals vary between 80 and 90% carbon, and anthracite has more than 90% carbon. Table 2-1 presents the ASTM ranking of ash free coal.

Gases are generated during the conversion of the sediment plant material to coal, and they are either adsorbed onto the coal particle surfaces or are dispersed into the pore spaces around the coal seam. The amount of gas formed depends on the rank or class of coal. Since coal rank is a function of temperature and time, it increases with depth, and as a result, more methane is likely to be contained with high rank coal rather than shallow, low rank coal. Kim (1977) showed that the volume of adsorbed gas increases with increasing coal rank from high volatile to anthracite, Figure 2-2 shows the relationship between the volume of adsorbed gas and coal ranking. The volume of adsorbed gas at 60 atm pressure for anthracite coal is almost twice the volume of adsorbed gas for the high volatile coal at the same pressure.

Methane is the dominant gas in the coalbeds (about 95%), with the remaining gases including ethane, carbon dioxide, nitrogen, helium and hydrogen. Hydrogen sulfide is found only in trace amounts, even in high-sulfur coals. In addition to these gases, large amounts of water are released during the maturation process. Because coal shrinks during the maturation process, it losses its capacity to retain water.

Coals' ability to retain carbon dioxide is stronger than methane. (Robertson et al., 1994) and (Stevenson et al, 1991) had experimentally shown that for binary and ternary mixtures of CO_2, CH_4, and N_2 the equilibrium gas and adsorbate phase compositions differ considerably, and that the total amount of gas mixture adsorbed is strongly dependent on composition and system pressure. CO_2 is the most strongly adsorbed gas, then CH_4, with N_2 being the least adsorbed. The

approximate adsorption ratios are 4:2:1 that is 4 molecules of CO_2 are adsorbed for 2 molecules of CH_4 and for every molecule of N_2, when comparing pure gases at the same temperature and pressure. The process of coalification and maturation results in coalbeds that are generally fractured, low-pressure, low-permeability, water-saturated gas reservoirs.
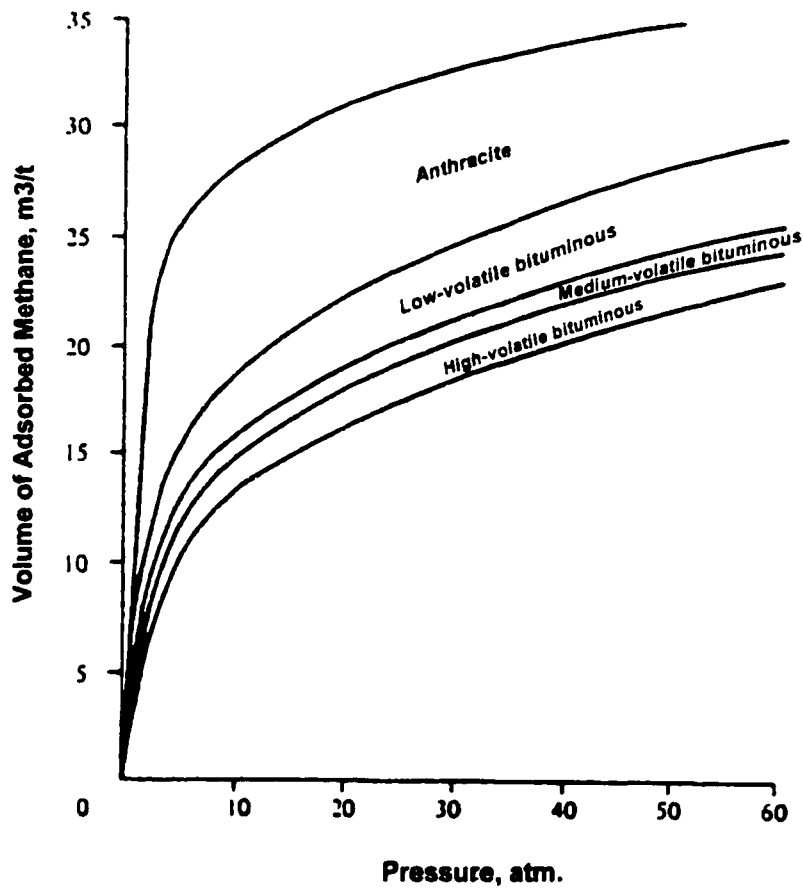
Figure 2-2 Variation of methane adsorption isotherm (0 °C) with coal rank.
(after Kim, 1977)

2.2.1 Gas Sorption in Coal

Sorption

Sorption is a term that has been used in the literature to refer the following range of physical-chemical processes.

i)   Absorption: A uniform penetration of one substance into the molecular structure of another substance (the process is reversible)

ii) Adsorption: A surface effect, whereby one substance is physically held onto the surface of another (reversible)

iii) Persorption: An extremely effective absorption of gas by a solid with the formation of an almost molecular mixture of two substances (irreversible).

iv) Chemisorption: An irreversible adsorption, whereby one substance is held to a surface of another by chemical forces.

Different conditions, such as pressure, temperature, nature of substances will determine the extent to which each of these processes can occur. Under the conditions of this research, chemisorption and persorption are considered irrelevant. Therefore, the sorption of gases on coal is considered as being totally physical in nature and reversible.

The Mechanism of Adsorption

Adsorption occurs due to the unbalanced forces that exist on a surface. Generally there is a field of forces around each atom and molecule of a substance which, by interaction, holds the molecules together, thus forming the substance. For example at the surface of a solid the average number of atomic or molecular neighbors is only half as great as below the surface. Therefore, there is an imbalance of forces at the surface of the solids (called the adsorbent), and a marked attraction on the surface toward the atoms and molecules in its

environment. This imbalance of forces can be neutralized by an attracted substance (called the adsorbate) such as molecules of an adsorbed gas.

The process of adsorption is spontaneous and continues until the free surface energy of the system, due to imbalance of forces, has reached a minimum. Van der walls forces are considered to be responsible for adsorption. These forces arise from the interaction between the electrons of neighboring molecules. Therefore, they are always present, but in ionic or homopolar lattices are overshadowed by electrostatic and valency forces respectively. They are much weaker than valency forces. Van der waals forces are also associated with the condensation of liquids. Therefore, the energy change accompanying adsorption is of the same order of magnitude as that for liquefaction of gases.

Theories of Adsorption

There are many theoretical models which could be used to describe the adsorption of gases into solids. The main difference between these models arises from the basic assumption made, and each model can be accurately used under appropriate conditions. For example, the Langmuir model (Langmuir et al, 1916) assumes that a monolayer of gas molecules occurs on the surface of solid during adsorption. On the other hand, the Brunauer, Emmet, and Teller (known as BET) approach assumes the formation of additional layers (Brunauer et al,. 1938).

2.2.2 Coal Ranking

The three ways of coal ranking are:

1.Proximate analysis, which depends on relating the ratio of fixed carbon versus fixed carbon plus volatiles; 2.The amount of heat given off when the coal is

15

burned; and 3.Reflectance index measurements, which are conducted by using a polished slide of coal and are directly related to its rank.

The reflectance test is highly dependent upon the maceral content of the coal. Macerals are known as the organic microconstituents of coal and vary with source material. There are three main groups of macerals: (1) Vitrinite, formed from the stemmy material in plants; (2) Liptinite, originating from leafy material; and (3) Inertinite, formed from nonflammable waxy material.

Macerals can be distinguished visually and are usually quantified petrographically by examination of a polished section of coal core under a microscope.

Glass	Group	Rank Criteria Limits of Fixed Carbon of BTU Mineral-Matter-Free Basis
Lignite	Brown Coal	Moist BTU, <8,300 *
	Lignite	Moist BTU, <8,300
Subbituminous	Subbituminous C Coal	Moist BTU, >8,300 and < 9,500
	Subbituminous B Coal	Moist BTU, > 9,500 and < 11,000
	Subbituminous A Coal	Moist BTU, >11,000 and <13,000
Bituminous	High-Volatile C Bituminous Coal	Moist BTU, > 11,000 or < 13,000
	High-Volatile B Bituminous Coal	Moist BTU, > 13,000 < 14,000
	High-Volatile A Bituminous Coal	Dty FC < 69% and moist BTU > 14,000
	Medium-Volatile Bituminous Coal	Dry FC > 69% and < 78%**
	Low-Volatile Bituminous Coal	Dry FC > 78% and < 86%
Anthracite	Semi-Anthracite	Dry FC > 86% and < 92%
	Anthracite	Dry FC > 92% and < 98%
	Meta-Anthracite	Dry FC > 98%

Table 2-1 ASTM Ranking of ash- free coal

* BTU British thermal unit   ** FC Fixed Carbon

2.2.2 Coal Structure

A porous structure generally contains three main pore systems. Micropores are usually defined as pores with radius less than 0.01 μm. Transitional pores between 0.01 to 0.1μm and macropores those which have a radius greater than 0.1μm. The micropores in coal make up about 70% of its total porosity and occur as part of the coal matrix. The macropore system consists of a naturally occurring network of fractures called the cleat system. The transitional pore system or what are sometimes called mesopores (smaller than macropores) do not generally appear in coal explaining why the coal is generally known as dual porosity rock or reservoir.

There are two kinds of cleats or fractures in coal: a face cleat and a butt cleat. These are considered the primary and secondary avenues, respectively, for fluid flow in coal. The two are commonly orthogonal or nearly orthogonal, and are nearly perpendicular to the bedding surfaces. The face cleat is laterally extensive, vertical and continuous throughout the seam. The butt cleat, also vertical, is in most cases discontinuous, ending at an intersection with the face cleat generally at a right angles, as shown in Figure 2-3. Face cleats usually control the flow of fluid to the wellbore because of their continuity. Butt cleats generally control the diffusion of gas from the coal matrix to the face cleats.

Cleat spacing is known to be affected by coal rank and bed thickness and it varies from millimeters to meters. Spacing generally decreases with decreasing layer thickness and with increasing rank. The in situ aperture width of cleats is another important attribute of cleat system geometry and permeability. It is difficult to obtain meaningful data under natural or replicated natural conditions. Estimates of cleat aperture under in situ confining pressure vary from 100 to 0.1 nm. Cleating in coal is determined by at least two diagenetic factors: the progressive compaction of organic matter due to coalification, and tectonic forces

17

acting on the coal (McCulloch et al., 1974). Permeability in coal beds is controlled by the cleat system in the coalbeds (Jones et al., 1988) and is generally low (< 10 md).

BUTT CLEAT

MATRIX BLOCKS CONTAINING MICROPORES
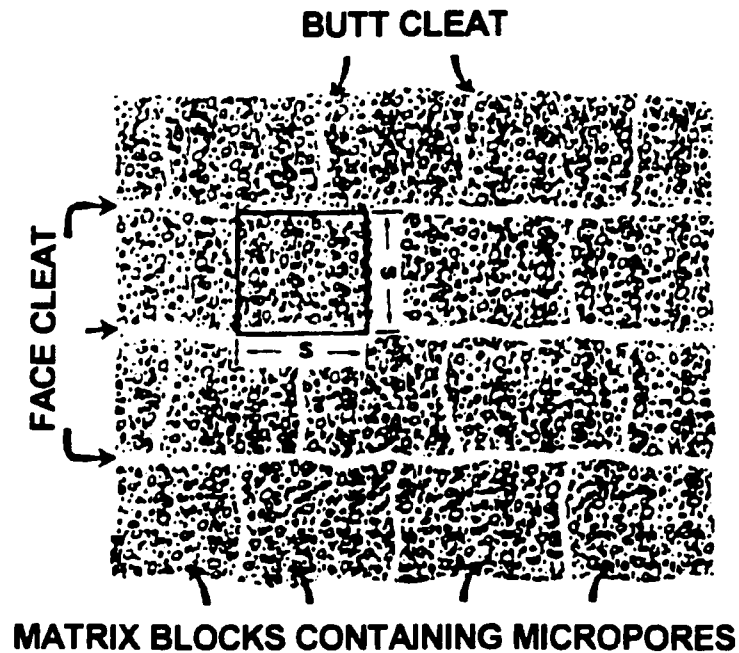
Figure 2-3 Cleating system

Finally, cleats are often confined to coal layers with bulk densities between 1.2 and 1.75 Mg/m^3. The upper density limit corresponds to rock comprising 50 % coal with the remainder mineral matter (roughly equal to ash content).

Apart from the cleat system, the bedding planes or surfaces are another set of fractures present in coal. However, these normally have no role in conducting fluids, because overburden weight induces high effective stress, and are of little primary interest as far as gas flow in coal is concerned (Harpalani et al., 1994). Although this is true, most researchers use a model consisting of several adjoining cubes, as shown in Figure 2-4 to represent coal.
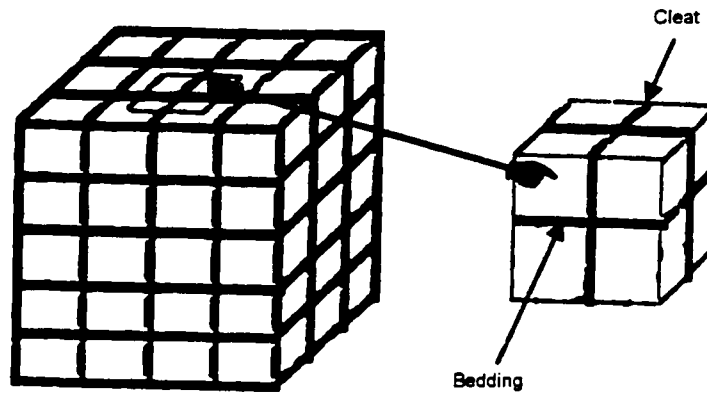
Figure 2-4 Cubes modeling for fractures in coal

To better reflect the inability of bedding surfaces to conduct flow, coal has been modeled as a collection of "matchsticks" as shown in Figure 2-5. This geometry has provided much better agreement between theoretical, laboratory and field data.
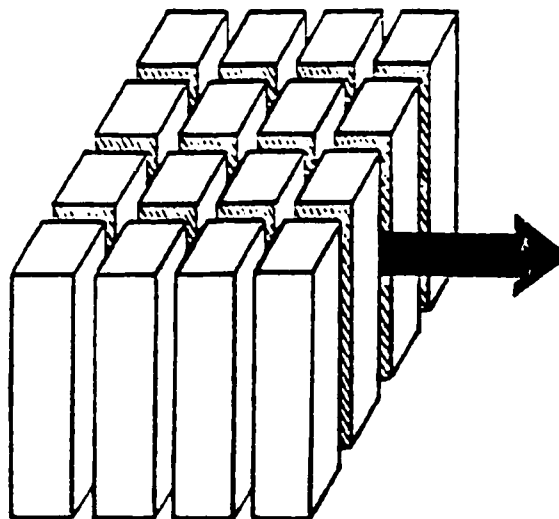
Figure 2-5 Matchsticks Modeling

Coal of any rank possesses certain porosity (King et al, 1944). Generally, the porosity is the factor responsible for the capacity of coal to store methane or any other fluid. However, it is important to distinguish the pore volume from the pore surface area. The internal surface area plays a great role in the capacity to adsorb gases (Kervelen, 1981). Generally the rate of reactivity in such process is higher with higher internal surface area. The external surface area is significantly less than the internal surface area.
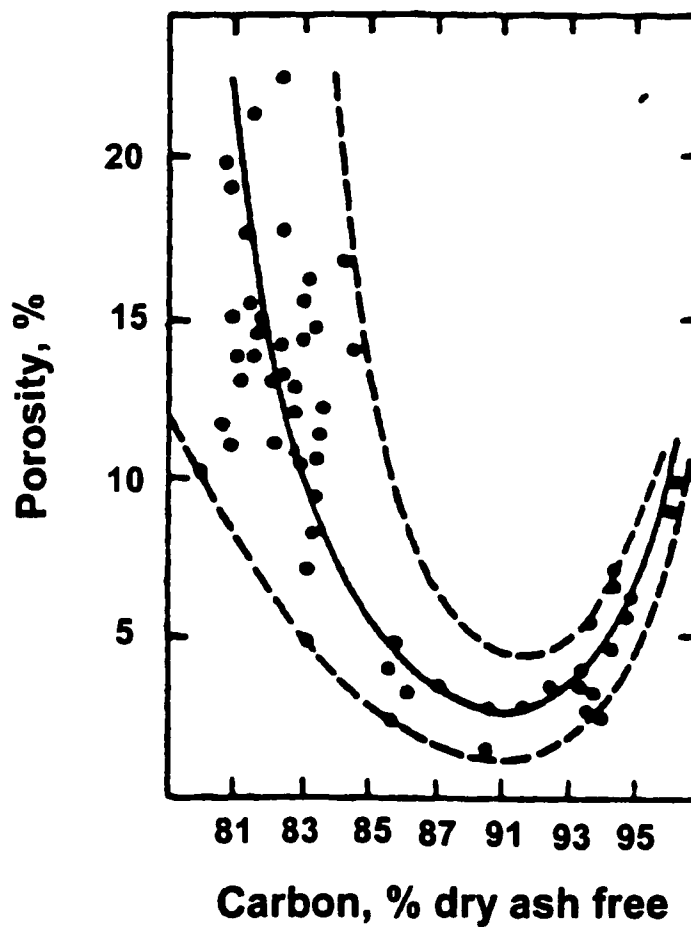
Figure 2-6 Variation of coal porosity with coal rank (After King, 1944)

2.2.3 Swelling and Shrinkage

Coal swelling due to sorption of liquids is a well known phenomenon reported by several researchers (Gregg, 1961 and Green et al., 1985). Other researchers have investigated swelling of coal in the presence of an absorptive gas. Moffat and Weale (1955) reported the swelling and shrinkage of coal with adsorption/desorption of methane to interpret sorption isotherms correctly. For pressures up to 15.2 MPa the volume of blocks of different coals were reported to increase by 0.2 to 1.6% clearly indicating swelling associated with sorption. At pressures between 15 and 71 MPa the bulk volume either decreased or remained constant. The authors concluded the constant or decrease in bulk volume was due to volume changes in the coal grains.

Swelling of coal under gas sorption influence has also been studied to investigate how the surface area and pore structures of coal are affected when an adsorptive gas is used to measure these properties. Because the surface area of coal determined by adsorption of carbon dioxide is higher than that obtained using nitrogen, the usual assumption that an inherent pore structure exists in coal which can be probed by molecules without influencing the coal structure itself is suspect. For bituminous coal samples, Reucroft (1986) examined whether the presence of CO_2 alters the volume of coal, and its subsequent effect on surface area measurements. There were two primary conclusions: (1) at room temperature (25°C) and a pressure of 0.14 MPa the length of the specimen increased on exposure to carbon dioxide by 0.36~1.31%; and (2) there was negligible change in length on exposure to nitrogen and helium at the same pressure and temperature. This work was followed by another study by Sethuraman et al., (1986) to evaluate the effect of pressure on swelling behavior of typical coals. The results indicated that swelling increased as pressure increased. The reported increase was between 0.75 and 4.18% for pressures up to 1.5 MPa. Also the higher the carbon content of the coal, the greater the degree

21

of swelling. However, only changes in length were monitored and the change in volume was estimated assuming isotropic behavior.

In a more recent study, Stefanska (1990), studied the simultaneous adsorption and swelling of coal cubes in carbon dioxide and methane at pressure ranging from 0.48 to 5 MPa. It was concluded that the adsorption induced swelling/shrinkage of coal in carbon dioxide was reversible and irreversible in methane. As expected, the degree of swelling of coal was found to depend on its rank and moisture content as these two factors affect the sorption capacity of the coal.

2.2.4 Permeability

Accurate knowledge of in situ permeability is important parameter for successful gas production simulation. Measurement of in situ permeability is very difficult because permeability is influenced by several factors, such as in situ stress condition, disturbance associated with drilling, water content of the coalbed, and gas pressure. Many of these factors change continuously during production due to varying pore pressures (effective stress) and gas desorption processes.

Gray (1987) postulated that shrinkage of the coal matrix due to gas desorption opens up the cleats and results in an increase in permeability. This increase in permeability would depend on initial in situ stress conditions and shrinkage characteristics of the coal. It should be mentioned here that changes in cleat porosity in situ would be due to shrinkage as well as to cleat closure owing to the increase in effective stress resulting from pressure depletion. This postulation is supported by more recent reported field data. Mavor et al., (1998) showed that natural fracture absolute permeability was increased significantly with continued gas production in the San Juan basin Fruitland formation. This conclusion was reached by examining two components of field results:

22

1) Absolute permeability measured from well test data during the production life of the wells increased, Table 2-2; and

2) There is an increase in bottomhole pressure during periods of constant gas production, illustrated in Figure 2-6.

The importance of understanding the influence of permeability is shown in Figure 2-7, where gas production rates rise dramatically while water production rates fall below the expected rates.

Well	Test Type	Average Pressure psi	Pressure Elevation ft ASL	Absolute Permeability md	E P to gas md	E P to Water md	Absolute Permeability Initial Absolute Permeability Ratio	Average Pressure Initial Pressure Ratio
VC 29-4	Open-Hole DST	775.9	4,896.3	16.6	0.0	16.6	1.0	1.0
VC 29-4	Shut-In	359.1	4,896.3	67.9	40.5	1.7	4.1	0.5
VC 32-1	Open-Hole DST	956.7	4,526.7	17.2	0.0	17.2	1.0	1.0
VC 32-1	Shut-In	527.0	4,526.7	46.7	28.4	1.1	2.7	0.6
VC 32-4	Open-Hole DST	929.8	4,581.0	19.5	0.5	13.7	1.0	1.0
VC 32-4	Shut-In	328.9	4,581.0	137.7	96.9	1.3	7.1	0.4
VC 32-4	Shut-In	382.5	4,581.0	137.9	85.9	1.5	7.1	0.4

Table 2-2 Summary of well tests supporting absolute permeability changes (after Mavor et al., 1998)
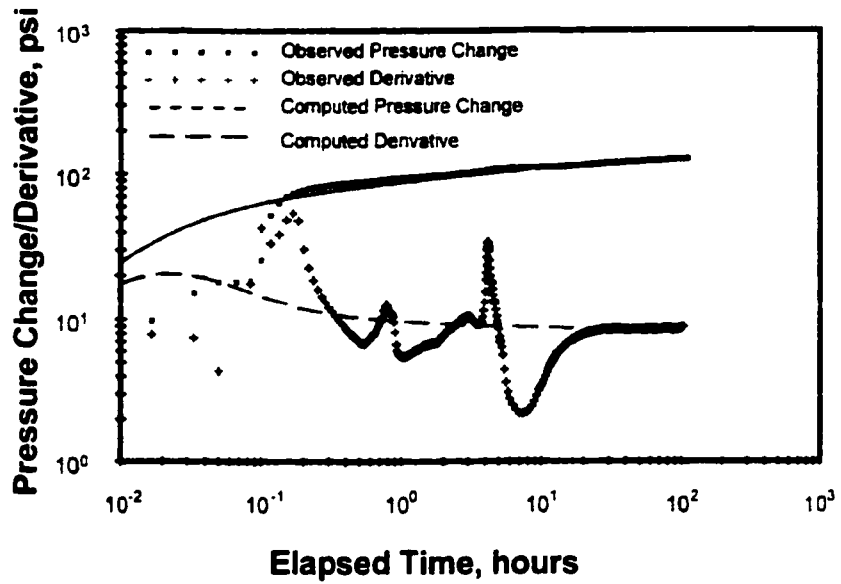
Figure 2-7 Shut-in diagnostic graph (after Mavor et al., 1998)
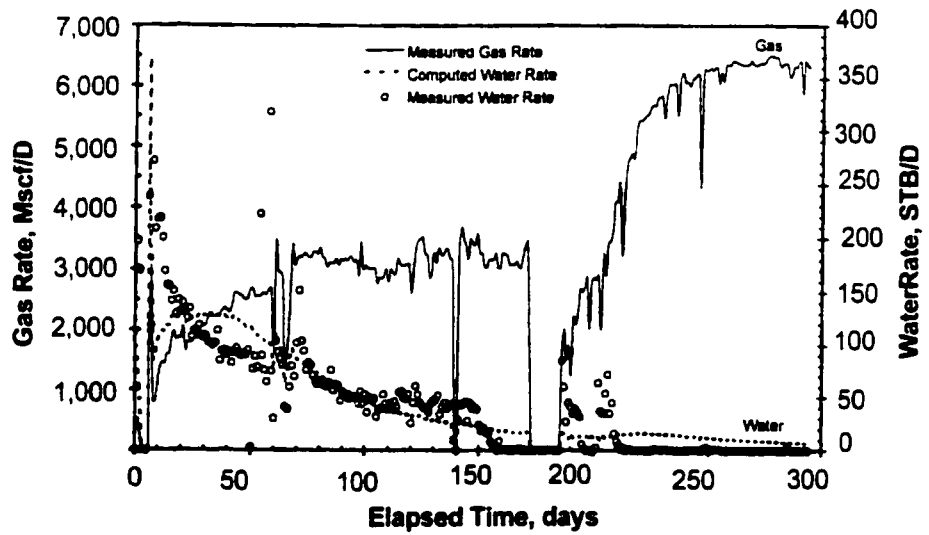
Figure 2-8 Comparison of measured and computed production rates (after Mavor et al., 1998)

For CO_2 injection, flow through the cleats can be influenced by many factors:

♦ Desorption of methane will open up the cleats due to the shrinkage causing an increase in permeability;

♦ Adsorption of CO_2 will result in swelling causing a reduction in permeability;

♦ Depending on the injection pressure, pore pressure might increase or decrease from the initial pore pressure which will alter the effective stress which, as a result, will have tremendous affect on the cleats permeability; and

♦ Changing pore pressure will affect grain compressibility thereby introducing another change in the permeability.

These simultaneous processes, occurring during CO_2 injection, make numerical simulation of the process difficult. In addition, shrinkage or swelling of the coal matrix during the desorption/adsorption process may not only widen or narrow cleat openings but may change the effective horizontal stress (σ_h') across the cleats. Modifying σ_h' will lead to further changes in cleat dimensions and a subsequent influence on permeability. Substantial shrinkage may even lead to a complete loss of horizontal stress. Pavel and Alena (1996) tested coal samples under triaxial stresses and concluded that gas permeability decreases with the increase in confining pressure. Overall, matrix shrinkage can have a significant impact on long-term gas production from coalbed methane reservoirs and can be an important factor influencing gas production from coal.

Harpalani and Richard (1989) state that the gas permeability of coal decreases with decreasing gas pressure. However, if the gas is an adsorbing gas, the permeability starts increasing once the pressure falls below the point at which significant desorption begins. The increase in permeability of coal below the pressure at which significant desorption begins is due to the shrinkage of coal matrix. The intact matrix of coal between the fracture shrink inward due to desorption of methane, thus enlarging the fracture width and resulting in higher

permeability.

More recently Harpalani and Chen (1994) concluded that the shrinkage of coal matrix on desorption of gas results in a matrix shrinkage coefficient which is significantly larger than the matrix (or grain) compressibility. For a sample from the San Juan Basin, the authors measured a shrinkage coefficient almost five times the matrix compressibility. A major consequence of the matrix shrinkage is a corresponding increase in the cleat (or fracture) porosity of coal. Depending on the initial cleat porosity the increase can be almost 80%. The results also suggest that shrinkage of the matrix and the associated increase in the cleat porosity can increase the permeability by as much as sixfold, depending on the initial porosity. It is therefore recommended that the coal matrix shrinkage be considered together with cleat contraction due to pore volume compressibility when simulating long-term gas production from coalbed methane wells.

As clearly demonstrated above, effective stress strongly influences coal permeability. Harpalani and McPherson (1986) studied the role of effective stress on coal permeability and found that the variation in coal permeability with respect to applied axial stress indicates that coal exhibited viscoelastic behavior. During loading, the stress at high points of contact among the coal macerals may exceed their failure level. The time-dependent crushing occurring at these points leads to a certain nonrecoverable component of the permeability-stress hysteresis. The percentage of permeability that is recovered during unloading is attributable to the elastic reopening of most pore closures that occur during loading, as supported by the effect of axial stress on volumetric strain. With successive loading-unloading cycles, however, the permeability losses become exaggerated when the coal is left either in a lightly stressed state between successive cycles or especially in a maximum stressed condition before unloading.

Mckee et al., (1988) also found similar behavior for their experimental work on coals from Northern Appalachian Basin and San Juan Basin, Colorado.

2.2.5 Coal Strength

Determination of field representative strength properties of coal by direct measurement is difficult due to its cleated structure. Cleats govern the strength response of the coal. Since cleats vary in orientation and size throughout the coal mass, coal samples from the same block of coal generally exhibit different strength characteristics. Moreover, small samples used in the laboratory will be quite different from that in the field. Field large-scale material behaviour can be represented as a continuum, whereas in the laboratory the cleats render a more discrete response. In addition to difficulties associated with establishing a unique strength profile for cleated coals, the reported laboratory tests performed on coalbeds have generally ignored the significance of stress path on the strength response. Most of the tests reported have been performed in compression and under high levels of confining stress which tend to close the cleats and thus overestimate the strength properties, particularly the apparent cohesion. As a result of these inconsistencies a wide range of cohesion values have been reported for coalbeds; this range is typically between 2 and 5 MPa. In analyzing field problems involving coal break-up and sloughing of the wellface in deep wellbores employed for methane extraction from San Juan Basin coalbed reservoirs, it was noted that the cohesion for coalbeds is very much smaller than the reported range. The true cohesion is shown to be ca. 5-10 kPa with an apparent cohesion (defined herein as the extrapolation of the linear portion of the Mohr-Coulomb failure envelop to the shear stress axis) of approximately 100 kPa which is considerably less than the previously reported range. The primary reason for the discrepancy between back analyzed and laboratory determined cohesion is due to the stress paths used to initiate failure. In the field, failure of coal is induced by a reduction in the effective stress through fluid injection

(tensile failure) whereas in the laboratory failure has been measured in compression. Another factor that has also contributed, rather significantly, to the high cohesion is the assumption that the failure envelope remains linear over the low stress range. The study by Vaziri (1997) indicates that coal's failure envelope is nonlinear and that the behavior at low levels of effective stress is markedly different from that at higher levels. To validate the numerical findings, direct shear tests were performed by subjecting coal samples to failure under low levels of effective confining stress. The test results indicated both a nonlinear failure envelope and apparent cohesion of 150 kPa, which is very close to that predicted from back-analysis of the field problem.

The mechanical properties of coal are significantly different from conventional rocks. It is not uncommon for Young's Modulus values for coal to be an order or orders of magnitude less than conventional reservoir rocks, such as sandstones. The mechanical properties of coal are important when hydraulic fracturing is used to stimulate production. The low value of Young's Modulus typically results in the creation of very wide hydraulic fractures, Additionally, it has been found from mineback experiments (Holditch et al., 1988), that very complex fracture systems are usually created during a hydraulic fracturing treatment. Not only are multiple vertical fractures often created, but also fractures propagating in multiple directions can be quite common. It is felt that this complex hydraulic fracture behavior is due to the presence of the cleat system, the complex structure of the coal matrix, and the stratigraphy of the coal seam with respect to the surrounding sediments.

The properties of coal containing gas are important to explain coal and methane outburst. For long period of time the physiocochemical interaction between pores gas and the surface of minicrack in coal or rock was ignored or considered in the way of effective stress (Terzaghi's theory). The results of the study done by (He and Shining, 1992) show that the behavior of the coal specimens containing gas

28

(CO_2 or N_2, at 2MPa) or containing no gas after rheological experiments are different. The specimen containing no gas are compressed and become hard; those containing gas are fractured and separated. These behaviors show that the pre-gas action cannot be simply described by effective stress. The physicochemical interaction between the crack surfaces of coal and the pore gas is important. The different adsorbabilities of gas in coal will make the specimens fail in different ways. It was found that the strong adsorptive gas, CO_2, fails the specimens easier and faster than the weak adsorption gases do, such as N_2.

The adsorption of a gas (CH_4 or CO_2 or N_2) in coal or rock is the physisorption. The adsorption is brought about by the force of attraction between the solid and gas molecules. When a specimen of coal containing no pore gas is compressed at high stress levels, the cracks in the specimen close easily until the yield strength of coal is reached. The attractive forces (Van der Waals) between the two surfaces of the closed crack make the compressed coal specimen stiff. If the pores of coal are filled with gas, and the surfaces of cracks in coal are adsorbed by the molecules of the gas, the attractive forces between the two surfaces of a crack are reduced subsequently and the coal will be much less stiff than the no gas coal specimens.

2.3 MINING DEGASIFATION OF METHANE

As a result of mining deep coalbeds, the problem of increased methane content associated with these deeper coalbeds has become a tremendous concern. The huge amount of released gas during mining and the subsequent methane outbursts prompted research in this area to understand the drainage properties of coal in order to design mine ventilation systems. Also the strength properties of coal in the presence of methane was also studied to better understand methane outbursts. Singh (1968) studied the desorption of gases for different

coals and used this data to classify whether a coal was prone to outburst or not.

More studies in the United Kingdom, Australia and United States resulted in different ventilation designs to improve mine safety by increasing air flow to dilute the gas to below the dangerous level and venting it to the atmosphere. Bise et al., (1989) conducted research to determine the optimal methane degasification scheme for a coal permeability range from 5 md to 60 md based on simulated methane flows and economic data. The overall finding were

♦ Borehole spacing of 152 m is the best choice in a horizontal degasification scheme because of the low labor and material costs associated with a lower number of boreholes to drill, along with substantial cumulative methane flows produced.

♦ For vertical scheme the results showed that every other panel scenario is optimal because it has lower numbers of wells than the every panel case.

♦ When optimal vertical and horizontal borhole strategies were compared, it was clear that in the lower permeability ranges, 5 to 10 md, the horizontal borehole method, with spacing intervals 152 m, was the most economical choice. In the higher permeability ranges, > 10 md, the vertical stimulation well method with the wells placed in every other panel proved to be the best method

Since methane is a fossil fuel and also the second most critical greenhouse gas next to carbon dioxide accounting for 45% of the global warming, interest in coalbed methane recovery has increased dramatically.

2.4 COALBED METHANE RESERVOIRS

2.4.1 Methane Formation

Gases in coalbeds are generated during the conversion of organic matter to coal. They are either adsorbed onto the coal or are dispersed into the pore spaces around the coal seam. The amount of gas formed depends on the rank of coal. Methane is the dominant gas (about 95%), with the remaining gases including ethane, carbon dioxide, nitrogen, helium and hydrogen; hydrogen sulfide is found only in trace amounts, even in high-sulfur coals. Large amounts of water are also formed during the coalification process.

2.4.2 Gas Existence

The gas content of a coalbed is made up of three components, free gas compressed in pore spaces, gas in solution, and gas adsorbed on the internal surface of the pores. The process of adsorption is different than that of absorption of gases. When gas is allowed to come to equilibrium with a solid or liquid surface, the concentration of gas molecules is always greater in the immediate vicinity of the surface than in the free gas phase, regardless of the nature of the gas or surface. The process by which this surface excess is formed is called adsorption. According to Young et al. (1962), the phenomenon of adsorption is like a condensation of vapor to form a film of liquid. It is distinguished from absorption, which involves bulk penetration of the gas into the structure of the solid by diffusion. In the case of coal and gas it is difficult to distinguish between those processes, so the term adsorption is used here for both types of phenomenon. The quantity of free and solution gas depends on the porosity of the coal, pressure of gas in the pores and the temperature. It usually makes up a small fraction, about 5-10% of the total gas content (McPherson 1975).

The greater part of the in situ gas content in coal is held on the surfaces of the coal pores and microfractures in adsorbed form. Since the internal surface area of coal can be as large as 90 m²/g, the quantity of adsorbed gas can be extremely high. It is, therefore, important to be able to determine the amount of adsorbed methane accurately. This can be determined by the adsorption isotherm which is the curve giving the quantity of gas adsorbed as a function of pressure at a given temperature.

Several researchers have studied the sorption behavior of coal and the effect of temperature, moisture, gas mixture, and particle size on sorption. Joubert et al., (1973, 1974) studied the effect of moisture on the sorption capacity of bituminous coal at a temperature of 30 °C and pressure up to 6 MPa. For all coals studied the capacity of coal to adsorb methane decreased with increasing moisture content up to a certain value characteristic of the coal type. Moisture present in excess of the critical value had no effect on methane sorption. At values of moisture content m (wt %), below critical value mc, Equation 2-1, an empirical equation developed by Ettinger (1958), fits the methane sorption data quite well:

$$\frac{V_d}{V_w} = C_o m + 1 \qquad [2\text{-}1]$$

where,

V_d = volumes of methane adsorbed on dry coal;

V_w = volumes of methane adsorbed moist coal; and

C_o = the correlation coefficient, with a value of 0.31 often used for bituminous coal.

When coal is at or above the critical saturation value, mc, methane sorption can be described by:

$$(1-\frac{V_w}{V_d})\max = C_1X_o + C_2 \quad (m \geq mc) \qquad [2-2]$$

where,

X₀ is the coal oxygen content in wt %.

The reduction in methane sorption capacity with increasing moisture is more significant for high oxygen coals due to their high moisture capacities.

The dependency of sorption capacity on moisture content was also studied by Bell et al., (1986) and results similar to those reported by Joubert and others were reported. One interesting observation of the study was that at pressures above 3.5 MPa, the moisture content had no effect on sorption capacity. Also, initial work by Bell (1986) reported a hysteresis between adsorption and desorption isotherms. However, an error in calculating the sorbed volumes was realized and later work by Bell (1989) confirmed that there was no hysteresis. Furthermore, Bell reported laboratory gas content being about 50% higher than that measured in the field, and attributed the discrepancy to a possible effect of stress on adsorption equilibrium.

The effect of particle size on the sorption capacity was studied by Ruppel et al., (1972). The amount of methane adsorbed on crushed and dried coal was measured as a function of pressure. Isotherms were measured at 30°C for Illinois coal and at 0°C, 30°C and 50°C for the others. Most measurements were made up to 150 bars with a few up to 240 bars. Isotherms were repeated using 6-8, 80-100 and 270-325 mesh coal. The conclusion of the study was that particle size in the range of 6 and 325 mesh has no effect on equilibrium adsorption.

In the above study, temperature effect on the sorption capacity of coal was also reported. There was a distinct decrease in the amount of adsorbed gas with increase in temperature from $0°C$ to $500°C$. A similar dependence was again reported by Yang et al., (1985). Ettinger et al., (1958) developed an empirical equation where, if the methane adsorption isotherm of a coal at $30°C$ is known, the isotherm at any other temperature can be established by:

$$V_t = V_{30} \frac{e^{n30}}{e^{nt}} \qquad [2\text{-}3]$$

where,

V_t = the methane adsorption capacity of dry coal at temperature t;

V_{30} = the methane adsorption capacity of dry coal at temperature t and $30°C$;

n_t = the index of the degree of the temperature coefficient at $t°C$; and

n_{30} = the index of the degree of the temperature coefficient at $30°C$.

Another relationship commonly used for bituminous coal is that starting at $23°C$, the volume of adsorbed gas falls at a rate of 0.8% per degree.

Harpalani et al, (1993) studied the effect of gas mixtures on the sorption isotherm. It was concluded that carbon dioxide is more adsorptive on coal than methane. They also established sorption isotherms for gas mixtures and compared the results with results obtained from theoretically established isotherm. Sorption results for the gas mixture obtained by the numerical technique compares very well with the sorption isotherm obtained experimentally. Similar results were obtained by Robinson et al, (1994).

2.4.3 Gas Release and Flow

Methane has been produced from conventional reservoirs (sandstone). Gas in these reservoirs is compressed in the pore space and with time, gas production rates decline and water production rates increase. In coalbeds, the high percentage of methane is adsorped to the coal surface under high pore pressure. The traditional method to recover methane depends on pressure reduction. Figure 2-8 provides a schematic illustration of the different production responses for sandstone and coalbed reserviors.

Benzene Rings

Coal   Sandstone

Conventional

Butt Cleats

Face Cleats   Sand Grain   Gas Filled Water
Dewatering   Stable   Decline   Porosity
              Production

Methane   Methane

Water   Water

Time   Time
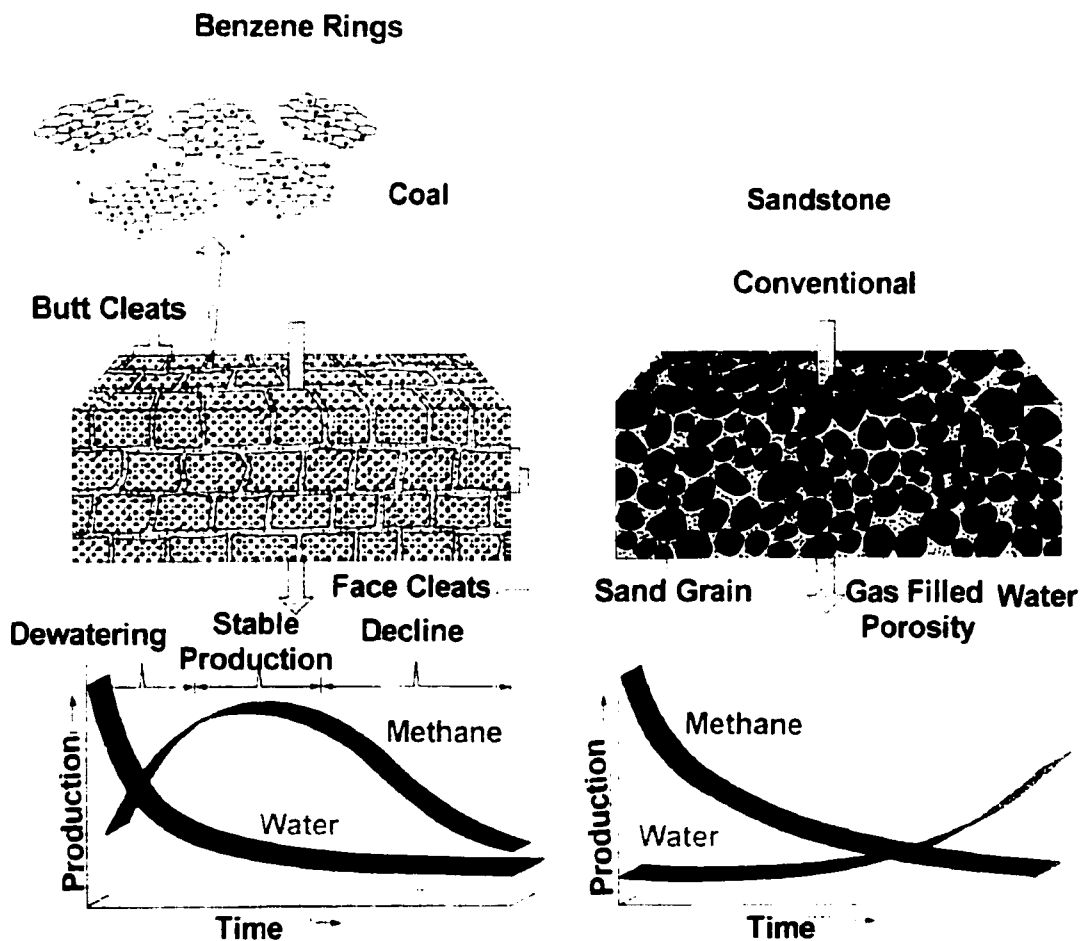
Figure 2-9 Coalbed and sandstone methane reservoirs

Once the pressure in the coalbed is reduced, coal becomes less capable of retaining methane in an adsorbed form. The gas molecules start detaching themselves from the surface of the pores and microfractures and the process of desorption is initiated. Desorption is the reverse of adsorption and occurs when the gas pressure within the pores is reduced. When the in situ gas content in the coal seam lies directly on the adsorption isotherm, methane is released immediately upon drawdown of water within the wellbore. However in many coalbeds the methane content does not lie on the desorption isotherm, and significant drawdown of pressure at the well bore must occur before methane can be released as shown in Figure 2-9.

After methane is desorbed it must diffuse through the solid matrix. Methane diffusion is governed by Fick's Law. Crank (1975) has shown that the differential equation representing Fick's Law for diffusion into or out of a sphere is:

$$\frac{D\delta}{r^2 \delta r}\left(\frac{r^2 c}{r}\right) = \frac{\delta C}{\delta t}$$

[2-4]

where,

C = concentration of gas (scf/tone);

r = is distance (ft);

t = time (days);

D = the diffusion coefficient (sq ft/day); and

D/r^2 = characterizes the diffusion for particular coal of interest when r equals the mean particle diameter "a".

Methane diffuses through a coal particle by means of a concentration gradient. Methane concentration is higher near the desorbing surface and low in the cleat of the coal therefore, the methane diffuses down the concentration gradient toward the cleat. Sawyer et al. (1987) have demonstrated that D/a^2 can be

toward the cleat. Sawyer et al. (1987) have demonstrated that D/a^2 can be related to sorption time, t, where sorption time characterizes the time of diffusion of the methane through the coal particle to the cleat. In general, sorption time is dependent upon the composition of the coal and the cleat spacing in the coal. Sorption times have been reported as low as less than 1 day to greater than 100 days for coal.

Short sorption times, when coupled with gas-saturated coals, result in immediate, high initial gas-production rate peaks within a few days of putting the well on production. In similar circumstances, long sorption times tend to generate broad gas-rate peaks that occur several months after start of production.
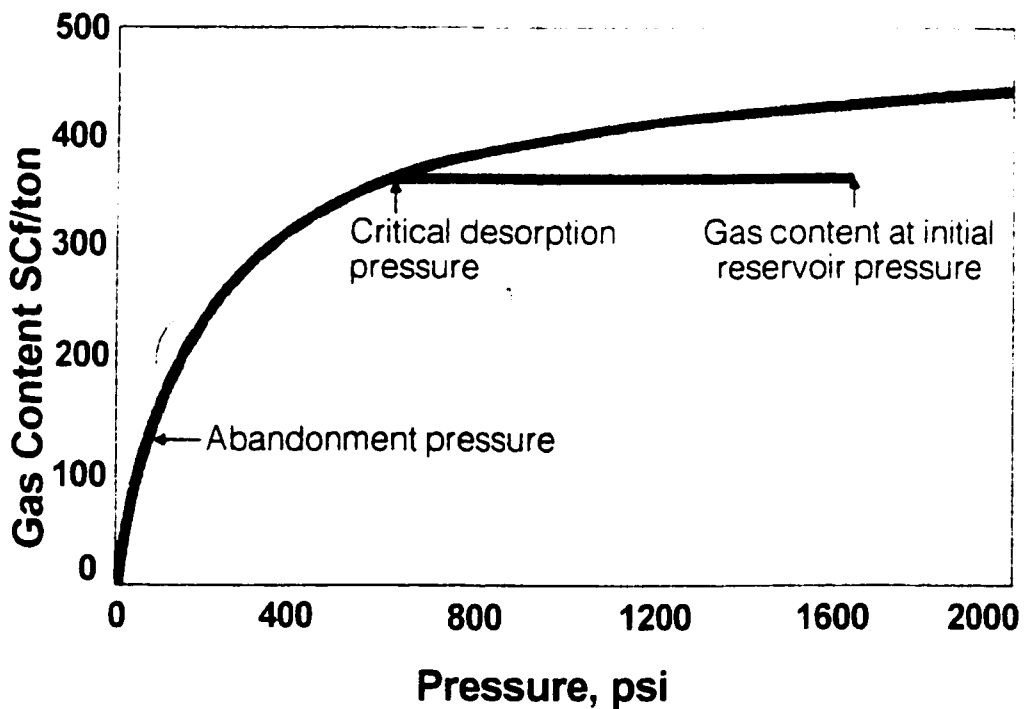
Figure 2-10 Adsorption isotherm

water according to Darcy's law and the gas-water relative-permeability for the coal.

2.5 CARBON DIOXIDE GEOLOGICAL DISPOSAL

Geological formations have been considered as potential permanent storage of CO_2. Many techniques have been used to dispose CO_2 underground and other techniques are still under development.

CO_2 has been used in enhanced oil recovery (EOR) operations. If CO_2 from power plants is desulphurized, it can be used in extracting more oil from depleted wells, or used as liquid to transport coal in a liquid/slurry pipeline. Primary oil extraction removes approximately a third of the oil present and EOR removes a further third before a well becomes uneconomical to operate Houpeupt (1976).

Frederick, et al (1981) stated that the disposal of CO_2 into abandoned oil and gas wells is considered feasible because in the United States alone there are 12 000 abandoned wells. However the liquid CO_2 will not remain at its liquefaction temperature of 27°C, but will be slowly heated to the temperature of the surrounding earth. Its final temperature will depend upon the depth of the well and could increase to > 95°C. At this temperature the CO_2 will be supercritical and the pressure will increase. If CO_2 maintain its placement pressure at 95°C, it will expand to five times its original volume, thus reducing the equivalent carbon storage capacity of the well. Also there is always risk of gas leakage from those wells, sudden release of the stored gas due to tectonic movements could be catastrophic.

Hitchon (1996) showed that the deep aquifers in Alberta Basin are capable of trapping huge amounts of waste CO_2. The capacity of these traps are so large that no other sinks would be needed to dispose of all Alberta's emissions over

the next century. On the other hand, this method of CO_2 disposal is expensive, of the order of $50/tonne if flue gas separation costs are included (Gunter et al., 1995).

Gunter et al (1996) conducted a research to evaluate the possibility of trapping CO_2 in deep aquifers, they concluded that CO_2 trapping reactions are expected to take 100s of years to complete. The concerns around this method of CO_2 trapping were over carbonate mineral precipitation reducing the aquifer permeability. Also this method is considered expensive because it does not generate any revenue to compensate for the cost of the operation. However a big project for CO_2 disposal in an aquifer is under operation in Sleipner field in the Utsira formation in Norway.

The use of coalbeds to trap CO_2 is still a new research area, CO_2 could be injected in deep coalbeds to displace the adsorbed methane on the coal particles. The EGR has already been tested in the field. Amoco was the first to successfully demonstrate the process in the field, the performance result of this test has not been released. However some technical problems remain to be solved. The advantage of such method of CO_2 disposal lays in its economical and environmental benefits. Gunter et al., (1996) stated: *the development of CO_2-EGR technology to exploit Alberta's CBM resources will lead to a synergy between an increased supply of fossil fuel and decreased global warming.*

2.6 COALBED METHANE RESOURCES

Methane is a colorless, odorless, tasteless, flammable gas. It is the first member of the paraffin (aliphatic or saturated) series of hydrocarbons. Methane is soluble in alcohol or ether, and slightly soluble in water. It is the major constituent of natural gas. In Canada Coalbed Methane estimation ranges from 200 to 3000 trillion cubic feet TCF (Nickols, et al. 1991) and it lies mostly in the Alberta basin.

In the united States 96% of CBM production comes from the San Juan Basin, located in southern Colorado and North Western New Mexico, and the Black Warrior basin in Alabama (Dawson, 1995). Estimates of CBM resources in the US range from 275 to 649 TCF.

2.7 CARBON DIOXIDE

Carbon dioxide is a compound of carbon and oxygen in proportion by weight of about 27.3 percent carbon to 72.7 percent oxygen. At normal atmospheric temperature and pressure, CO_2 is colorless, odorless, and about 1.5 heavier than air. CO_2 is relatively nonreactive and nontoxic. It will not burn, and it will not support combustion or life. When dissolved in water, carbonic acid (H_2CO_3) is formed. The pH of carbonic acid varies from 3.7 at atmospheric pressure to 3.2 at 23.4 atm.

Carbon dioxide may exist simultaneously as a solid, liquid, and gas at a temperature of $-69.9°F$ ($-56.6°C$) and pressure of 60.4 psig (416 kPa). Figure 2-10 shows the triple point and full equilibrium curve for carbon dioxide.

At temperatures and pressures below the triple point, carbon dioxide may be either a solid (dry ice) or gas, depending upon temperature conditions.

Above the critical temperature, which is $87.9°F$ ($31.1°$ C), Carbon dioxide can not exist as a liquid regardless of the pressure.
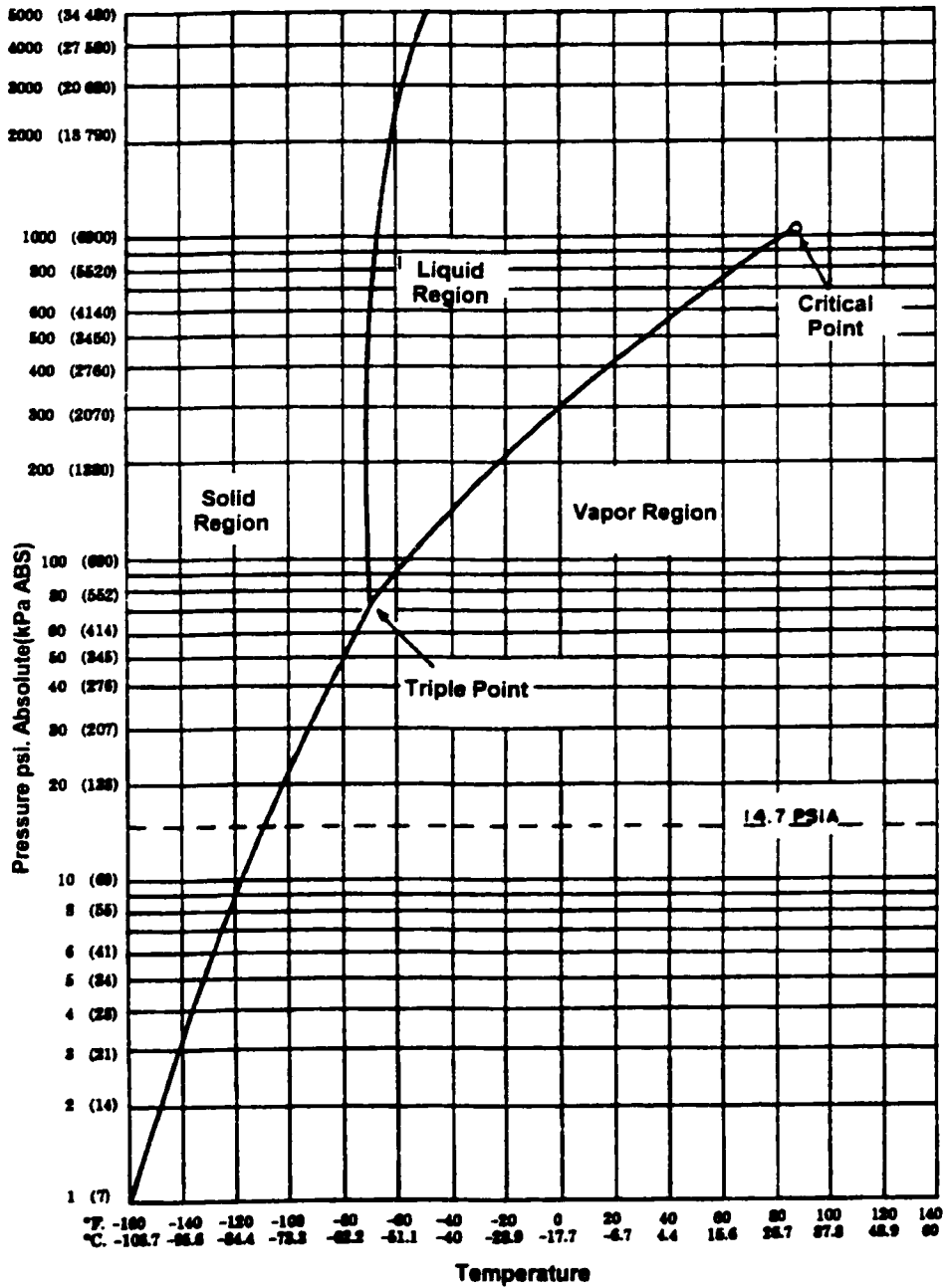
Figure 2-11 Carbon Dioxide Phase Diagram (Modified from the Handbook of Compressed Gases)

CHAPTER 3 CHARACTERIZATION TESTS

3.1 INTRODUCTION

Petrophysical properties of coal play an important role in the geomechaical response of coal to CO_2 injection. Under different coalification conditions, gas retention characteristics, porosity permeability and other similar properties will vary. This chapter describes the sampling program to obtain samples of coal from two open pit mines in Alberta. The procedure and results for the coal characterization tests are also presented and discussed.

3.2 FIELD SAMPLING

Coal samples were collected from two different sites, Coal Valley Luscar open pit mine in west central Alberta and Cardinal River open pit mine, Figure 3-1. Sampling took place in September 1998. The Luscar coals belong to the Tertiary age Val D' or seam of the Upper Coalsuper Formation, as shown in Figure 3-2. Samples were collected from fresh cuts as big blocks Figure 3-3.

Field sampling was attempted using three methods:

1) a portable coring machine; 2) chain saw and 3) retrievable of block samples created by excavator.

The portable coring machine, as shown in Figure 3-4, was built at the University of Alberta. This coring machine allows 25 cm diameter specimens to be cored to a length of 40 cm. An attempt was made to drill perpendicular to the bedding plane. As a result of excavation induced disturbance on the bench and

preferential shearing along the bedding planes, it was not possible to obtain high quality samples of the required size.

An attempt was made to use a chain saw to cut "blocks" of intact coal. This was also unsuccessful as the excavation induced disturbance caused the coal to "fall apart".

From the attempts and the experience of other researchers in attempting to obtain high quality coal samples (Kaiser et al., 1979, Noonon et al., 1972), it was concluded that high quality, consistent samples of coal could only be obtained by collecting large, intact blocks of coal that were cut by the excavator. The volume of the blocks was approximately 0.3 m^3. High quality test specimens could be taken from the blocks using special coring equipment in the laboratory. All blocks were isolated with expanding foam and wrapped in plastic for transportation to the University of Alberta where they were stored.

3.3 CHARACTERIZATION TESTS

In order to characterize the two kinds of coals used in the experimental program the following tests were carried out:

- Specific gravity;
- Bulk density;
- Water content;
- Porosity;
- Surface area;
- Proximate analysis;
- Ultimate analysis;
- Reflectance Test; and
- Maceral content.

The first three tests and porosity test using mercury intrusion were run at the University of Alberta laboratory. Porosity tests using nitrogen, surface area, proximate analysis, ultimate analysis, reflectance test and maceral content were done at CANMET Western Research Center (CWRC) in Devon Alberta.

A summary of the test results for these characterization tests is provided in Table 3-3. The detailed characterization test results can be found in Appendix A.

3.3.1 Specific Gravity

Specific gravity tests were conducted according to ASTM D 854-92. In general no difficulties were encountered during the testing, however some coal particles stayed on the water surface due to surface tension. This was overcome by adding a drop of soap to break the surface tension. For the Luscar coal, Gs = 1.43 and for Cardinal River, Gs = 1.52. These results compare very well with what was reported in the literature on similar kinds of coal (Handbook of Physical Properties of Rocks).

3.3.2 Moisture Contents

Moisture content tests were conducted according to ASTM D5142-90 and it is defined as the moisture weight in the sample over the weight of the dry sample. Cardinal River coal specimens were substantially drier than the Luscar coal specimens, with moisture contents of 0.8% and 7.2%, respectively. Moisture content results from the proximate analysis tests confirmed that Cardinal River coal specimens were drier than Luscar coal specimens, 0.6% for Cardinal River coal and 5.5% for Luscar coal. The slight difference in the moisture content results could be attributed to the variation of moisture content in the coal blocks.

3.3.3 Bulk Density

Bulk density tests were conducted according to ASTM D4404-84. The results were 1.38 and 1.23 Mg/m^3 for Luscar and Cardinal River coal specimens respectively. Also, bulk density was calculated from the weight and the volume of the triaxial coal specimens, bulk density from those specimens were 1.4 and 1.26 Mg/m^3 for Luscar and Cardinal River coal respectively. This difference in the bulk density represents the difference between the two methods used to determine the bulk density and the variation of the bulk density through the block samples.

Dry bulk density was 1.28 Mg/m^3 for Luscar coal and 1.21 Mg/m^3 for Cardinal River Coal. The slight difference in the dry bulk density between the two coals could be attributed to difference in the porosity.

3.3.4 Porosity and Surface Area Tests

Porosity tests were conducted using two different methods, firstly by using mercury intrusions according to ASTM D4404-84 and secondly by using Nitrogen intrusion according to ASTM D3663-92.

Mercury intrusion test is done by placing an air dried sample with known weight in the porosimeter after setting a zero reading. The porosimeter is then closed and mercury injected until it comes from the bleeding valve. The difference in the reading gives the volume of the sample. After closing the bleeding valve, pressure is raised incrementally and both the absolute pressure and the volume of intruded mercury were recorded until the pressure of interest is reached. The volume of intruded mercury after correcting for the system deformation represents the pore volume.

Porosity and surface area using nitrogen are determined by measuring the volume of nitrogen gas adsorbed at various low pressure levels by the coal sample. Pressure differentials caused by introducing the coal surface area to a fixed volume of nitrogen in the test apparatus are measured and used to calculate BET surface are and the porosity.

Porosity for Luscar CV and Cardinal River CR coals was low and lower than what's reported in the literature, approximately 2% and 3% for Luscar coal specimens and Cardinal River coal specimens respectively. Luscar coal has lower porosity than Cardinal River coal, this was reflected on larger dry bulk density for Luscar coal.

As mentioned before porosity tests were conducted using two techniques; mercury intrusion and nitrogen intrusion. From the mercury intrusion test higher porosity was found than nitrogen intrusion that could be attributed to bigger sample size used in mercury intrusion.

Porosity was also calculated from the bulk density and specific gravity. From this calculation Luscar coal porosity was 4% and Cardinal River was 19%. The difference in the porosity results between intrusion test procedure and the calculated porosity is likely the result of the low pressure used in the intrusion tests. This low pressure was unable to force nitrogen or mercury into the majority of the micropores. The difference in porosity provides an indication that more micropores are present in the coal specimens than indicated by mercury or nitrogen intrusion.

The surface areas for both coals were low 1.45 m^2/g for Luscar specimens and 0.13 m^2/g for Cardinal River specimens. There was no explanation for the extremely low surface area of Cardinal River specimens.

3.3.5 Maceral Contents and Reflectance Tests

The following sections describe the detailed process required to determine the maceral content and to perform the reflectance tests. The objective of this test is to determine the percentage of Vitrinite, Liptinite, Inertinite, and Minerals content in each sample in order to rank the coal and determine the effect of these material on the potential of gas adsorption. As mentioned in chapter 2 higher coal rank will have higher adsorption capacity and in return higher volume change. That means the adsorption process is related to the existence of the Liptinite and Vitrinite fragments rather than the inertinite.

Sample Preparation

After crushing and sieving the two coal samples, 20 gram representative samples were obtained from the material passing mesh # 30 (0.589 mm), Figure 3-5.Four molds are cleaned and lubricated. Five grams of coal are placed in each of the molds. Epoxy is mixed (5 - 1 resin to hardener) in separate container and then casted in the molds. Using a rod the mixture is distributed evenly in the mold. Tags are placed in the specimens after allowing them to harden for 24 hours. Specimens are then removed from the molds and cleaned using water and soap. The surface is then prepared by grinding and polishing through four steps, Figures 3-6, 3-7:

1- Using 100 pieces 240 GRIT sanding paper and water
2- Using 100 pieces 600 GRIT sanding paper and water
3- Using 10 pieces and Micropolish A 0.3 Micron Alpha Alumina
4- Final polishing by silk and Micropolish B 0.05 Micron Gamma Alumina.

Sample numbers are presented in Figure 3-8:

- Cardinal River 39-98
- Cardinal River 40-98

- Luscar Mine 41-98
- Luscar Mine 42-98
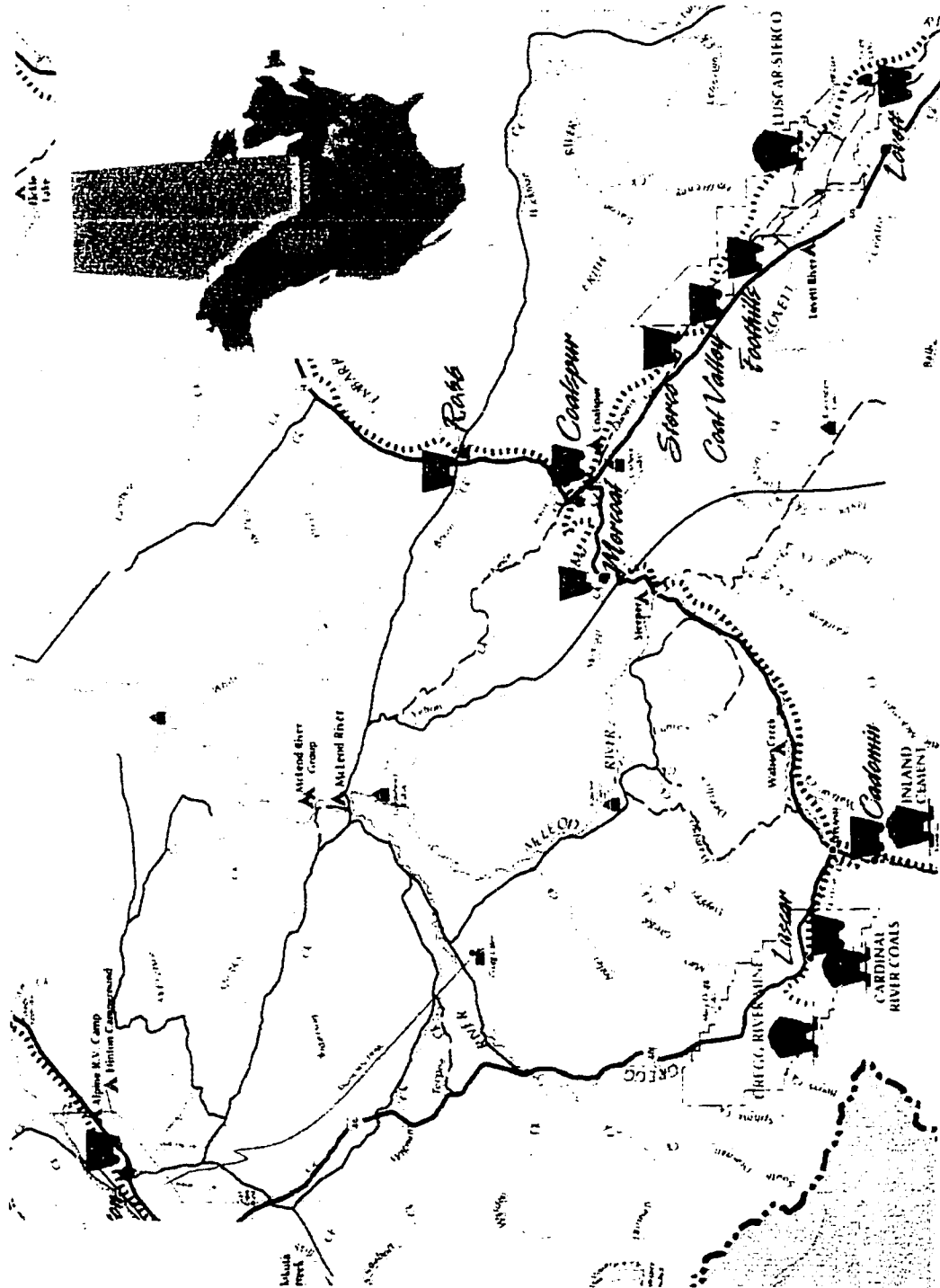
Figure 3-1 Map of the sampling locations
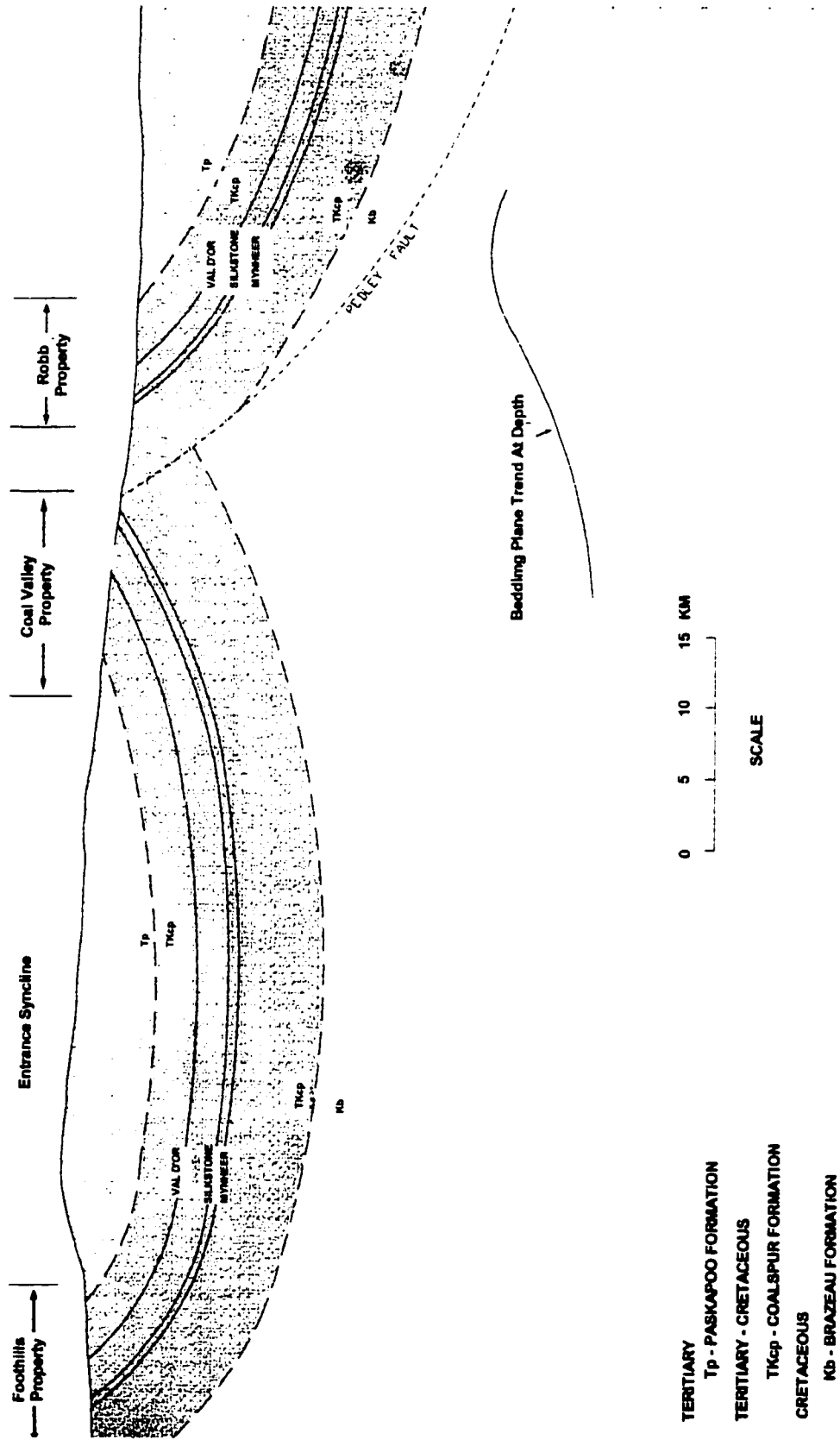
Figure 3-2 General cross section in Luscar mine

TERTIARY
Tp - PASKAPOO FORMATION
TERTIARY - CRETACEOUS
TKcp - COALSPUR FORMATION
CRETACEOUS
Kb - BRAZEAU FORMATION

SCALE

0   5   10   15 KM

Foothills Property

Entrance Syncline

Coal Valley Property

Robb Property

Bedding Plane Trend At Depth

PEDLEY FAULT

VAL D'OR
SILKSTONE
MYNHEER

Tp
TKcp
Kb

Figure 3-3 Coal blocks from Luscar mine

Figure 3-4 Portable coring machine
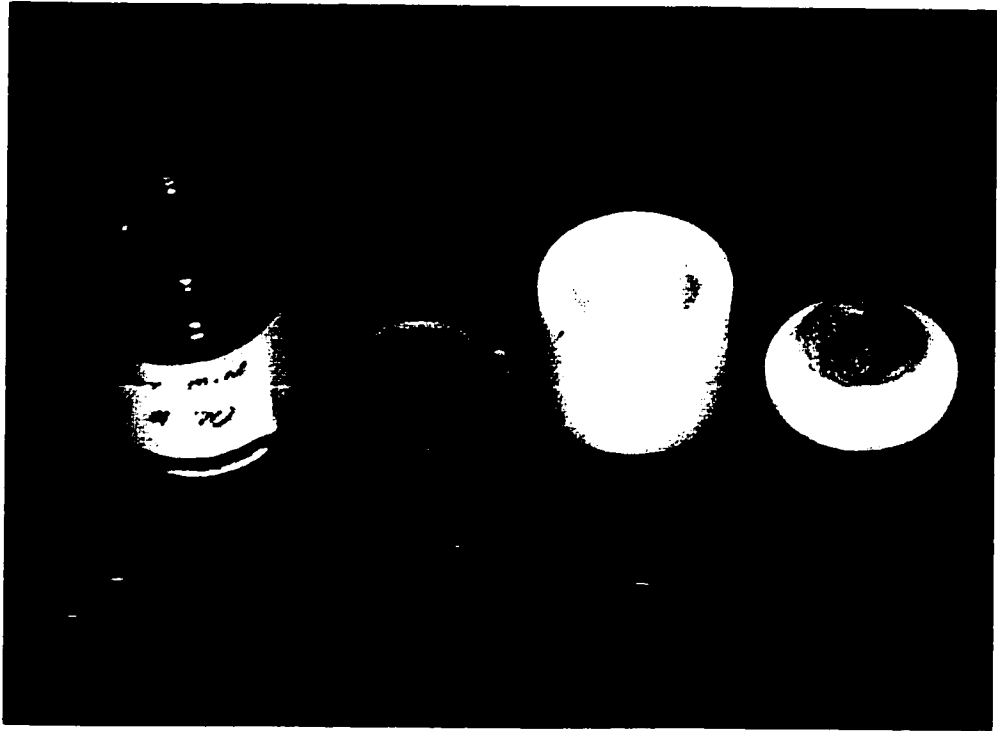
Figure 3-5 Coal samples after crushing
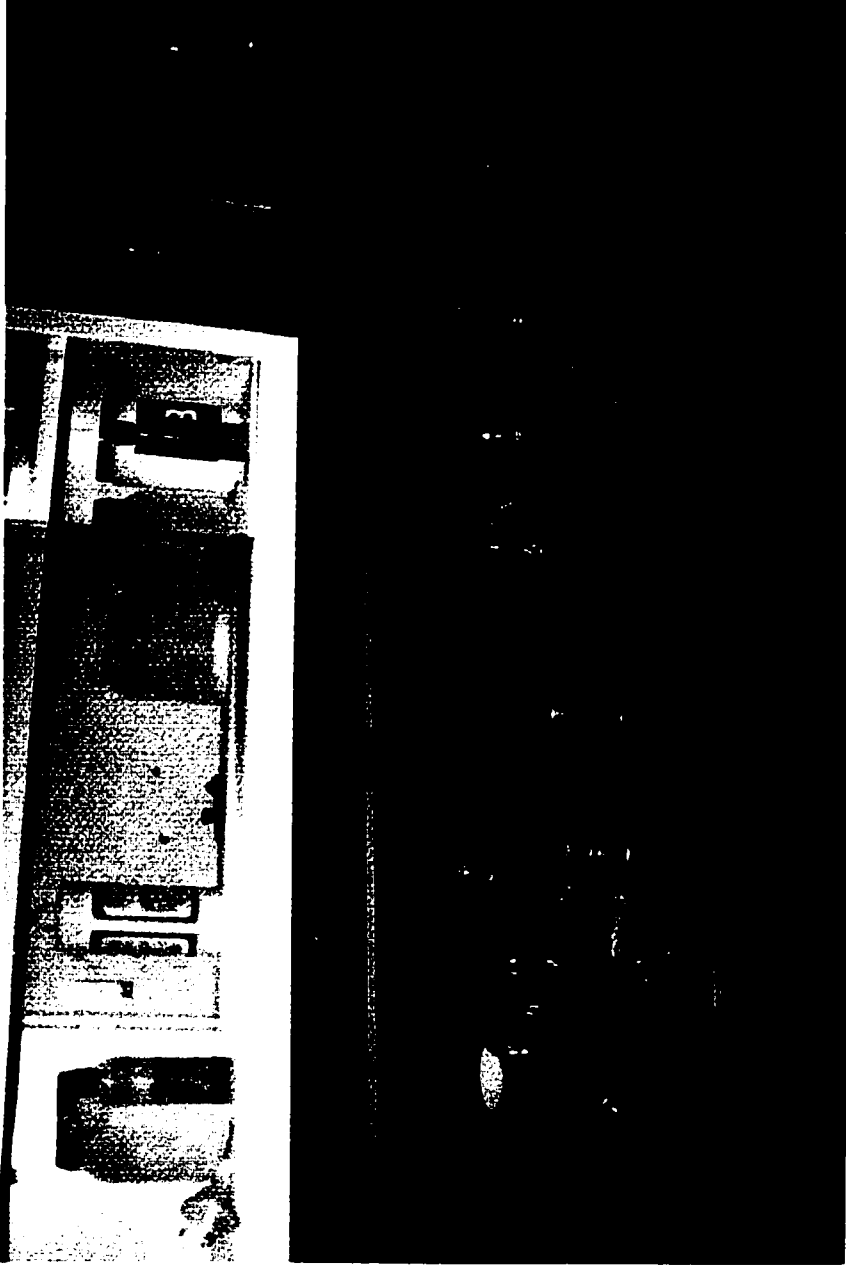
Figure 3-6 Polishing equipment
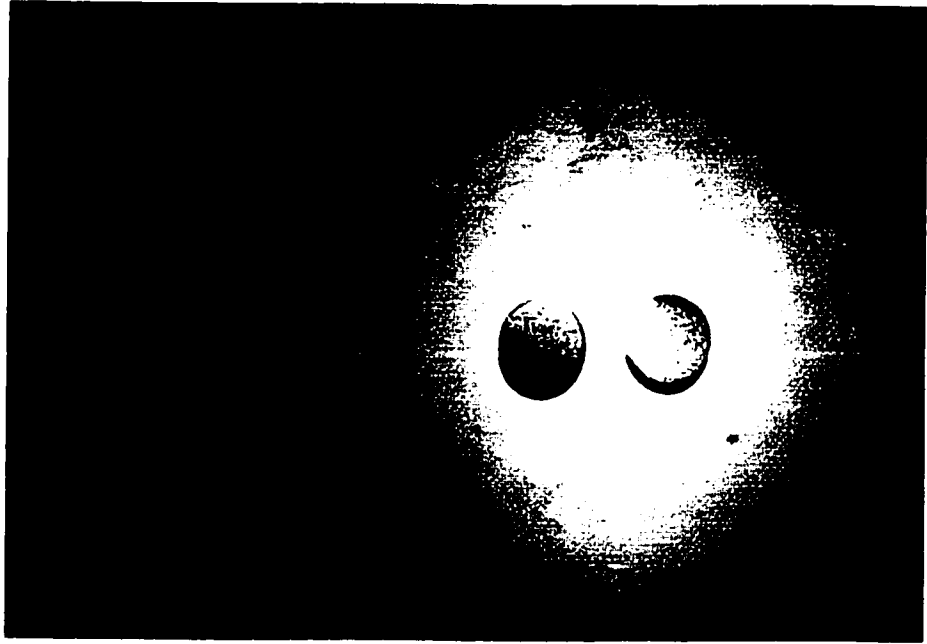
Figure 3-7 Polished samples
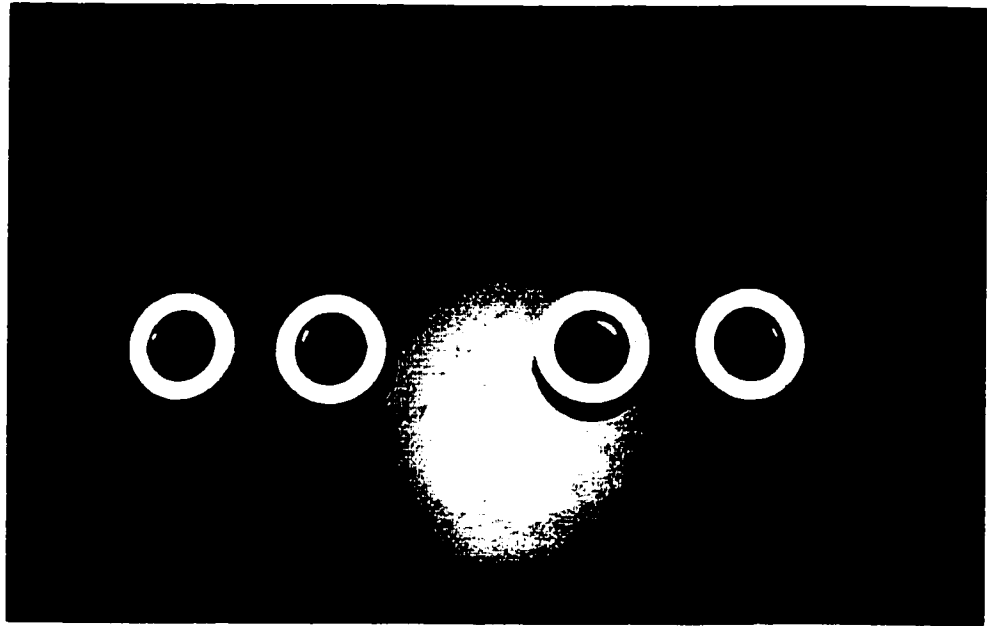
Figure 3-8 Samples numbers

1.2 Test Procedure

Maceral Content:

- Specimen was placed under the Universal ZEISS microscope equipped with white and fluorescent light; combined magnification is X640, Figure 3-9.

- First the specimen was emerged by water and inspected using Fluorescent light; Fluorescent excitation is 400 to 440 nanometers.

- The sample then was cleaned and immersion oil was placed on the polished surface

- The Specimen was then inspected using polarizer and analyzer to distinguish between the vitrinite and inertinite.

- Photomicrographs were taken each time, Figures 3-10, 3-11, 3-12, 3-13, 3-14 and 3-15 show the different coal components under the microscope.

- Using a moving stage and a swift automatic point counter model E, Vitrinite, Liptinite, Inertinite, and Minerals matter were measured based on 500 counts.

- The counting is repeated for all specimens

- Each specimen is recounted and checked for 5% difference in the maceral contents.
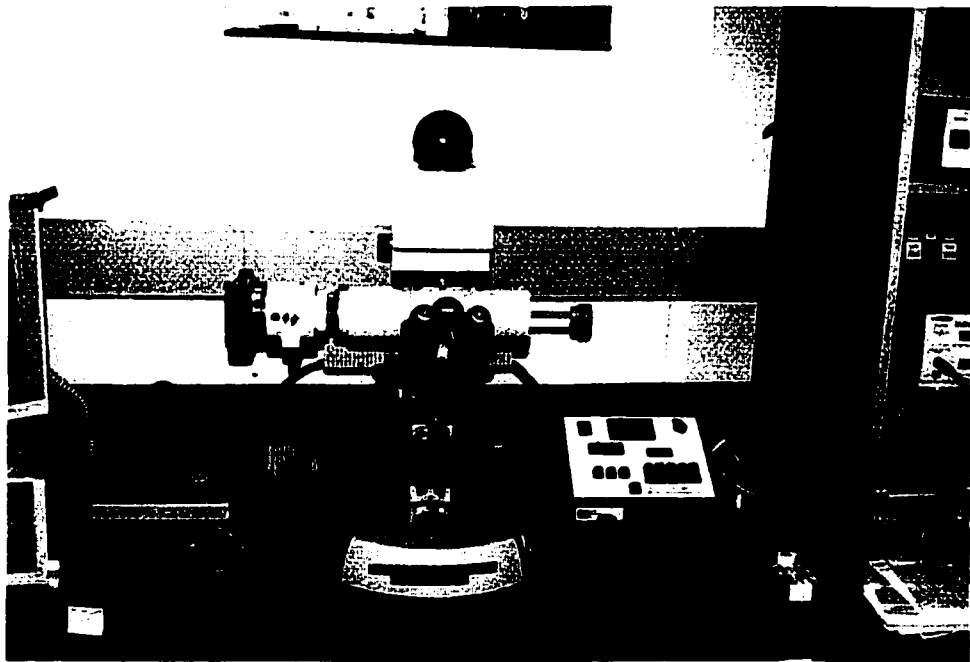
Figure 3-9 Microscope
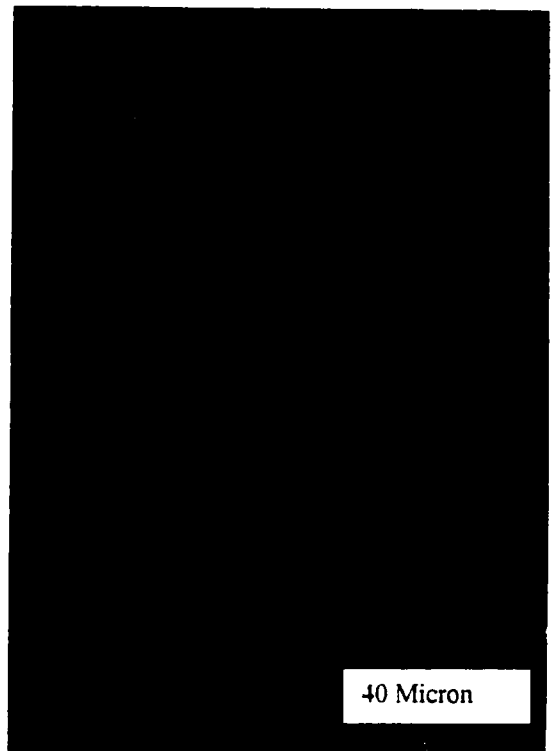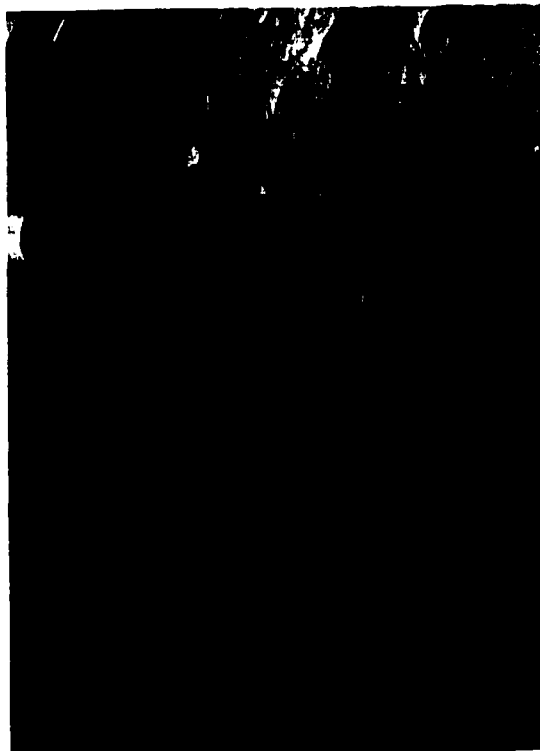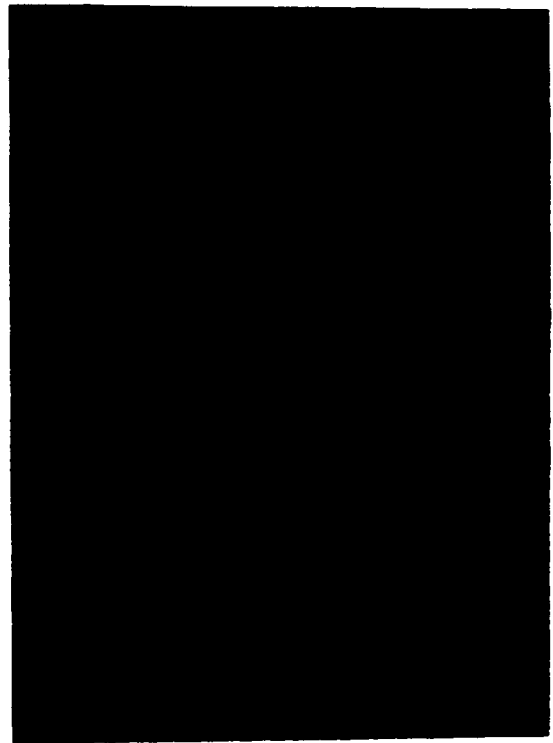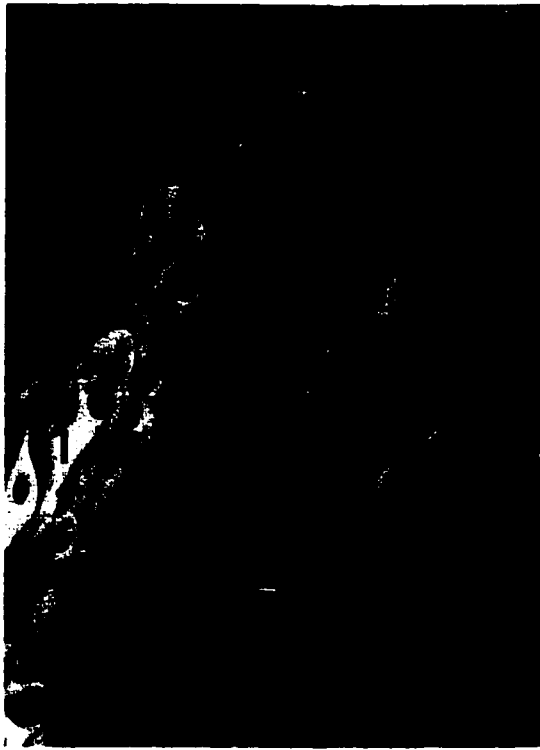
Figure 3-10 Cardinal River under white light (I=Inertinite, L=Liptinite, V=Vitrinite)
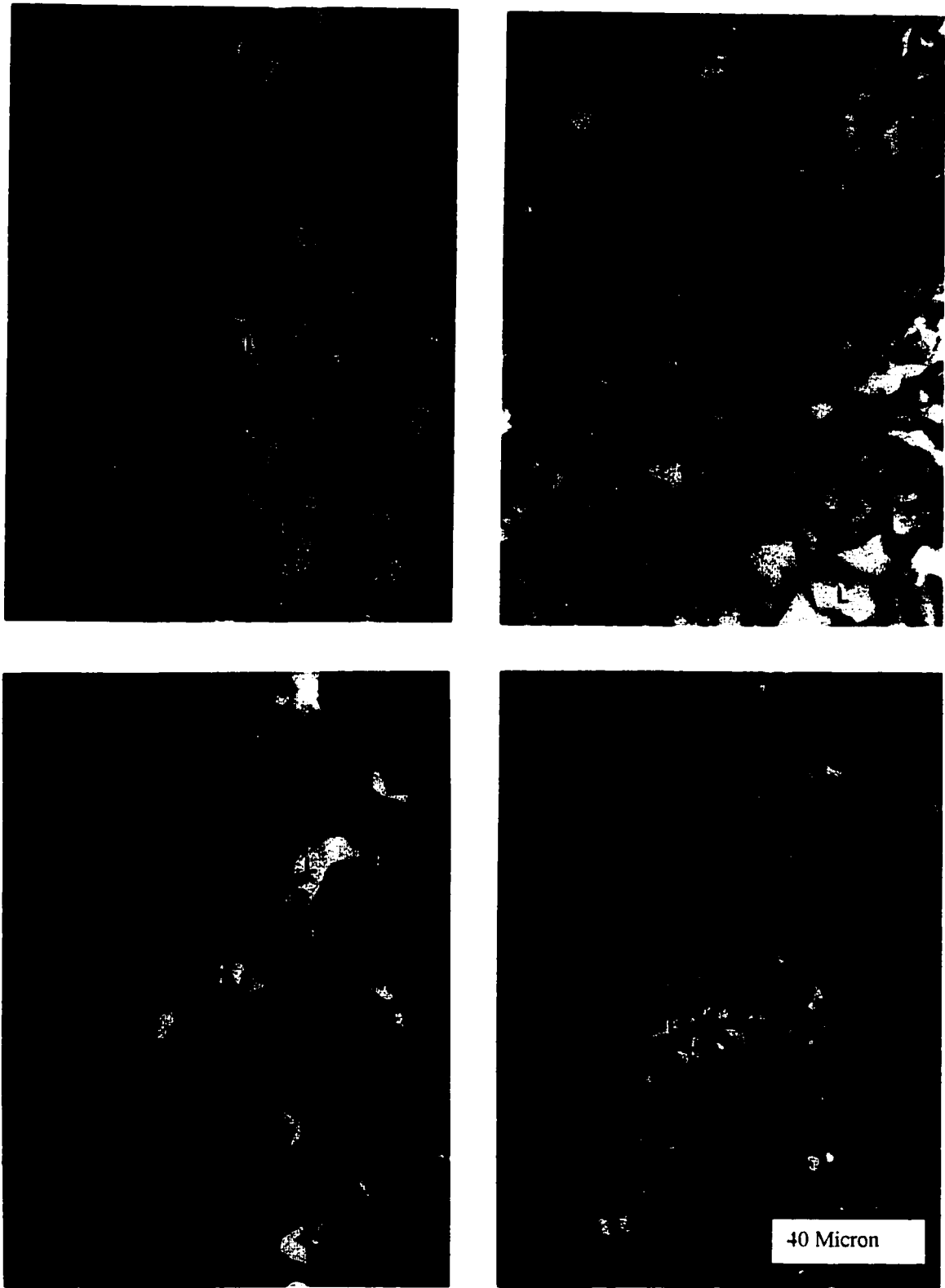
Figure 3-11 Cardinal River coal under fluorescent light (I=Inertinite, L=Liptinite, V=Vitrinite)
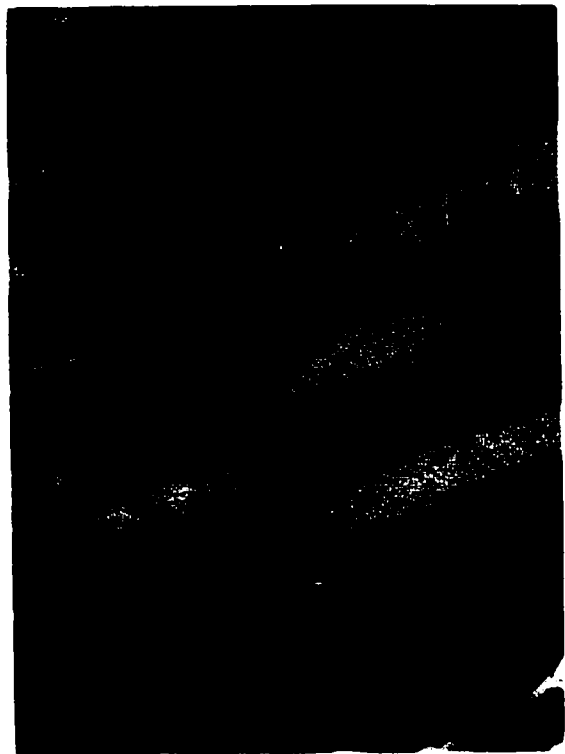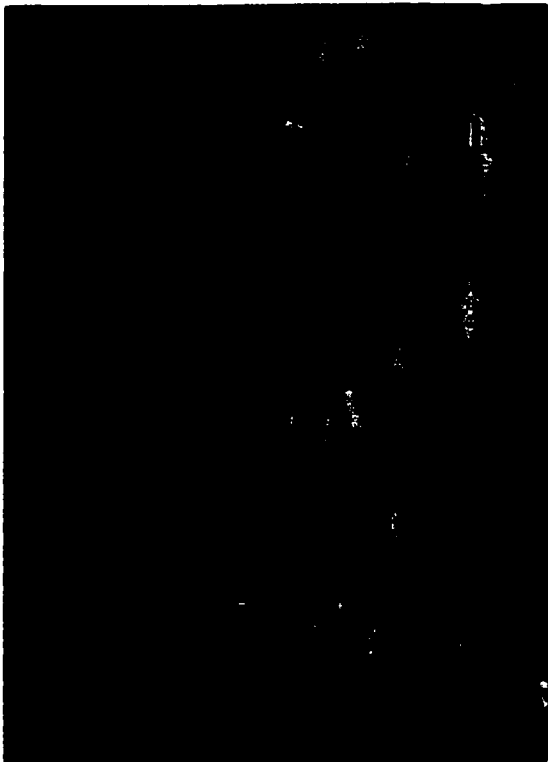
Figure 3-12 Cardinal River coal under fluorescent light (I=Inertinite, L=Liptinite, V=Vitrinite)
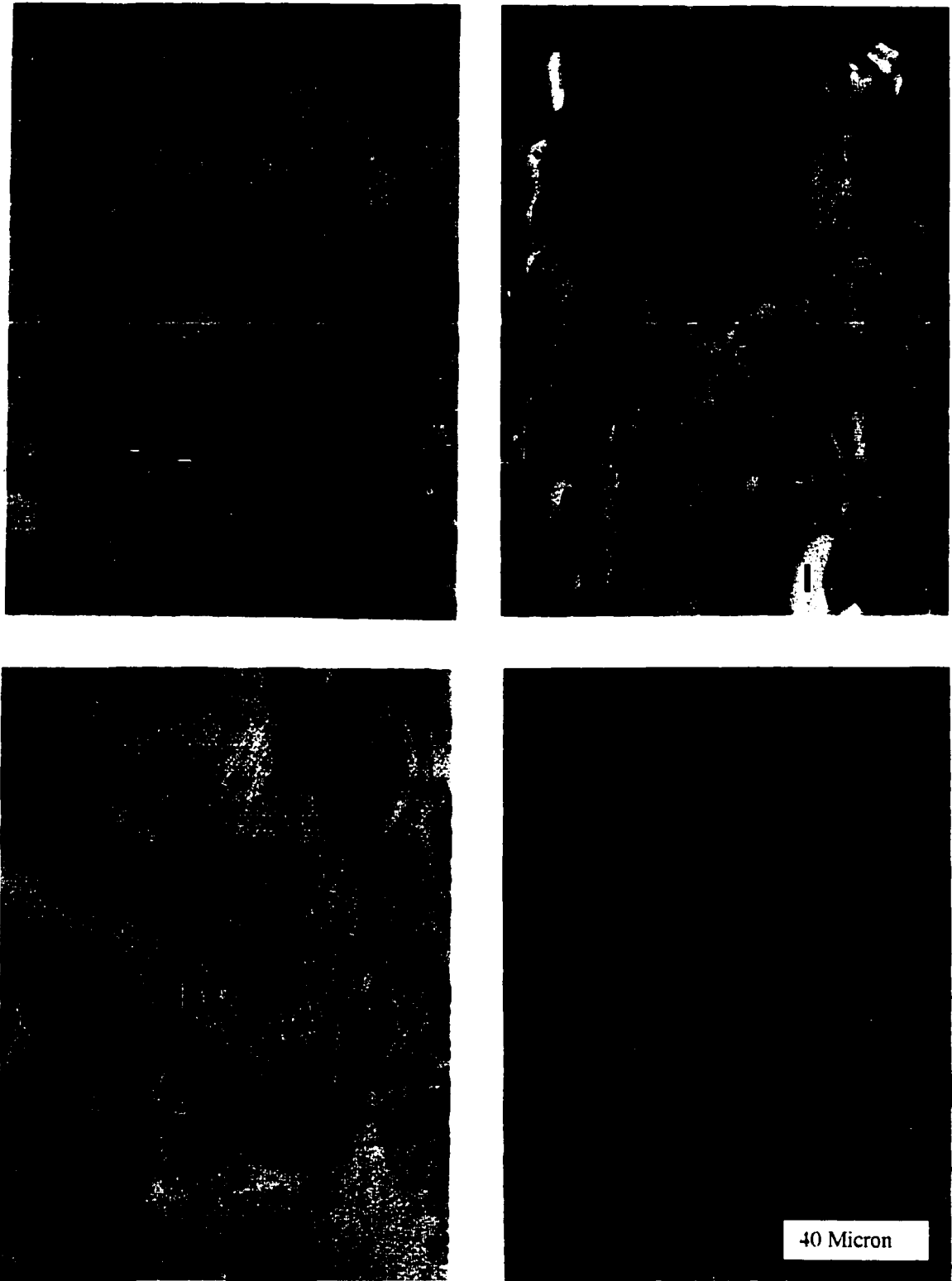
Figure 3-13 Luscar coal under white light (I=Inertinite, L=Liptinite, V=Vitrinite)
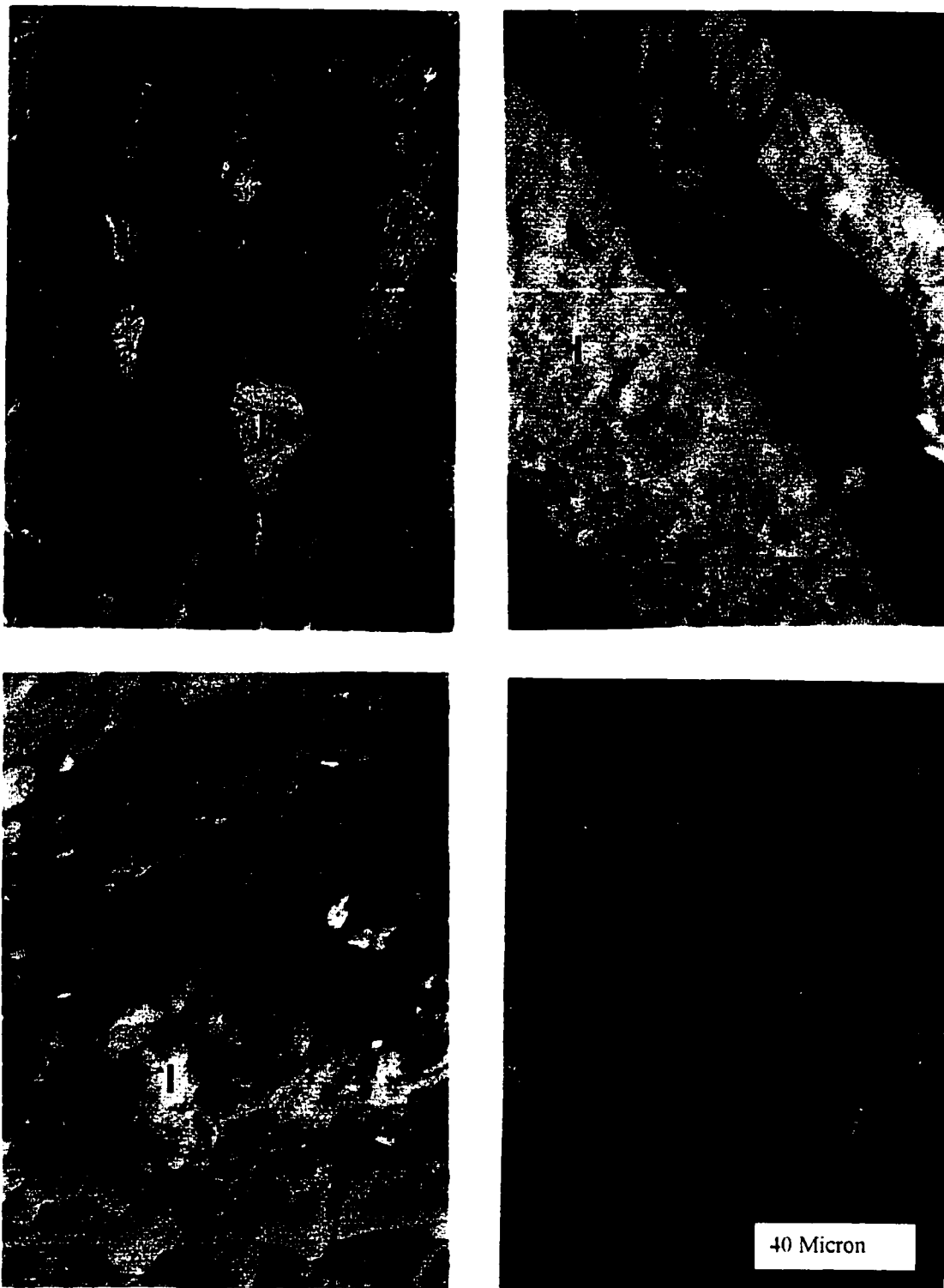
Figure 3-14 Luscar coal under white light (I=Inertinite, L=Liptinite, V=Vitrinite)
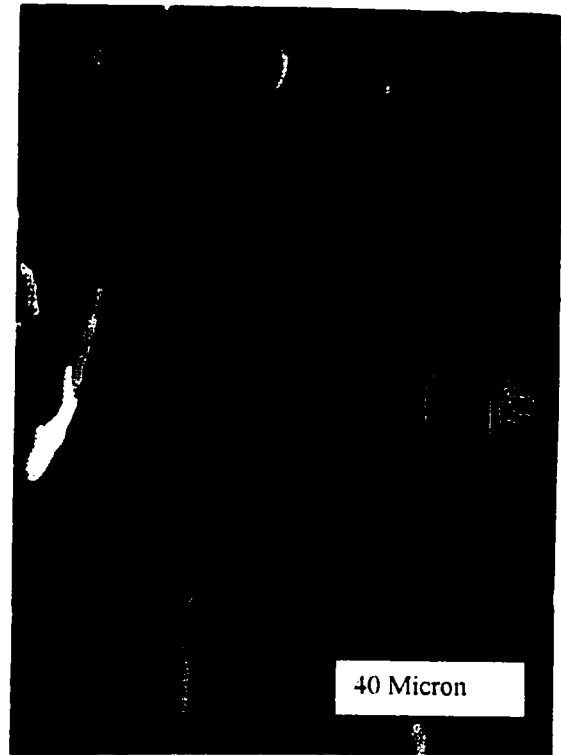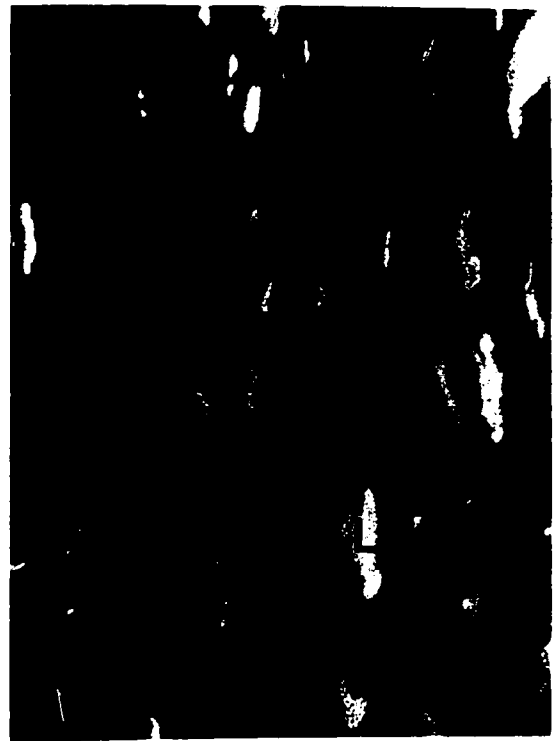
Figure 3-15 Luscar coal under fluorescent light (I=Inertinite, L=Liptinite, V=Vitrinite)

Reflectance Test

- Reflectance test was carried out using PHOTAN software and photo multiplier. The microscope is standardized using a standard series of 6 special calibrating glasses. Glasses, which have the same range of reflectance to the coal samples, were only used to standardize the microscope.

- Immersion oil with reflectance index ne = 1.518 at 23° C was placed on the samples.

- Light was reflected from the surface of clean vitrinite flakes and compared with the standard reflectance by PHOTAN then reported on the screen.

- Hundred measurements were taken for each sample.

- Random measurements were taken for samples 41-98 and 42-98, where maximum measurements are taken for samples 39-98 and 40-98 by rotating the stage 90 degrees and reporting the higher value.

Maximum refractive index, minimum refractive index, mean refractive index and standard deviation were obtained.

Test Results

Maceral Contents

Table 3-1 summarizes the final results for 4 specimens and the recount results. Maceral content revealed high percentage of Vitrinite in Cardinal River coal compare to Luscar coal. Luscar coal has a high percentage of Inertinite. This could also be seen through the microscopic pictures presented in this chapter.

Coal	Speciemen Number	Content	First Count Number of Points	First Count Percentage	Recount Number of Points	Recount Percentage
Cardinal River	39-98	VITRINITE	379/500	75.80%	378/500	75.60%
		LIPTONITE	33/500	6.60%	25/500	5%
		INERTINITE	80/500	16%	92/500	18.40%
		MINERALS	8/500	1.60%	5/500	1%
	40-98	VITRINITE	353/500	70.60%	368/500	73.60%
		LIPTONITE	33/500	6.60%	21/500	4%
		INERTINITE	106/500	21.20%	96/500	19.20%
		MINERALS	8/500	1.60%	14/500	2%
Luscar Mine	41-98	VITRINITE	218/500	43.60%	240/500	48%
		LIPTONITE	55/500	11%	50/500	10%
		INERTINITE	200/500	40%	184/500	36.80%
		MINERALS	27/500	5.40%	26/500	5.20%
	42-98	VITRINITE	230/500	46%	224/500	44.80%
		LIPTONITE	59/500	11.80%	60/500	12.00%
		INERTINITE	191/500	38%	187/500	37%
		MINERALS	20/500	4%	29/500	5.80%

Table 3-1 Maceral content results

Reflectance Test

Table 3-2 summarizes the final results of reflectance tests

Sample	39-98	40-98	41-98	42-98
Sample Descirbtion	Cardinal River	Cardinal River	Luscar	Luscar
Catalogue No	LaF9-850-322	LaF9-850-322	LaF12-836-423	LaF12-836-423
Class No	4	4	3	3
Refractive Indice Ne	1.8567	1.8567	1.84	1.84
Reflected Calculated	1.0085	1.0085	0.9207	0.9207
Determide	1.025	1.025	0.94	0.94
Measurements	100	100	100	100
Minimum Reflectance	0.937	0.94	0.53	0.54
Maximum Reflectance	1.095	1.099	0.641	0.656
Mean Reflectance	1.015	1.011	0.583	0.584
Standard Deviation	0.035	0.041	0.027	0.027
Coal Ranking	Medium Volitil	Meduim Volitile	High Volitile	High Volitile

Table 3-2 Reflectance test results

3.3.6 Proximate Analysis

Proximate analysis test was conducted according to ASTM D5142-90 to obtain the fixed carbon percentage, ash content, Volatile matter and moisture content. Coal passed mesh #35 (0.495 mm) was used in this test.

This test was done by heating the coal specimens to different temperatures, all measurements were taken under rigidly controlled conditions of temperature, time, atmosphere, specimen mass and equipment specifications. Firstly moisture content is determined by establishing the loss mass of the analysis specimen of coal or coke when heated to the desire temperature. Volatile matter is determined by measuring the loss mass of the moist or dried analysis specimen of coal or coke when heated to higher temperature. If appropriate, the measured mass loss establishes the volatile matter after correcting for moisture content. Ash is determined by measuring the mass of the residue remaining after burning the coal or coke.

Proximate tests results revealed that Luscar coal has higher ash and volatile matter percentage than Cardinal River coal. Also Cardinal River coal contains higher percentage of fixed carbon than Luscar coal. This means Cardinal River coal should be capable of adsorbing more gas than Luscar coal. However the difference on those proximate analysis percentages was not substantial, which means both coals could behave in similar way during the adsorption and the triaxial permeability tests.

3.3.7 Ultimate Analysis

Ultimate analysis was conducted according to ASTM D5373-93 to obtain Carbon, Hydrogen, Nitrogen and Sulfur. Coal passing the #35 mesh (0.495 mm) was used in this test.

Carbon, hydrogen, and nitrogen are determined concurrently in a single instrumental procedure. In the configuration used for this test, the gases are conducted through a series of thermal conductivity detectors and gas absorbers aligned so that, at the water vapor detector level, the gases pass through the sample side of the detector, water vapor absorber, and the reference side of the detector. At carbon dioxide detector level, the gases are then conducted through the sample side of the detector, a carbon dioxide absorber, and the reference side of the detector. Finally, the resultant gases, which contain only nitrogen and the carrier gas, pass through the sample side of the nitrogen detector and are vented. At this detector level, high-purity carrier gas is used as the reference gas. In these ways, the detectors determine the thermal conductivities solely of the specified components. In some systems, the procedure consists of simply weighing a test specimen, placing the test portion into the instrument, and initiating the (subsequently automatic) analytical process. In other systems the analytical process may be controlled manually to some degree. The analytical process consists of the complete conversion of the subject materials in an oxygen stream to carbon dioxide, water vapor, nitrogen oxides, and ash respectively; and subsequent, quantitative determination of the gaseous in an appropriate reference gas stream. The conversion of the subject materials to their corresponding gases occur largely during combustion of the sample at an elevated temperature in an atmosphere of purified oxygen.

Sulfur analysis is usually done by burning a weighted sample in a tube furnace at a minimum operation temperature of $1350°C$ in a stream of oxygen. During combustion, all sulfur contained in the sample is oxidized to gases oxides of sulfur (sulfur oxide, SO_2, and sulfur trioxide, SO_3) and the chlorine in the sample is released as Cl_2. These products are then absorbed into a solution of hydrogen peroxide (H_2O_2), where they dissolve forming dilute solutions of sulfuric (H_2SO_4) and hydrochloric (HCl) acids. The quantities of both acids produced are directly dependent upon the amounts of sulfur and chlorine present in the original coal

sample. Once the amounts of each acid present have been determined, the percentage of sulfur contained in the coal may be calculated.

Again Cardinal River Coal exhibited higher percentage of carbon 85%, compare to Luscar coal 68%. Hydrogen percentage was around 5% for both coals. Less nitrogen resulted from the analysis on Luscar coal 1%, where nitrogen in Cardinal River coal was 1.5%. Sulfur was low in both coals 0.20%. Higher carbon percentage results in more adsorbed gas in the sorption test.

3.4 COAL RANKING

Based on the results of maceral content test, reflectance tests, proximate and ultimate analysis, and according to ASTM classification Luscar coal was ranked as High Volatile Bituminous C and Cardinal River coal was ranked as Medium to High Volatile A. The final results are presented in table 3-3.

Both coals are located almost in the same field in ASTM classification charts, they could considered high volatile coal and they are expected to exhibit similar behavior during the adsorption test. However since Cardinal River samples have higher porosity, it is anticipated that the permeability results will vary between the two coal types.

Coal	Experiment	Test	Result	Repeatability	Unit	ASTM Method	Classification
Luscar	Specifc Gravity	Specifc Gravity	1.431	N/A	N/A	ASTM D854	High Volitile Bituminous C
	Moisture	Moisture	7.2		%wt	ASTM D5142	
	Bulk Density	Bulk Density	1.378		g/cc	ASTM D4404-84	
	Porosity	Porosity(Mercury)	2.08		%	ASTM D4404-84	
		Porosity(Nitrogen)	0.52		%	ASTM D3663-92	
		Surface Area	1.454		m^2/g	ASTM D3663-92	
	Proximate Analysis	Moisture	5.55	0.27	%wt	ASTM D5142	
		Ash	10.52	0.28	%wt	ASTM D5142	
		Volatile Matter	28.44	0.69	%wt	ASTM D5142	
		Fixed Carbon	55.49	N/A	%wt	ASTM D5142	
	Ultimate Analysis	CARBON	67.72	0.64	%wt	ASTM D5373	
		HYDROGEN	4.74	0.16	%wt	ASTM D5373	
		NITROGEN	1.05	0.11	%wt	ASTM D5373	
		SULFUR	0.27	0.04	%wt	ASTM 4239M	
	Maceral Content	VITRINITE	46.4	N/A	%	N/A	
		LIPTONITE	11		%		
		INERTINITE	37		%		
		MINERALS	5.6		%		
	Relectance	Relectance Index	0.584				
Cardinal River	Specifc Gravity	Specifc Gravity	1.52	N/A	N/A	ASTM D854	Medium to High Volitile A
	Moisture	Moisture	0.77		%wt	ASTM D5142	
	Bulk Density	Bulk Density	1.222		g/cc	ASTM D4404-84	
	Porosity	Porosity(Mercury)	3		%	ASTM D4404-84	
		Porosity(Nitrogen)	0.1		%	ASTM D3663-92	
		Surface Area	0.136		m^2/g	ASTM D3663-92	
	Proximate Analysis	Moisture	0.68	0.21	%wt	ASTM D5142	
		Ash	3.61	0.14	%wt	ASTM D5142	
		Volatile Matter	27.29	0.67	%wt	ASTM D5142	
		Fixed Carbon	68.42		%wt	ASTM D5142	
	Ultimate Analysis	CARBON	85.09	0.64	%wt	ASTM D5373	
		HYDROGEN	5.28	0.16	%wt	ASTM D5373	
		NITROGEN	1.49	0.11	%wt	ASTM D5373	
		SULFUR	0.21	0.04	%wt	ASTM 4239M	
	Maceral Content	VITRINITE	75	N/A	%	N/A	
		LIPTONITE	4.5		%		
		INERTINITE	19		%		
		MINERALS	1.5		%		
	Relectance	Relectance Index	1.013				

Table 3-3 Final results

CHAPTER 4 MULTIPHASE GEOMECHANIC TESTING FACILITY

4. 1 Introduction

To achieve one of the objectives of this research, it was necessary to design, construct, commission, and utilize a specialized geomechanical testing facility capable of testing under simulated CO_2 injection conditions. This required a new triaxial cell design to fit within an environmental chamber and be connected to positive displacement pumps capable of handling multiphase fluids. This chapter outlines the major design requirements for this facility and provides the details of the components with the system.

4.2 DESIGN REQUIREMENTS

A series of permeability tests were conducted to investigate the effect of different gases adsorption on Coal Valley (CV) and Cardinal River (CR) bituminous coal intrinsic permeability. The tests were performed under different gas pressures to evaluate the behavior over a range of injection pressures. The confining pressure was also varied between 6 MPa and 16 MPa to study the influence of different in situ confining stresses. Intact small coal samples 1" diameter were used to reach adsorption in short time. Using intact samples allowed the separation of the effect of micro porous and macro porous on the test's results. As will be shown, some samples had existing shear planes.

The lack of previous complete geomechanical properties data under triaxial conditions for coal has been predicated by the requirement for unusually high pressure triaxial test equipment and sealing against gases. The initial coalbed formations properties in Alberta were obtained from ARC reports; where in-situ pore pressure is around 11 MPa and the total overburden pressure is 27 MPa. The triaxial test equipment must therefore be capable of applying cell

pressures in excess of 27 MPa and pore pressures of 11 MPa which are well beyond the capacity of conventional testing apparatus. For this test program, a special triaxial testing facility was assembled capable of cell pressure up to 45 MPa. This allowed a minimum initial pore pressure of 20 MPa at the highest initial effective test pressure of 25 MPa.

In previous research studies, Harpalani et al., (1993) concluded that coal saturation with gases takes a long time (four months for 3 ½ " diameter sample). Other researchers (Ates et al., 1987) showed that adsorption time for small samples (54 mm diameter and 12.7 mm thickness) takes around 24 hours. Consequently, small samples were used in this research to allow rapid saturation of the coal. The specimens dimensions were around 1" diameter and 2" height. During the adsorption test, samples were left for longer times to assure full adsorption. This time period ranged between 24 to 36 hours and was stopped only when the syringe pump stopped adding more gas to the sample.

One of the design challenges is keeping the cell and the plumbing under a constant temperature, $52^{\circ}C$ which is the in-situ temperature and the temperature above the critical point where CO_2 stays in the gas form regardless of the pressure. This requirement constrained the cell design with certain dimensions (to fit within the environmental chamber). Even though the cell was designed to fit in the tight space inside the environmental chamber, it is still capable of testing samples with diameter up to 2".

Volume change measurements are important components of this work, during the adsorption or compressibility tests, however these measurements are expected to be small because of using small samples. Also CO_2 is known to diffuse through normal latex membrane. To accommodate the previous requirements an the cell was designed as double wall cell. The internal cell is to be filled with mercury and connected to differential pressure transducer. The

transducer will deduct any changes in the mercury level when it happens during adsorption or compressibility tests. The mercury will act as barrier for CO_2 diffusion through the membrane. The membrane used is heat shrink Teflon which is proved to prevent CO_2 diffusion.

Finally the safety during the operation of these equipment under the test conditions was an important issue. All joints and flow lines were tested for leakage using GT gas detector capable of measuring very small percentage of CO_2 or CH_4 in the air. High performance ventilation system was used at all times to release any leaked gas to outside the building as well as small amounts of gas kept in the lab during the testing.

4 .3 Description

The high pressure triaxial testing facility includes the following major components:

1) High pressure triaxial cell
2) High load capacity testing machine
3) Confining pressure system
4) High pore pressures system
5) Plumbing
6) Environmental chamber
7) Measurement System.
8) Data acquisition system

The following sections provide pertinent design details for each of these major components.

4.3.1 Triaxial Cell Design

A high pressure triaxial cell was specially designed for this test program. Figures 4-1 and 4-2 illustrates the triaxial cell and its components. The cell is capable of withstanding cell pressures up to 45 MPa and applying axial ram loads up to 150 KN. Dimensionally, the cell was designed to fit within an environmental chamber, described in # 4.3.6.

In order to measure volume change, an internal cell was designed to be filled with mercury and connected to a differential pressure transducer. The second port of the transducer is to be connected to the cell pressure. Any change in the sample volume during the test will be reflected by a change in the mercury level and measured directly by the differential pressure transducer.

The cylindrical cell was designed to be 16.5cm diameter cylinder and 32.5 cm tall. The top cap and base are threaded to the cell body with 10 threads per inch and 3.8 cm total length of engagement.

Figures 4-3, 4-4, 4-5, 4-6, 4-7 and 4-8 provide the final Autocad design specifications for each component of the cell, more detailed design is provided in Appendix B.

4.3.2 High Load Capacity Machine

A high load capacity testing machine was used during the test. The high load capacity machine is an Instron Model 4202 which has the capacity of 150 kN axial load and can achieve ram speed over the full 1000 to 1 range of the instrument. The load cell in the Instron provides a 50 to 1 range and includes a built-in preamplifier for immunity to interference. Series 4200 uses a new series

72

of self identifying strain gage transducers.

4.3.3 Confining Pressure System

The confining cell pressures were applied by pumping water using a Jeffri pump. The capacity of the pump is 40 MPa. The pump could maintain constant pressure by activating a step motor at slight changes in the water pressure.

4.3.4 High pore pressures system

Pore pressures in the range (0 to 11 MPa) were provided by an ISCO syringe pump which also provided constant flow rates for the permeability tests. Gas was pumped by the syringe pump until the desired pressure was maintained. The permeability measurements were controlled by using a Jeffri pump to maintain the back pressure.

The back pressure Jeffri pump had the same specifications as the cell pressure pump and was used to maintain constant back pressure during permeability tests.

4.3.5 Plumbing

All the systems pipes were stainless steel pipes capable of tolerating high pressures. The transducer plumbing should allow transducer removal, if necessary, without shutting down the test in progress. A differential pressure transducer used for measuring pressure requires extensive valving not only to place it in operation but also to remove it without over pressure damage. In this case, the valve arrangement shown in Figure 4-9 was used. To safely pressurize the transducer, the drain valve was closed and the bypass valve opened. Then, both shutoff valves were opened to apply line pressure to both sides of the transducer. Finally the bypass valve was closed. To depressurize the

transducer, the bypass valve was opened and the shutoff valves closed, and the drain valve opened.

4.3.6 Environmental chamber

For this testing program, maintaining a constant temperature was extremely important. Constant temperature was required for two components of the system: (1) syringe pumps and piping; and (2) the triaxial cell. The syringe pumps and pipes were wrapped with heating tape and covered with insulation. Thermocouples were used to control the heating tapes to insure a constant temperature.

The triaxial cell was also placed in a special environmental chamber. The environmental chamber used in this research was an Instron 3119-005 temperature chamber which provided an accurately controlled air temperature environment. It is a small chamber with inside dimensions of 48.5cm x 24 cm x 23 cm and it has a temperature range of −70 to 250°C (-94 to 482°F). Figure 4-10 provides a picture of the environmental chamber.

4.3.7 Measurement System

The confining and pore pressures were measured by pressure transducers attached to the ports of the pumps. The differential pressure during permeability tests was measured by a differential pressure transducer placed between the upstream and the downstream flow lines. The volume of pumped (adsorbed) gas was measured by an LVDT mounted on the upstream syringe pump and calibrated against volume change inside the pump. The volume change of the coal sample, as was explained in the cell design, was measured by means of a differential pressure transducer that detects the change of mercury level in the internal cell.

The excitation voltages for the LVDT, pressure transducers and load cell were supplied by a constant voltage power supply.

4.3.8 Data acquisition system

A high performance data acquisition system was used to collect and record data during the tests. This data acquisition system consisted of a personal computer, HP 3497a signal acquisition hardware, and Labview software.

4.4 CALIBRATION OF ELECTRONIC MONITORING DEVICES

The electronic monitoring devices were calibrated prior to undertaking the test program. Calibration checks were repeated periodically during the testing program and second full suite of calibration was carried out half way through the testing program.

The pressure transducers were calibrated using a dead weight table hydraulic pressure calibrator. The differential pressure transducer, which was used to measure pressure difference between upstream and downstream during the permeability test, was calibrated using a dead weight table hydraulic pressure calibrator. The LVDT mounted on the syringe pump was calibrated against the change in volume of the syringe pump cylinder. The differential pressure transducer, which was used to measure volume change was calibrated using a dead weight table hydraulic pressure calibrator. Table 4-1 summarizes the calibration results and the detailed calibration plots are presented in Appendix C.

4.5 SUMMARY

A high pressure triaxial double wall cell was developed to handle high pressures. The apparatus was described and its design was presented.

The triaxial permeability setup used, was discussed and explained. Issues of calibration of equipment and plumbing were explained.

The complete flow process sheet for the multiphase testing facility is shown in Figure 4-11. Figure 4-12 provides an overall view of the testing equipment.

ELECTRONIC MEASURMENT DEVICE	Function	CALIBRATION	Calibration Date
Pressure Transducer	Cell Presssure	408.13 psi/V	April 17th 1999
Pressure Transducer	Upstream	9.979 psi/mv	Jun 10th 1999
Pressure Transducer	Downstream	388.36 psi/V	April 17th 1999
Differential Pressure Transducer	Permeability	2.0497 psi/V	April 17th 1999
		10.948 psi/V	May 3 1999
		20.032 psi/V	Jun 10th 1999
Linear Voltage Displacement Transducer	Volume of Gas	25.194 cc/V	Jun 10th 1999

Table 4-1 Calibration table

77
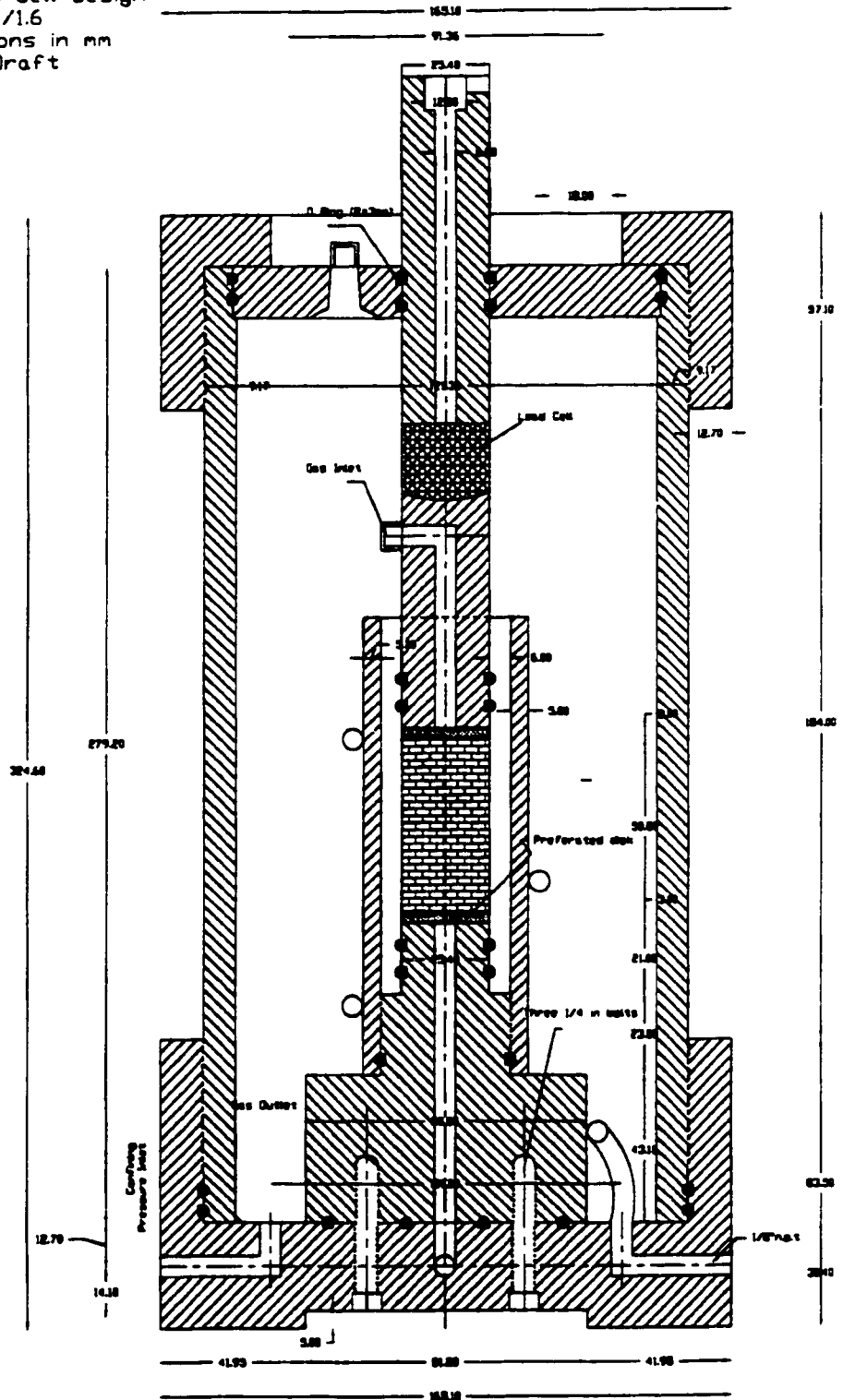
Figure 4-1 Section in the triaxial cell
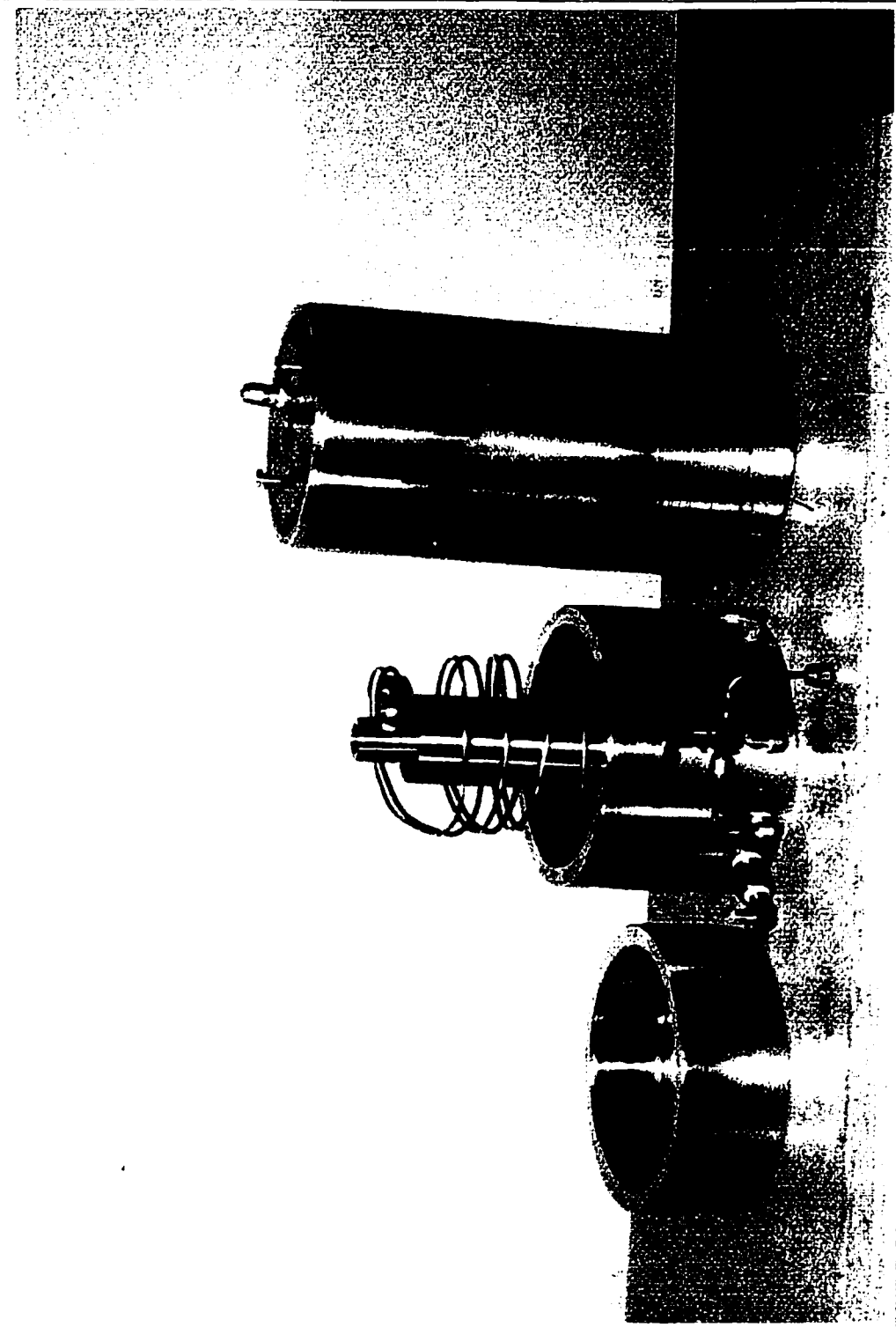
Figure 4-2 Triaxial cell component

Section A-A

Figure 4-3 Cell's base design

80
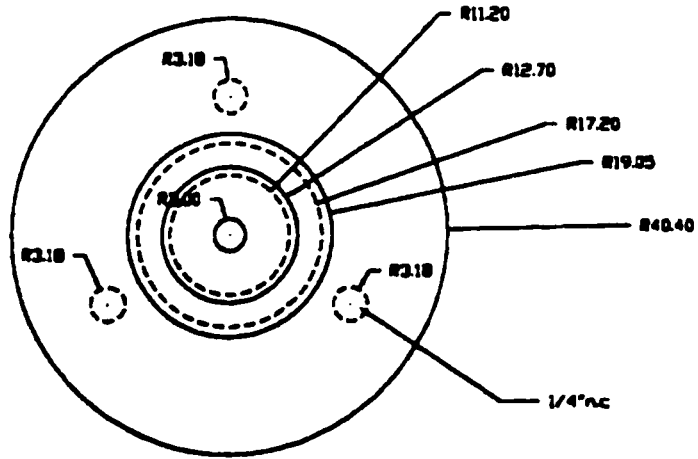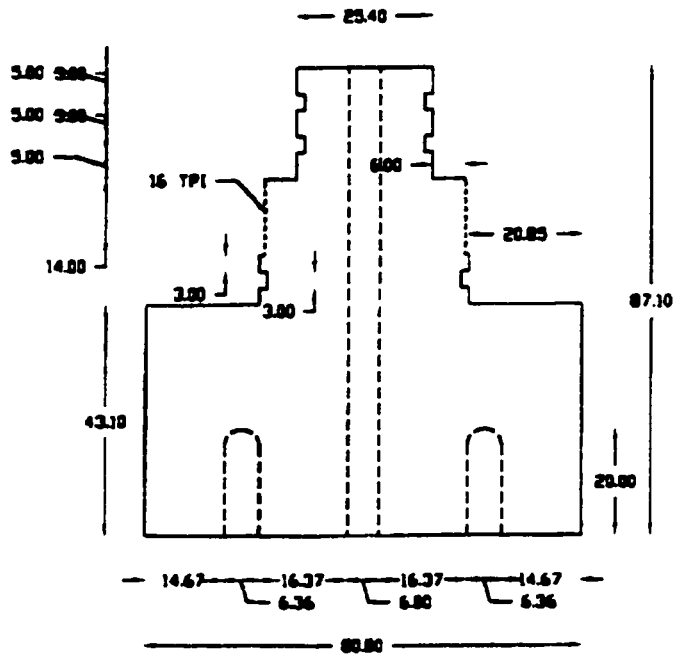
Stanless 3/6

Figure 4-4 Internal cell's base design
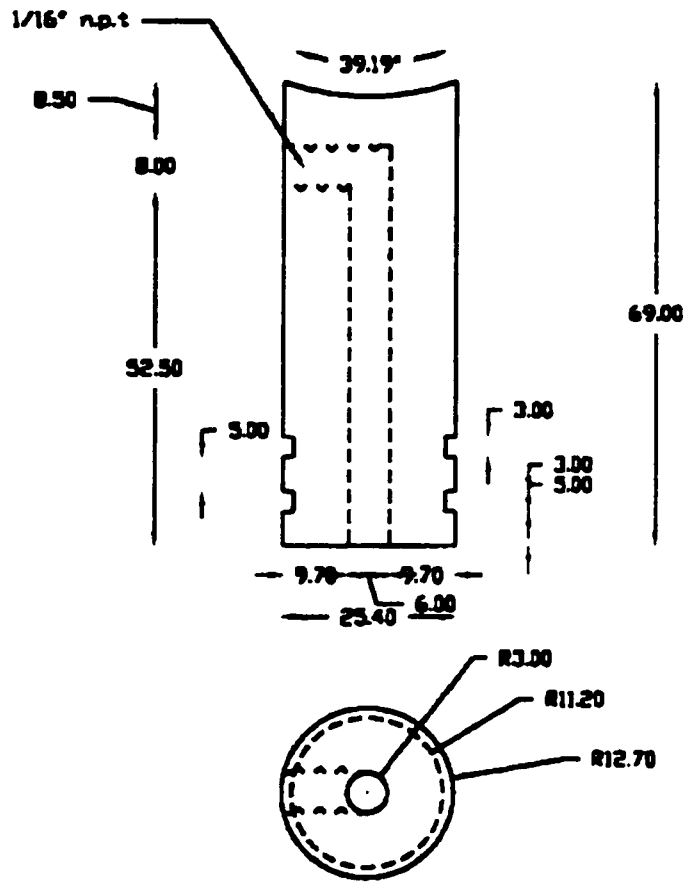
Figure 4-5 Top cap design
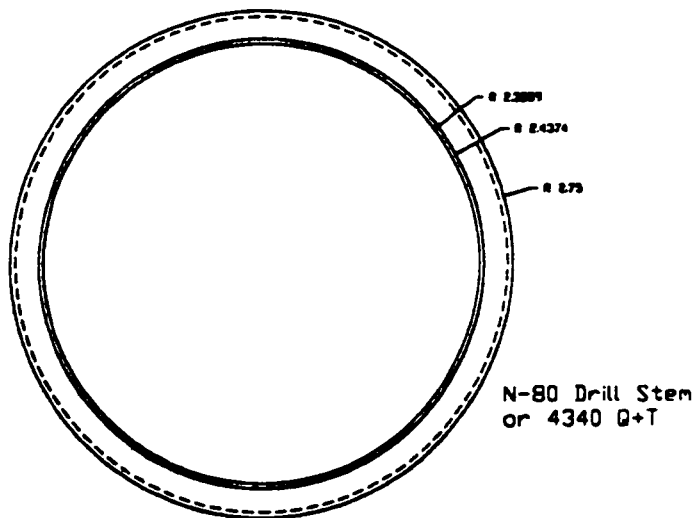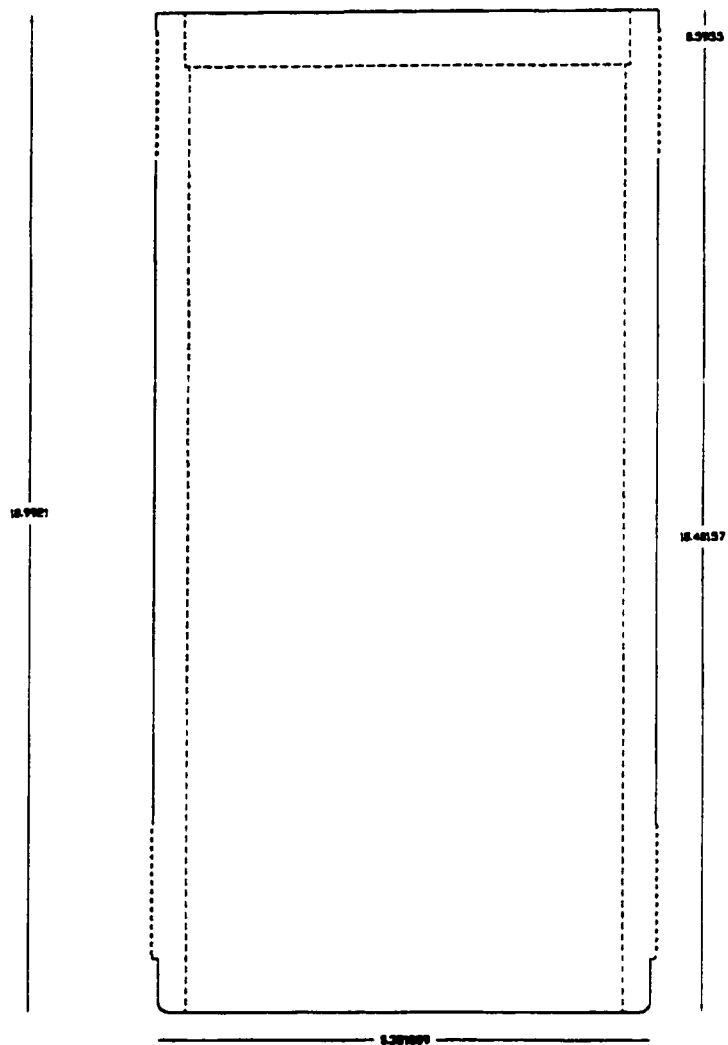
Figure 4-6 Cell's body design

N-80 Drill Stem
or 4340 Q+T
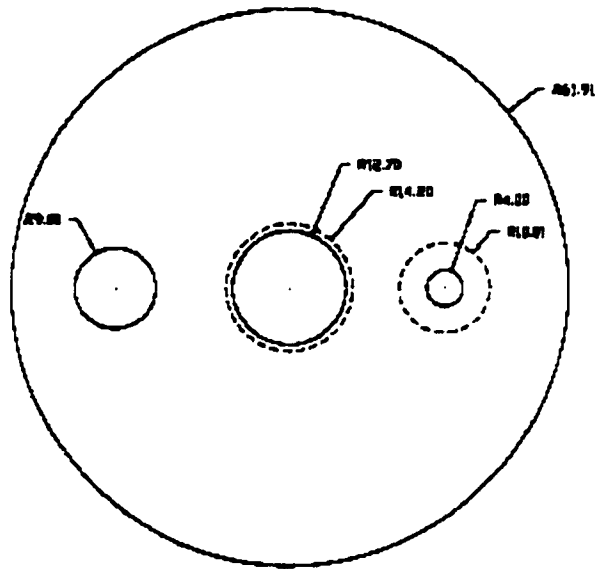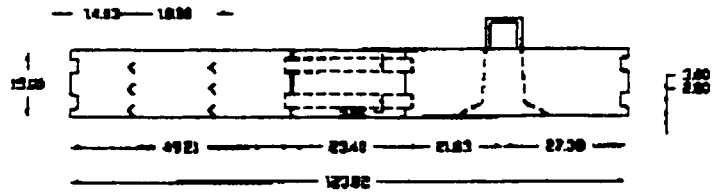
Figure 4-7 Cell's top cap design (a)
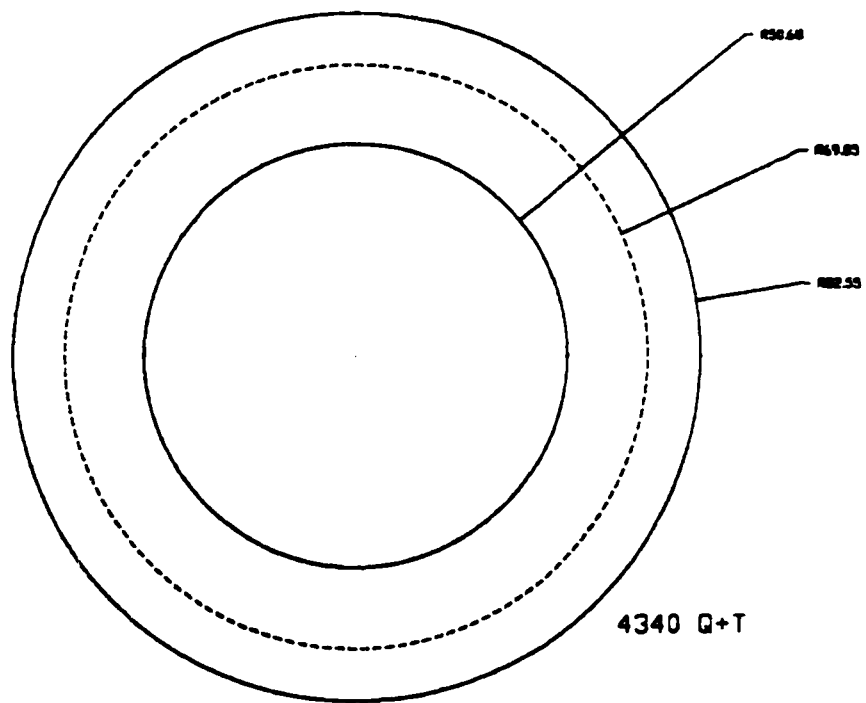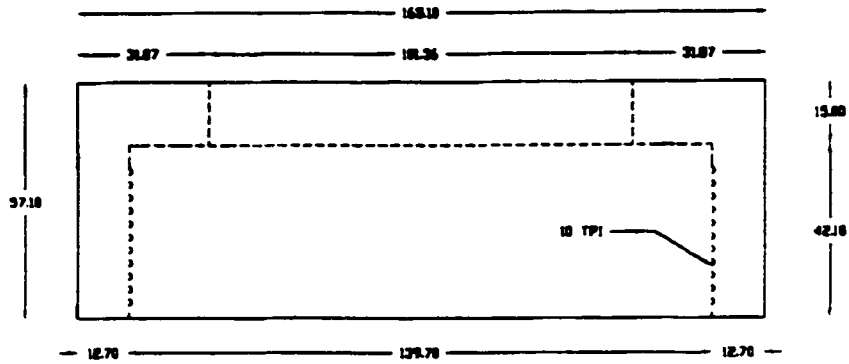
Figure 4-8 Cell's top cap design (b)
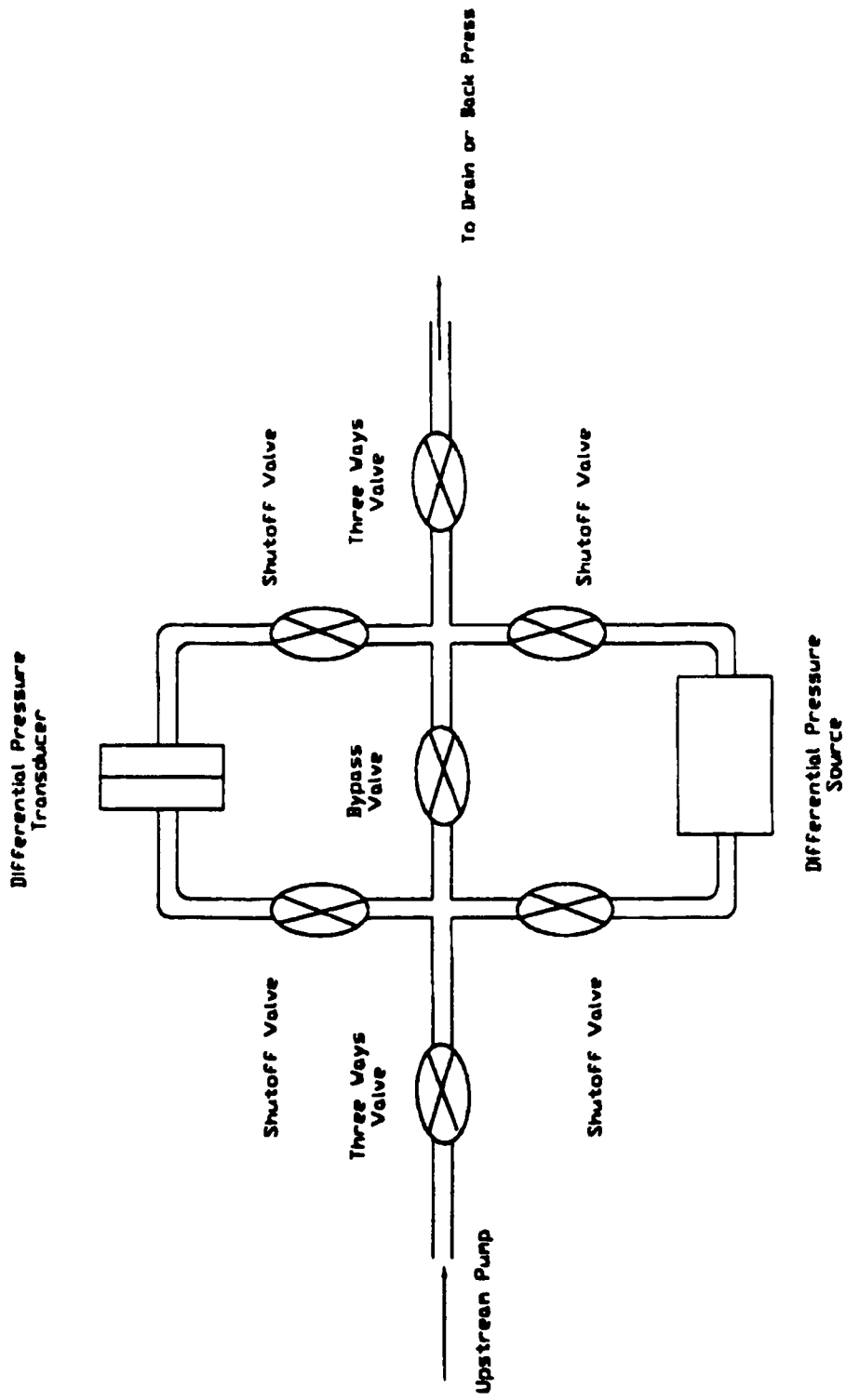
Figure 4-9 Typical valve arrangement for differential pressure transducers

Figure 4-10 Environmental Chamber
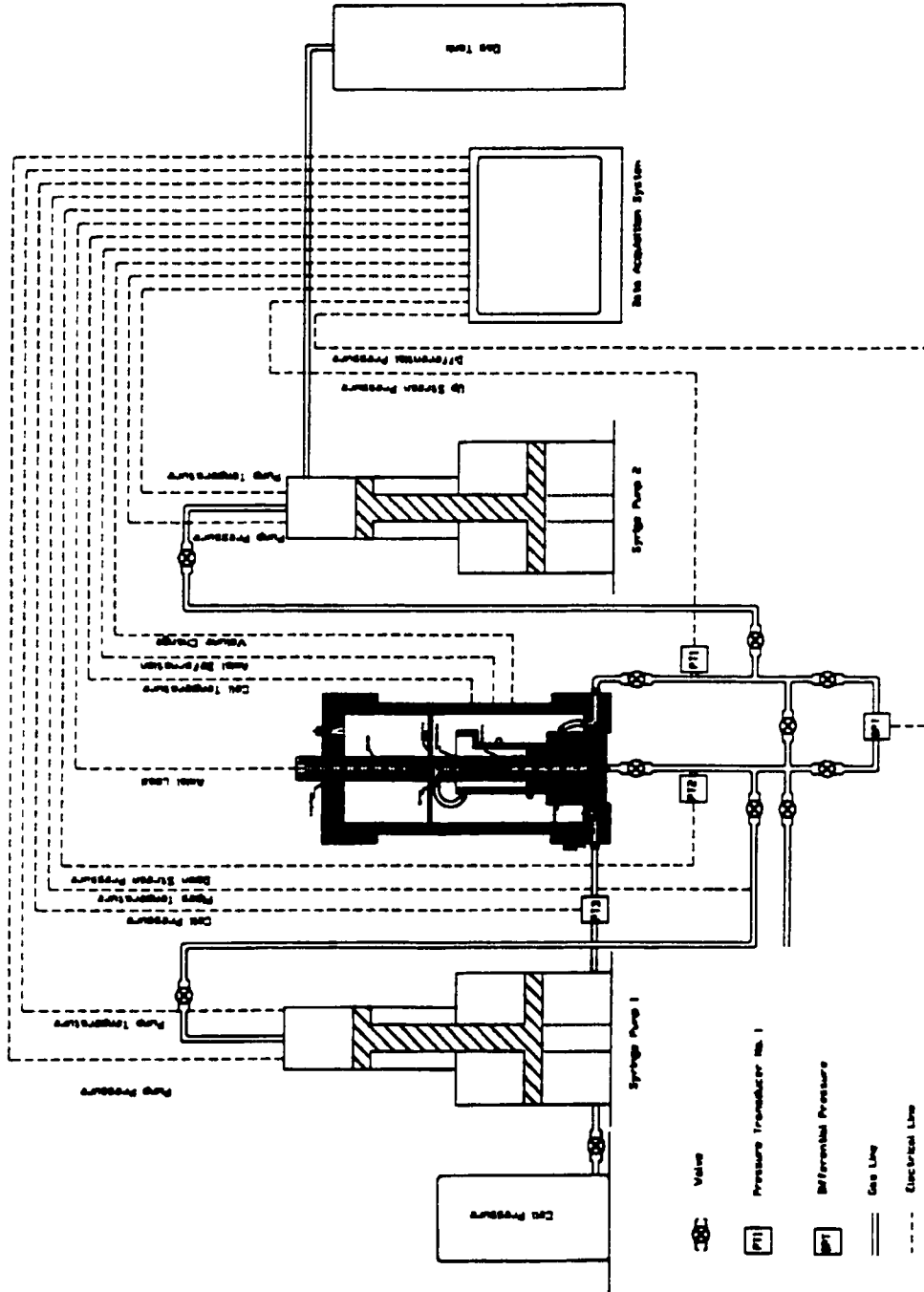
Figure 4-11 Testing Set up
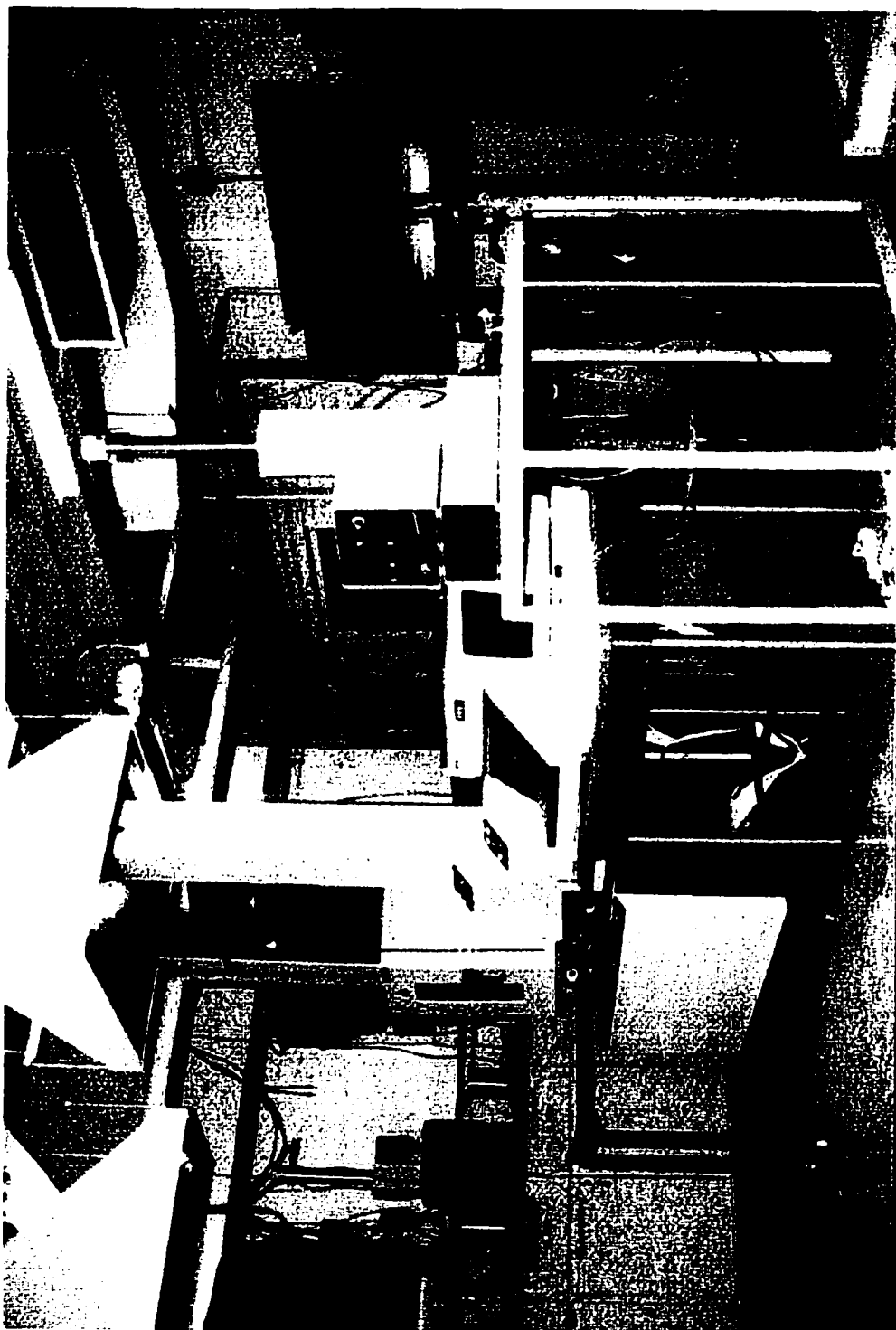
Figure 4-12 Testing Facilities

CHAPTER 5 INTRINSIC PERMEABILITY TESTING

5.1 INTRODUCTION

This chapter describes the coal sampling program as well as the testing procedures for the gas absolute permeability testing. While not used in obtaining specimens for this testing program, a method to freeze a coal specimen while preserving its structure is described. The steps followed for each component of the test are described. Intrinsic permeability experimental work with gas as the permeable requires a clear understanding of the gas density, viscosity and volume change relationships. The treatment of these variables for the adsorption and intrinsic permeability testing is described.

5.2 FIELD SAMPLING

5.2.1 Location

The samples used for this research were obtained from coal outcrops in the Coal Valley and Cardinal River mines. These coal mines are located approximately 100 km south of Hinton, Albreta; their location is identified in Figure 3-1.

The Coal Valley mine is operated by Luscar which mines high volatile bituminous coal for export to Japan to be used in coal-fired power plants. The Cardinal River medium volatile bituminous coal is used at the Genesse power plant.

5.2.2 Sampling

sampling is explained in details in chapter 3.

5.3 CORING

Coring was done by using a 1" diameter diamond core barrel and a GM3512 coring machine from ABARBOGA MASKINER shown in Figure 5-1. The bit rotation was set on high speed (3000 rpm) and the penetration on low rate (0.010 inch per revolution) in order to minimize disturbance. Air was used to cool the bit during coring Figure 5-2 illustrates the coring setup. The diameter of the core was almost 1", and the coring avoided any cleats in order to get intact coal samples. However, some samples exhibited some shear planes which altered some of the permeability results. After many trials intact coal samples were obtained. The length of the samples was between 1.5" to 2.5". Samples were then double wrapped in plastic to minimize oxidization and stored in a moisture room.

5.4 FREEZING AND CORING

Due to the high number of initial failures in attempting to recover high quality core specimens from the intact blocks, an attempt was made to initially freeze a water saturated coal specimen prior to coring. Substantial experience exist with other materials in the use of one dimensional freezing techniques to preserve the intact structure of soils.

The coal blocks were cut to smaller pieces (0.027 m^3). Those pieces were then placed in a container and water was added slowly and in stages. This allowed the samples to be saturated without causing negative suction inside them. The saturation process took one week where water level was raised every day. Specimens then were exposed to low temperature from one face, by isolating the rest of the specimen. Water inside the specimen started to freeze and the extra volume of frozen water moved to the warm side, the freezing front advanced slowly till the whole specimen was frozen. The specimen was then cored in a

cold room and cores were wrapped and stored in the cold room. However, these samples were not used in the adsorption and permeability because good quality samples were obtained by regular coring. Also freezing and thawing might has an affect on test results.

5.5 TEST SETUP PROCEDURE

The following sections describe the specimen preparation and triaxial cell setup procedures. These procedures are followed for all types of tests; adsorption, permeability, compressibility or compression.

5.5.1 Specimen Preparation

The edges were trimmed using grinding stone machine and sand-paper to finish the ends at right angle with the cylindrical axis. Weight and dimensions were then taken accurately by using electronic scale capable of measuring fractions of gram and a caliber capable of measuring fractions of mm. Table 5-1 summarizes the samples weight, dimensions and any relevant comments.

The specimen was placed on a stainless steel porous disc in the bottom base an another stainless steel porous disk was placed on the top. A 0.5 mm thick heat shrink Teflon tube was used to confine the specimen. The top cap was placed on the stainless steel disc, the heat shrink tube was then heated to the desire temperature to form a non permeable sleeve around the specimen and the caps. Teflon was used because it significantly retards gas diffusion through it. The specimen was then removed with the sleeve on it, silicon was placed in the internal surface of the sleeve and placed again on the caps. Another heat shrink sleeve was placed around the sample and heated. Finally O-rings and clamps were placed around the top and bottom caps. The assembly of the sample inside the cell is illustrated in Figure 5-3.

5.5.2 Triaxial Cell Setup

The cell was closed, filled with water and placed inside the environmental chamber. Gas outlet and inlet lines were connected as well as all instrumentation lines. The loading ram was lowered and a small seating load (10 psi) was applied on the specimen. The cell pressure outlet was connected to the pump and air was bled from the top valve. The cell pressure pump was then pressurized to the desired effective stress with no pore pressure. Both the upstream syringe pump and downstream pump as well as all gas pipes were heated to 52 °C by using band heaters. Thermocouples were used to control the temperatures and all lines were insulated with fiberglass insulation. The cell was left 24 hours to assure a stable temperature of 52 °C inside the cell. A small flow rate of gas was used first to flush the system and the sample of any air. The flow was stopped when the GT gas detector started giving high readings of gas concentration in the outlet.

The upstream syringe pump and the flow lines were pressurized to the required gas pressure. During this stage the required gas to stabilize the pressure drop by temperature lost was measured and used later in the calculation to correct the adsorption results. The gas was then allowed to flow to the sample after setting the syringe pump on constant pressure. The cell pressure was then set in total stress equal to the gas pressure and the required effective stress. After adsorption and permeability tests were done in this stage, gas pressure was raised to the second stage pressure this was followed by increasing the total cell pressure by the same amount of gas pressure to keep the effective stress constant. This process was repeated until the last point on the adsorption isotherm was reached at that effective stress level. At this point the total stress was increased to the second required effective stress level and only permeability tests were done. After the permeability tests at the new effective stress level on the last point of the adsorption isotherm was done, total stress was dropped by the amount of gas pressure is needed to reach the required gas pressure on the

isotherm. This was repeated until the first point on the adsorption isotherm was reached.

5.6 ADSORPTION TEST

The accepted procedure for conducting adsorption tests is detailed by Harpalani (1986). Every attempt was made to follow this procedure but some modifications were necessary in order to facilitate testing with whole core, not crushed core under the permeability testing conditions.

The first step in the adsorption test is the pressurizing of the syringe pump and the flow lines to the desired gas pressure. Note that the specimen is isolated from this increase in gas pressure by a valve immediately upstream of the specimen. During this period of time the volume of gas needed to stabilize the pressure drop by heat lost was measured and later used to correct the adsorption results. Once the desired gas pressure is reached and stabilized, the syringe pump is switched to constant pressure mode. At this point, the valve upstream of the specimen is opened to permit the gas to flow into the specimen. The downstream valve remains closed for the adsorption test.

The drop in pressure associated with opening the valve immediately begins to be compensated for by the syringe pump, which is attempting to return to its constant pressure setting. Several trial experiments showed that approximately three minutes was required for the pump to return to the constant pressure set point. At this point, if no adsorption was to occur, the syringe pump would remain static. But as adsorption begins to occur within the coal matrix, the pressure will slowly decline. When a pressure drop is sensed by the syringe pump, it will pump additional gas into the specimen in order to maintain a constant pressure. Equilibrium is achieved when the syringe pump no longer has to pump additional gas into the specimen. The volume of pumped gas is considered the adsorbed

volume of gas because the temperature was constant in all the system components. As well, and as important the effective stress is held constant during the test.

The adsorbed volume was calculated by subtracting the initial change in volume in the syringe pump from the final volume change. This number was then corrected to standard pressure and temperature using the Universal Gas Law:

$$\frac{P_1 * V_1}{Z_1 * T_1} = \frac{P_{st} * V_{st}}{T_{st}}$$

[5-1]

where,

$T_{st} = 0° \, C = 273 °K$;

$P_{st} = 760$ mm of mercury $= 101.36$ kPa $= 14.7$ psi; and

Z is the compressibility factore.

The standard presentation of the adsorption isotherm plots absolute volume of adsorbed gas per gram of coal versus gas pressure. Absolute volume refers to the volume of adsorbed gas at standard temperature and pressure. The adsorption isotherms obtained in this research and a discussion of these results is provided in Chapter 6.

5.7 ABSOLUTE PERMEABILITY TESTS.

Permeability tests were conducted at the conclusion of each adsorption test. In order to minimize the pressure imbalance between the downstream pumping system, which was isolated during the adsorption test, and the upstream pressurized system, valves are closed which isolate the specimen. A bypass

valve is opened which permits the upstream and downstream pumping system to equilibrate at the desired gas pressure. The bypass valve is then closed and the valves to the specimen are opened allowing flow through the specimen.

The fundamental premise for the measurement of permeability was to set a fixed flow rate using the upstream syringe pump and measure the pressure loss across the coal specimen. Flow rates that were used in the permeability tests were 1.5, 4, 15 and 40 ml/hour. Flow rates were modified in order to minimize the differential pressure across the coal specimen. This was necessary to ensure additional CO_2 sequestration or adsorption did not occur during the permeability tests. Flow was continued until steady state was achieved, as evidenced by a constant pressure differential across the specimen. This permeability test was repeated for various gas pressures and effective stress levels.

To compete the hydraulic conductivity of the specimen, the pressure differential at steady state flow was used to calculate the hydraulic gradient, i. The gradient versus flow velocity, as set by the syringe pump, provides permeability; as originally proposed by Darcy (1856). For gas flow, it is the intrinsic permeability which is important. The intrinsic permeability is a material property, and it is related to the material characteristic such as specific gravity and porosity. It does not change with changing the permeant. The density of CO_2 and CH_4 were obtained from Tables 3 IUPAC (1973) and 5 IUPAC (1976) The viscosity of CO_2 and CH_4 were obtained from the Journal of Physical and Chemical Engineering Data (1990) and the Journal of Chemical and Engineering Data(1965). Figures 5-4 and 5-5 provide these relationships for CO_2 and CH_4. Knowing the viscosity and density at a particular test temperature and pressure allows the calculation of the intrinsic permeability, K_o, using Equation 5-2;

$$K_o = K * \frac{\upsilon}{\rho * g}$$ [5-2]

where,

K₀ = Intrinsic Permeability;

K = Permeability;

υ = Viscosity;

ρ = Density; and

g = Acceleration of Gravity.

The standard presentation of the intrinsic permeability plots intrinsic permeability in micro darcy versus effective stress in MPa and intrinsic permeability in micro darcy versus gas pressure in MPa. The intrinsic permeability plots obtained in this research and a discussion of these results are provided in Chapter 6.

5.8 ISOTROPIC COMPRESSIBILTY TESTS

Compressibility tests were to be conducted at the conclusion of the adsorption test. The intent was to examine any change in matrix compressibility as a result of gas adsorption. Procedurally, once adsorption had ceased, the isotropic effective confining stress on the specimen could be cycled by increasing and decreasing the cell pressure. The challenge for these tests, however was the accurate measurements of small volume changes of the specimen. Recall that the triaxial cell was designed as a double wall cell. An internal cell was filled with mercury and connected to a differential pressure transducer. Volume changes during the compressibility tests are determined by using this internal cell. When the effective stress is increased, the coal specimen will compress and its volume will decrease. This causes the mercury level in the internal cell to drop which is detected by the differential pressure transducer. Volume strains plotted against

isotropic effective confining stress represents the compressibility under a particular gas pressure.

While in theory, the mercury filled double wall cell held great promise for exacting measurements of specimen volume changes, many difficulties were encountered in implementing this system. The difficulties were mainly the leakage of mercury into the sample. Under high confining pressure the Teflon, sleeves were not capable of sealing against such a heavy metal. Latex rubber membranes were attempted but they failed to seal against the mercury. Consequently, the measurement of isotropic compressibility was eliminated from the research program.

5.9 GENERAL COMMENTS ON THE TESTS

Prior to presenting and discussing the results it is important to address some of the challenges and the limitations on the results. During some of the permeability tests, the differential pressure transducer exceeded its limits. This was overcome by recalibrating the transducer after those tests were completed. Differential pressures during those permeability tests were obtained from the upstream and downstream pressure transducers. During the permeability test on Luscar specimen using CO_2 and at a total stress of 3.6 MPa, it was not possible to measure permeability. That was due to many factors such as high effective stress, high gas pressure, low porosity and the limitation of the equipment to provide small flow rates.

Adsorption tests with methane failed due to leakage in the syringe pump. In fact the leakage of methane from the seals was so overwhelming, this also lead to limited permeability test results with methane. Adsorption isotherms for methane reported in this thesis were obtained from the literature.

4.10 SUMMARY

This chapter described the experimental procedures followed for permeability and compressibility tests conducted on Luscar and Cardinal River coals. The intrinsic permeability under isotropic stresses was determined for gas pressures up to 12 MPa. Isotropic stresses varied from 6 MPa to 16 MPa effective stress.

Carbon dioxide and methane were used separately in the permeability tests to evaluate the alteration of the intrinsic permeability using different gases and different in situ stresses.

Coal	Code	Test	Flow Rate ml/hour	Effective Stress psi	Gas Pressure psi
Cardinal River	CR1	Adsorption	400	870	550
		Permeability	4	870	550
		Permeability	15	870	550
		Permeability	40	870	550
		Adsorption	400	870	900
		Permeability	4	870	900
		Permeability	15	870	900
		Permeability	40	870	900
		Adsorption	400	870	1400
		Permeability	4	870	1400
		Permeability	15	870	1400
		Permeability	40	870	1400
		Adsorption	400	870	1700
		Permeability	4	870	1700
		Permeability	15	870	1700
		Permeability	40	870	1700
		Permeability	4	1450	500
		Permeability	15	1450	500
		Permeability	40	1450	500
		Permeability	4	1450	800
		Permeability	15	1450	800
		Permeability	40	1450	800
		Permeability	4	1450	1200
		Permeability	15	1450	1200
		Permeability	40	1450	1200
		Permeability	1.5	1450	1700
		Permeability	4	1450	1700
		Permeability	15	1450	1700
		Permeability	4	2320	600
		Permeability	15	2320	600
		Permeability	40	2320	600
		Permeability	4	2320	920
		Permeability	15	2320	920
		Permeability	40	2320	920
		Permeability	1.5	2320	1200
		Permeability	4	2320	1200
		Permeability	15	2320	1200
		Permeability	1.5	2320	1500
		Permeability	4	2320	1500
		Permeability	15	2320	1500

Table 5-1 Summary of test program

Coal	Code	Test	Flow Rate ml/hour	Effective Stress psi	Gas Pressure psi
Coal Valley	CV1	Adsorption	400	870	540
		Permeability	4	870	540
		Permeability	15	870	540
		Permeability	40	870	540
		Adsorption	400	870	930
		Permeability	4	870	930
		Permeability	15	870	930
		Permeability	40	870	930
		Adsorption	400	870	1400
		Permeability	4	870	1400
		Permeability	15	870	1400
		Permeability	40	870	1400
		Adsorption	400	870	1700
		Permeability	1.5	870	1700
		Permeability	4	870	1700
		Permeability	15	870	1700
		Permeability	4	2320	500
		Permeability	15	2320	500
		Permeability	40	2320	500
		Permeability	1.5	2320	950
		Permeability	4	2320	950
		Permeability	15	2320	950
		Permeability	1.5	2320	1400
		Permeability	4	2320	1400
		Permeability	15	2320	1400
Cardinal River	CR2	Permeability	4	870	550
		Permeability	15	870	550
		Permeability	40	870	550
		Permeability	4	870	930
		Permeability	15	870	930
		Permeability	40	870	930
		Permeability	4	870	1400
		Permeability	15	870	1400
		Permeability	40	870	1400
Coal Valley	CV2	Permeability	4	870	550
		Permeability	15	870	550
		Permeability	40	870	550
		Permeability	4	870	930
		Permeability	15	870	930
		Permeability	40	870	930
		Permeability	4	870	1400
		Permeability	15	870	1400
		Permeability	40	870	1400

Table 5-2 Summary of test program (Continued)

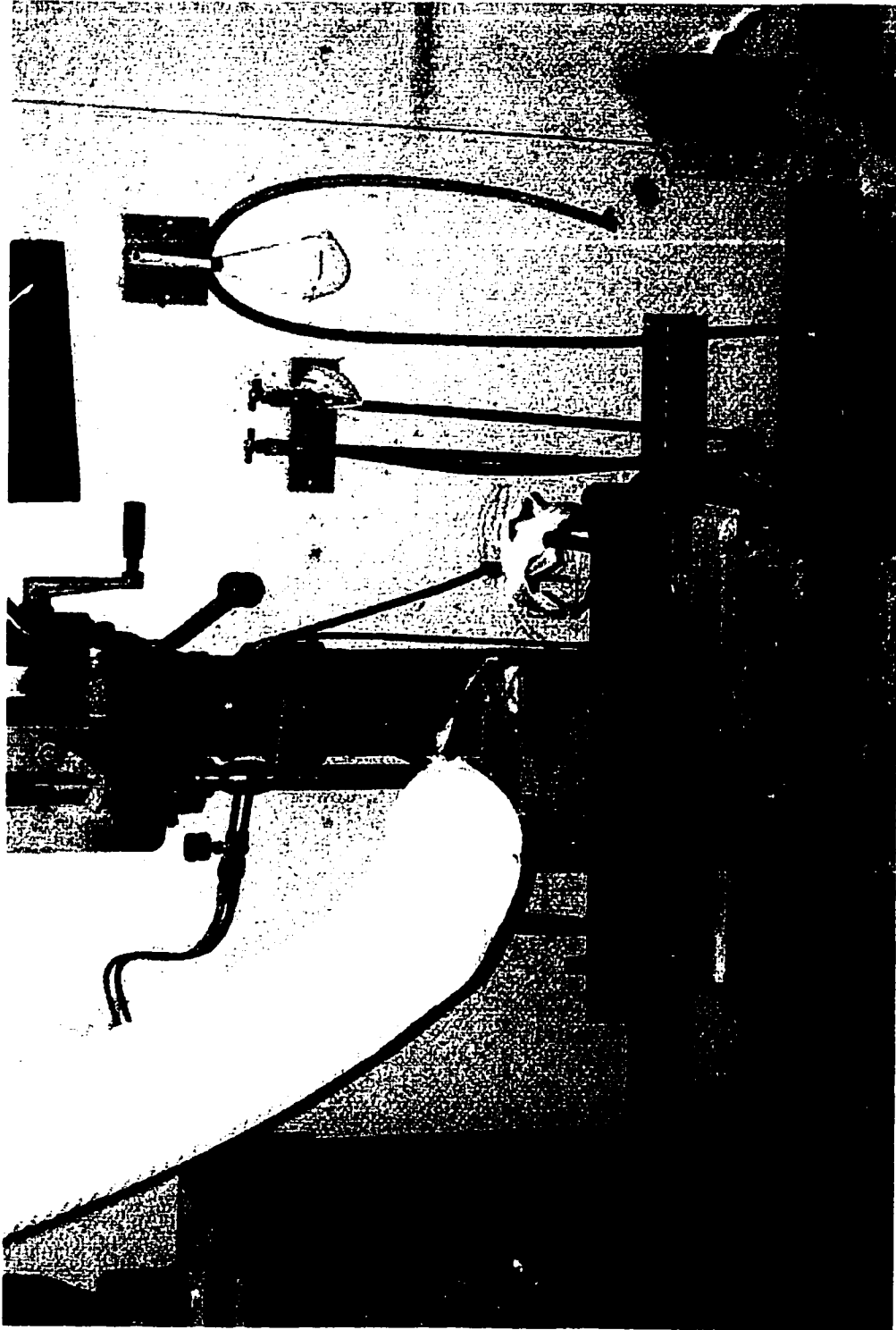| Sample	Symbol	Diameter mm	Length mm	Weght g	Use	Remarks
Cardinal River 1	CR1	24.5	41.86	29.17	CO_2 Testing	shear plane at 45
Cardinal River 2	CR2	24.4	46.67	28.6	CH_4 Testing	Intact
Coal Valley1	CV1	24.4	34.71	25.04	CO_2 Testing	Intact
Coal Valley2	CV2	24.3	40.75	26.27	CH_4 Testing	Intact

Table 5-3 Samples properties

Figure 5-1 Coring (a)

Figure 5-2 Coring (b)

Figure 5-3 Sample placing

250

200

Viscosity/kPa s x 10^-6

150

---- Saturation line

100

100MPa
90
80
70
60
50
40
30
20
15
10

50

8
6
4
0.1

0

200   400   600   800

Temperature/K
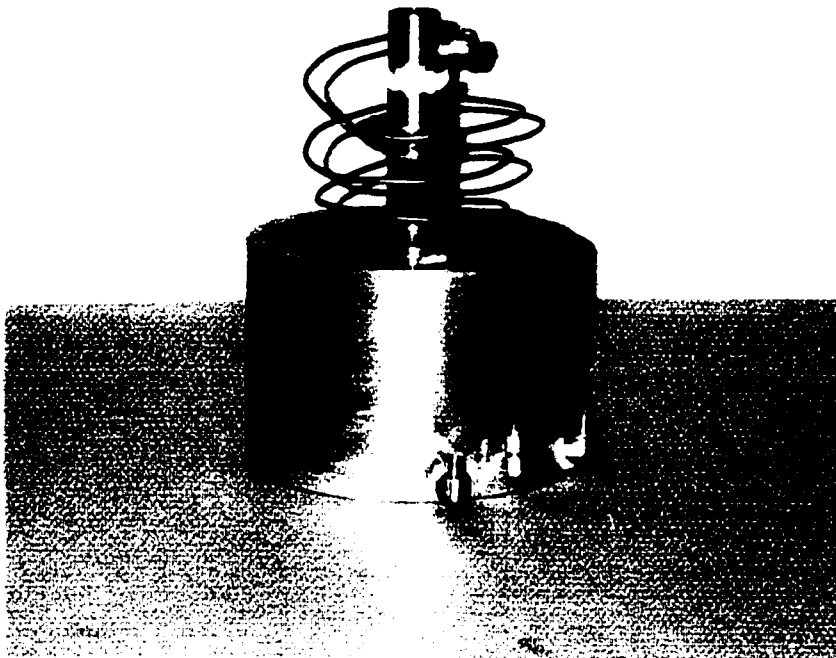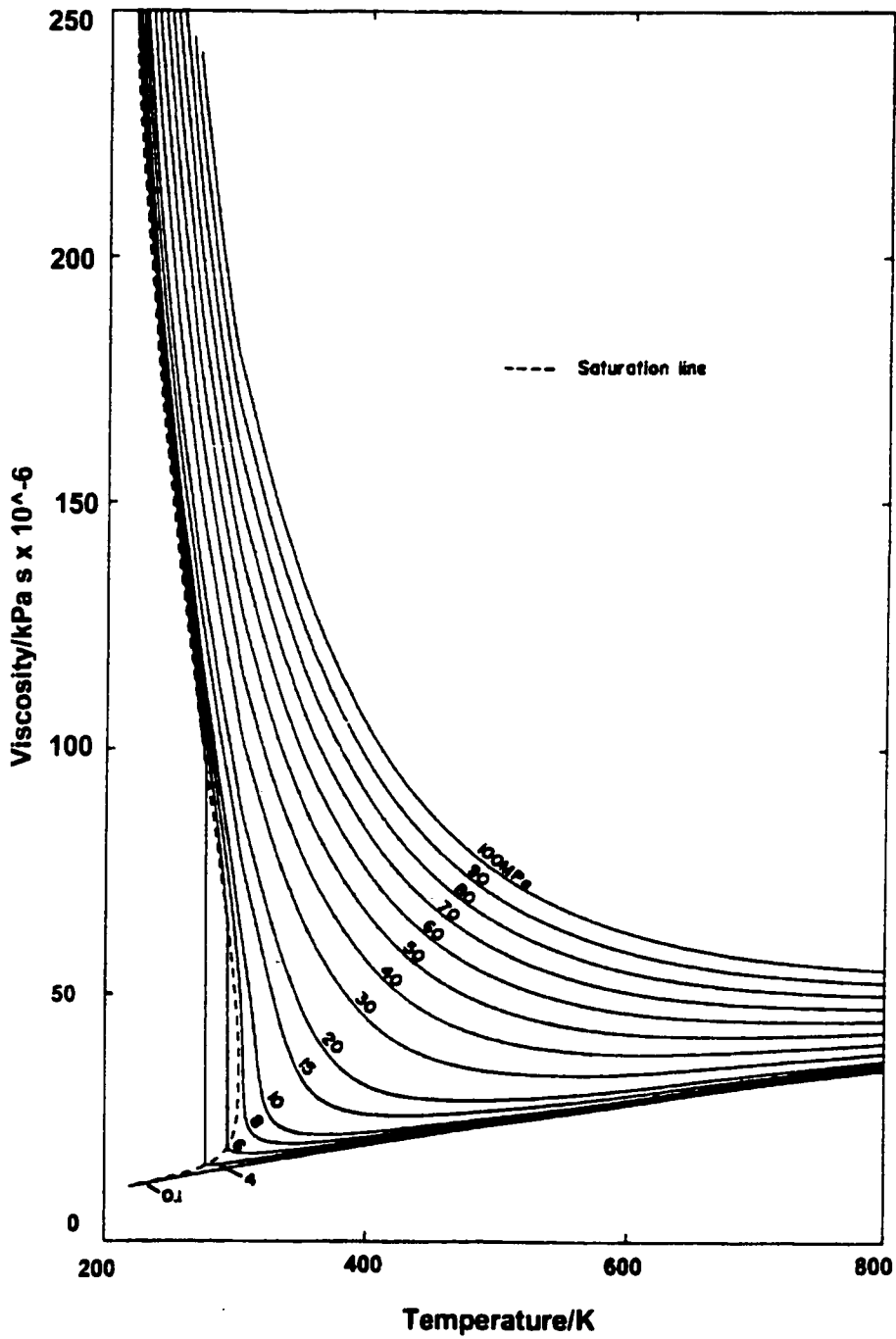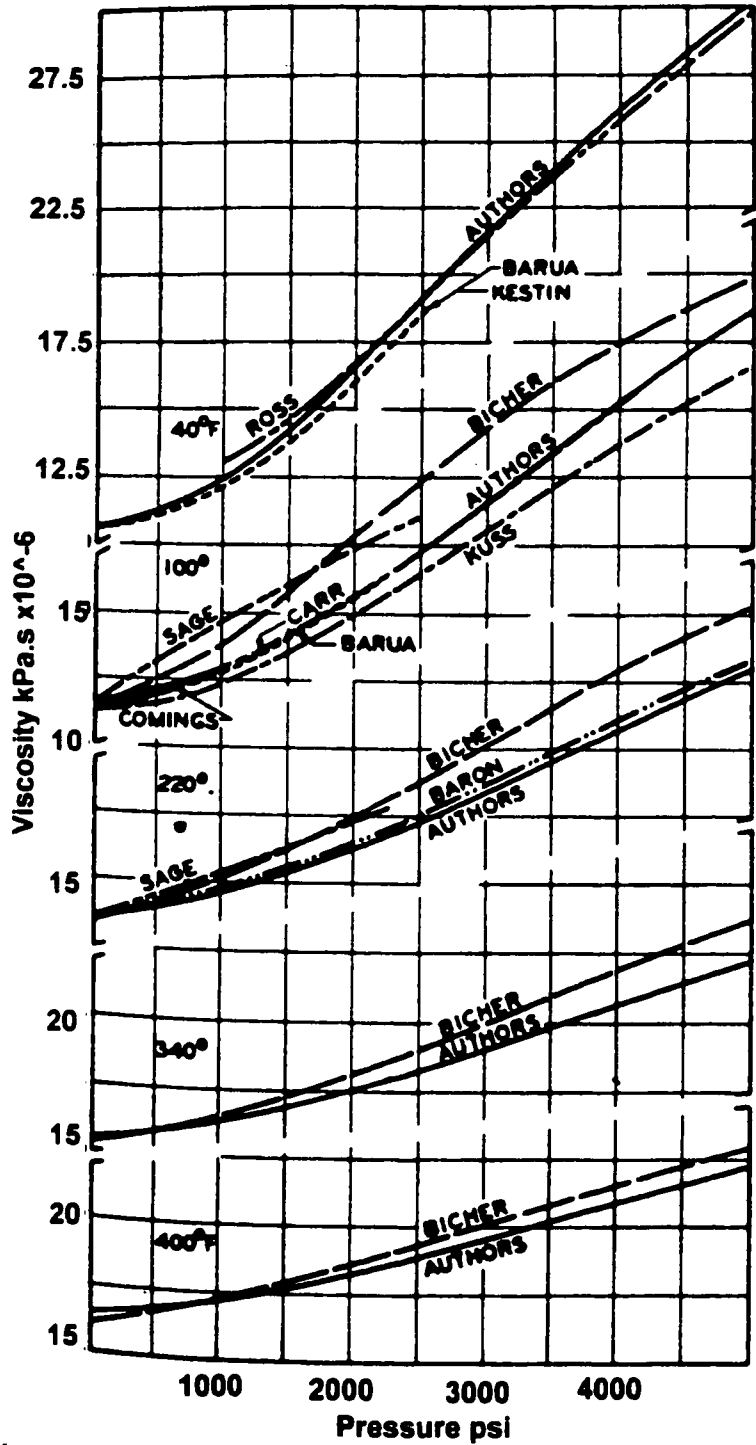
Figure 5-4 The viscosity of carbon dioxide along isobars

(After Vescovic et al., 1990)

Figure 5-5 Viscosity of methane for different pressures and temperatures (After Carmichel et al., 1965)

CHAPTER 6 RESULTS AND DISCUSION

6.1 INTRODUCTION

Performance or success of geological sequestration of greenhouse gases and co-production of methane from coalbed methane reservoirs will be highly dependent on the initial intrinsic permeability of the coalbeds and its variation throughout the injection process. Unfortunately, permeability is extremely variable and difficult to measure reliably. The permeability of coal, which is a rock containing a multiple fracture system, is a function of the permeability of the unfractured medium, the width of fractures, the fracture spacing and the angle between the fractures and direction of the overall pressure gradient across the medium. This multiple fracture system also gives rise to significant stress-dependency of permeability within coal. During CO_2 injection, pore pressures are elevated, effective stress decreases, CO_2 is adsorbing and methane is desorbing; all processes which impact the permeability of coal.

This chapter presents and describes the results of permeability tests conducted on Coal Valley (CV) and Cardinal River (CR) coal specimens. The permeability tests were conducted under different gas pressures and different effective stresses to examine the separate roles of gas adsorption and compressibility on coal permeability. Permeability tests were conducted using CO_2 and CH_4.

A component of the testing program includes the measurement of the gas adsorption isotherm on intact coal specimens. The results from these adsorption measurements are presented and discussed.

6.2 ADSORPTION ISOTHERMS

As discussed in Chapter 5, the test procedure adopted for this research permitted the measurements of the volume of adsorbed gas, CO_2 or CH_4, at each gas pressure increment. Figure 6-1 illustrates the CO_2 adsorption isotherms obtained for CR coal and CV coal. Table 6-1 provides a summary of the CO_2 adsorption test results. Figure 6-1 also shows that the medium volatile CR coal adsorbed more CO_2 than the high volatile CV coal. While the difference was not substantial, it follows the results of many researchers (Kim et al., 1977) who have shown that the volume of adsorbed gas increases with increasing rank. CR coal has a slightly higher grade than CV coal which results in more carbon surface available for adsorption of CO_2 molecules. Table 3-3 shows the ranking difference between CR coal and CV coal.

Due to experimental difficulties, no CH_4 adsorption isotherms were obtained for CR and CV coal specimens. However, Figure 6-2 illustrates the range of CH_4 adsorption isotherms obtained by other researchers. The isotherm for CO_2 is also plotted in Figure 6-2, clearly showing the increased adsorption capacity of CO_2 above CH_4.

Adsorption tests were done on the ambient in situ moisture content. Equilibrium moisture content was not used because Bell (1986) showed that moisture content does not affect the adsorption capacity at pressures above 3 MPa, which is below the lowest adsorption pressure used in this research. For CO_2, the adsorption isotherms obtained for CR and CV coal match closely to the isotherms obtained for other coals, as shown in Figure 6-1. While the CR and CV adsorption isotherms are in general agreement, it is apparent that the adsorption isotherms obtained on CR and CV intact coal specimens are slightly higher than those reported in the literature. The primary reasons for this are:

1. CR and CV are different coals, they have different rank;

2. The difference may be different because the coal samples were relatively dry.

3. Experimental error due to correction to standard temperature and pressure. The temperature error was estimated to be $\pm 0.1\ ^\circ C$ and the pressure error, based on a sensor accuracy of $\pm 1.0\%$ full scale, was estimated to be ± 413 kPa. These errors result in negligible errors in corrected gas isotherms due to the tests procedure which minimized the volume of gas affected by these errors.

Of particular importance, is the match in the substantial increase in adsorption capacity beyond a gas pressure of approximately 9 MPa. Robinson et al. (1994) were one of the first researchers to document this behavior. Note that this does not occur for CH_4, as shown in Figure 6-2.

The adsorption process involves the attachment of gas molecules to the coal surface. As gas pressure increases, the gas molecules will continue forming a single layer of adsorbed gas. At a particular gas pressure, in this case approximately 9 MPa, a process of multilayer adsorption will begin whereby gas molecules begin forming a second layer of attached gas on the top of the initial or first adsorbed layer. Another explanation is after reaching such high gas pressure the adsorbed gas could be subjected to capillary condensation and begin behaving in a liquid like manner even though it is still in the gas phase. (Stanford Geothermal Program, 1996). Capillary condensation results in the adsorbed gas reaching a high density and when the adsorbed volume is adjusted to absolute conditions, provides a high volume of adsorbed gas.

6.3 PERMEABILITY

Chapter 5 described the permeability test procedure and the calculation of intrinsic permeability. In the following paragraphs, permeability results will be

presented and discussed. Table 6-2 summarizes the permeability results.

6.3.1 Intrinsic Permeability Change with Effective Stresses

Figure 6-3 illustrates the permeability test results for CO_2. The permeability results in Figure 6-3 clearly shows the dramatic change in permeability with changing effective stress. The changes are significant; a drop in intrinsic permeability between 51% to 90% of its original value for a change in effective stress from 6 to 16 MPa. k_o/k_{oi} ranged from 0.1 to 0.49 depending on the level of CO_2 pressure. These results indicate that the pore volume is compressed by increasing the effective stress. This is very important, because when injecting CO_2 in the field, pore pressure will increase due to the injection process causing reduction in the effective stress which in turn results in increase in the intrinsic permeability ranging between 200% and 890% from the starting intrinsic permeability. However, note that for any given effective stress level, the magnitude of k_o is a strong function of gas pressure, not just σ'. Other researchers typically show k_o versus σ' as a single curve (Harpalani et al.,1989., and Konechny et al., 1996).

Figure 6-4 illustrates the permeability test results for CH_4. Figure 6-4 shows the expected results that σ' still has a strong influence on k_o but that the dependence on CH_4 gas pressure is reduced substantially. By comparing the thickness of the band of CH_4 pressures, shown in green for CR coal and orange for CV coal, to the thickness of CO_2 pressures showing in Figure 6-3, it is clear that the CH_4 data is tending towards a single k_o versus σ' curve. This relates fundamentally to the relative gas adsorption isotherms shown in Figures 6-1 and 6-2.

Figure 6-3 also shows a possible trend that higher permeability coal, specially the CR1 coal specimen which contained a fracture, had less sensitivity or lower reduction in k_o due to increased effective stresses. This is shown by the lower

slope for the CR1 specimen than the CV1 specimen.

In numerical simulation of carbon dioxide injection into aquifers, Hitchon (1996) showed that permeability has a very significant effect on the amount of CO_2 injected. For the same injection conditions, which included an injection pressure set to 90% of fracture pressure, 15 times more CO_2 volume could be injected when the aquifer permeability increased from 6.2 to 100 md, an increase of 1500%. Figure 6-3 clearly shows this permeability increase can occur within the coalbed methane reservoirs due to effective stress reduction alone. If it is assumed the in situ stress is 15 MPa, then the injection pressure will be 13.5 MPa (90% of fracture pressure) and the in situ effective stress would drop to 1.5 MPa. From the results of CV coal shown in Figure 6-3, this will result in permeability increase from approximately 2 μd to 30 μd; similar impact simulated by Hitchon (1996) may be expected to occur within the coal seams, possibly, at sub fracture injection pressure.

6.3.2 Intrinsic Permeability Change with Gas Pressures

Figures 5-6 and 6-6 illustrate intrinsic permeability change with CO_2 and CH_4 gas pressure, respectively for the same effective stress in Figure 6-5, intrinsic permeability was reduced by 75% when CO_2 pressure was increased from 3.5 MPa to 12 MPa. This dramatic change is a result of coal swelling due to gas adsorption.

Note that for each curve in Figure 6-5 and 6-6, effective stress is held constant so that permeability variations are due solely to the adsorption process.

Figure 6-5 shows that permeability reduction due to CO_2 adsorption behaves in a bi-linear manner. At stress levels below approximately 8.5 MPa, the permeability appears to be reduced severely with increasing gas pressure. At high CO_2

pressure the permeability reduction becomes less. This phenomena could be explained by looking at the adsorption isotherm. At pressures below the transition zone CO_2 is adsorbed in a single or monolayer causing the coal to swell and in turn reduce the permeability. At CO_2 pressures above the transition zone or 8.5 MPa, the injected gas is believed to be forming a multilayer making the adsorbed gas denser without affecting the pore space.

This phenomena does not occur with CH_4 over the pressure range used for these tests. It is believed that CH_4 does not create multilayer adsorption zone at these gas pressures. An increase in CH_4 pressure does result in a reduction in permeability, as shown in Figure 6-6. . However, the rate of permeability reduction with CH_4 pressure was less than the rate of reduction in permeability with CO_2. This is reflected by the size of CH_4 molecules. CH_4 molecules are relatively smaller than CO_2 molecules, so that at the same gas pressure a smaller volume of CH_4 will be adsorbed.

The rate of change in permeability for CO_2 and CH_4 is summarized in Figure 6-7. Clearly CO_2, effects a substantially higher drop in k_o than CH_4, as discussed above. Note also that even at low gas pressures, reductions of 2 to 3 times occur mainly due to the rapid initial adsorption that occur at low pressures.

Coal	Pressure MPa (psi)	Adsorped Gas (cm³)	temperature K	Z Comp factor	Adsorbed Volume at STP* (cm³)/gram	Cumulative (cm³)/gram
CR1	3.25 (470)	19	320	0.859525	22.0	22.0
	6.55 (950)	8	320	0.68142	20.2	42.2
	9.6 (1400)	6	320	0.36804	44.7	86.9
	11.7 (1700)	10	320	0.35446	94.1	181.0
CV1	3.8 (550)	22.6	320	0.859525	29.2	29.2
	6.55 (950)	5	320	0.68142	13.7	42.8
	9.6 (1400)	1.75	320	0.36804	13.0	55.9
	11.7 (1700)	8	320	0.35446	75.3	131.1

Table 6-1 CO₂ Adsorption results

* Standard temperature and pressure.

114

Coal	Effective Stress MPa	Effective Stress psi	Gas Pressure psi	Gas Pressure bars	Permeability m/hour	Density KN/m³	Viscosity kPa s	Intrinsic Permeability Micro Darcy
CR1	6	870	530	36	1.75E-05	0.686	2.00E-08	143.2
			1050	72	1.61E-05	1.85	2.20E-08	53.8
			1450	100	3.00E-05	4.4	2.80E-08	53.7
			1750	120	2.18E-05	5.77	4.00E-08	42.5
	10	1450	570	40	8.98E-06	0.788	2.00E-08	64.1
			930	64	1.32E-05	1.54	2.00E-08	48.1
			1260	87	8.23E-06	2.94	2.50E-08	19.7
			1750	120	8.08E-06	5.5	4.00E-08	16.5
	16	2320	660	45	4.54E-06	0.915	2.00E-08	27.9
			920	63	6.77E-06	1.456	2.00E-08	26.2
			1200	83	7.17E-06	2.277	2.60E-08	23.0
			1500	103	7.01E-06	4.4	2.80E-08	12.6
CV1	6	870	530	36	3.07E-06	0.686	2E-08	25.2
			930	64	2.69E-06	1.54	2E-08	9.8
			1450	100	3.05E-06	4.4	2.8E-08	5.5
			1750	120	4.84E-06	5.77	4E-08	9.4
	16	2320	530	36	3.94E-07	0.686	2E-08	3.2
			920	63	2.73E-07	1.456	2E-08	1.1
			1450	100	2.93E-07	4.4	2.8E-08	0.5
			1750	120	N/A	5.77	4E-08	N/A
CR2	6	870	550	36	1.55E-06	0.2358	1.30E-08	24.0
			950	64	1.82E-06	0.42	1.36E-08	16.6
			1400	100	1.76E-06	0.628	1.47E-08	11.6
CV2	6	870	530	36	3.05E-07	0.21	1.25E-08	5.1
			650	44	3.00E-07	0.28	1.30E-08	3.9
			1050	71	4.91E-07	0.42	1.37E-08	4.5

Table 6-2 CO_2 Permeability results

** The rest of changes in permeability with effective stresses for CR2 and CV2 were back calculated from the relationships obtained from CV1.
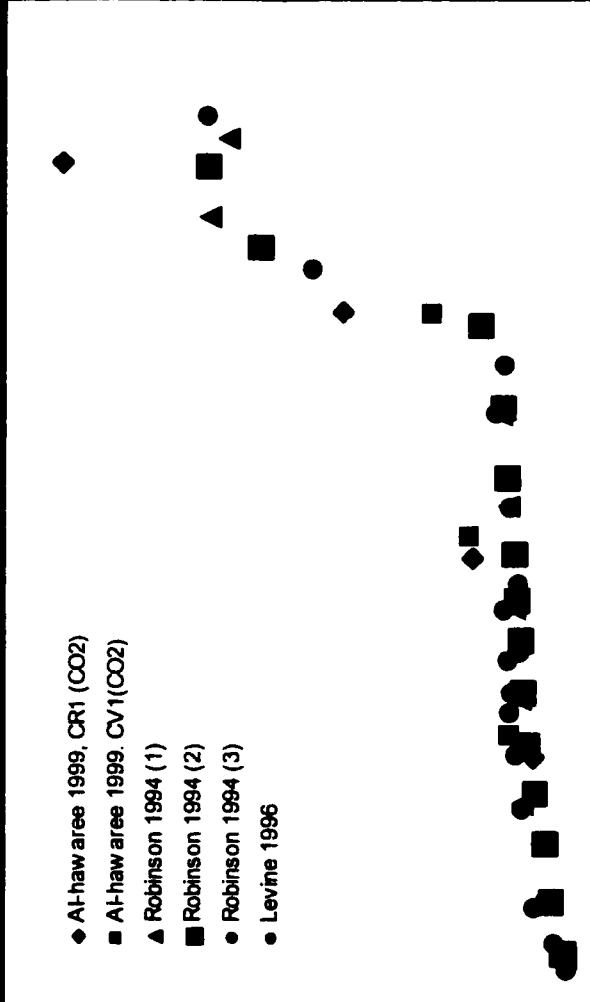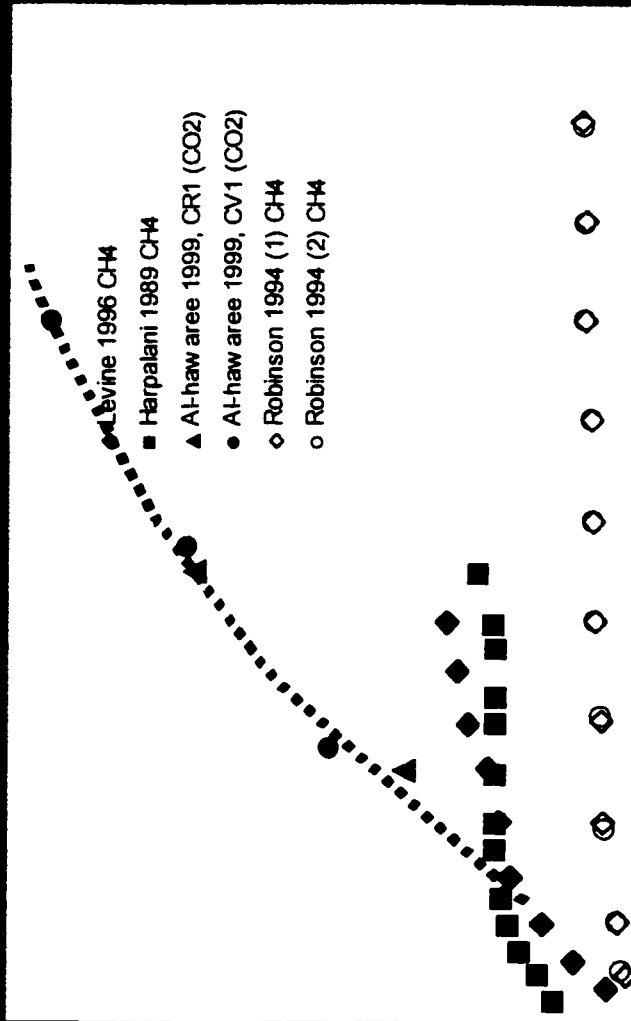
Figure 6-1 CO₂ Adsorption isotherms

Levine 1996 CH4
■ Harpalani 1989 CH4
▲ Al-haw aree 1999, CR1 (CO2)
● Al-haw aree 1999, CV1 (CO2)
◇ Robinson 1994 (1) CH4
○ Robinson 1994 (2) CH4

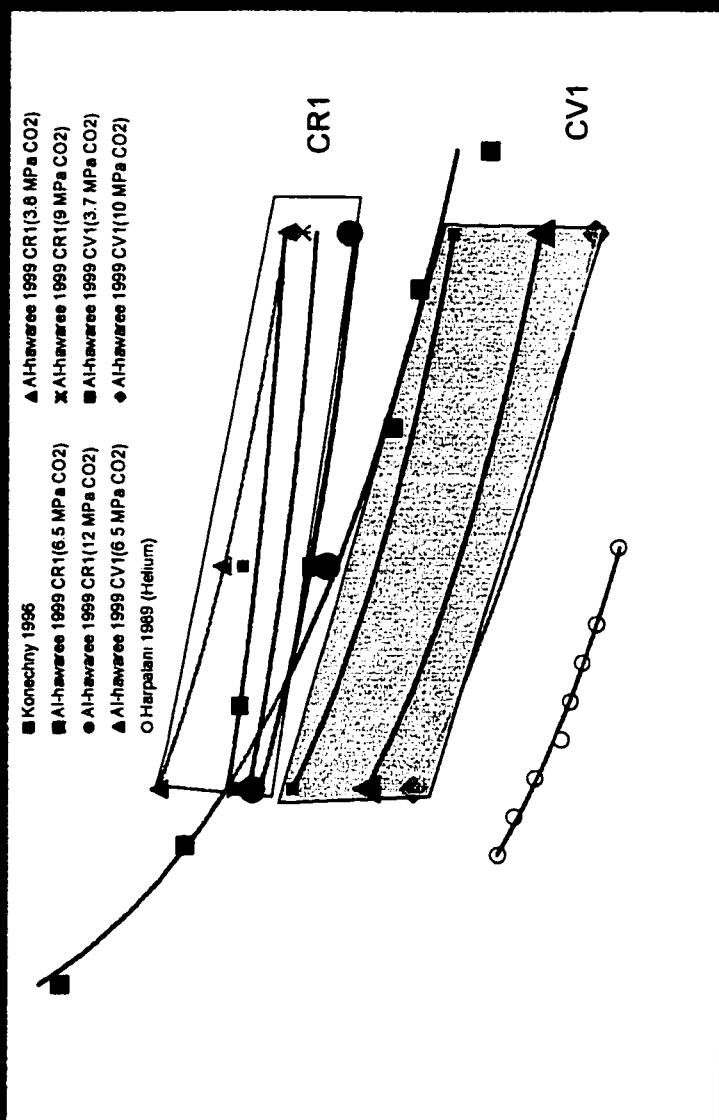**Figure 6-2 CH₄ Adsorption isotherms**

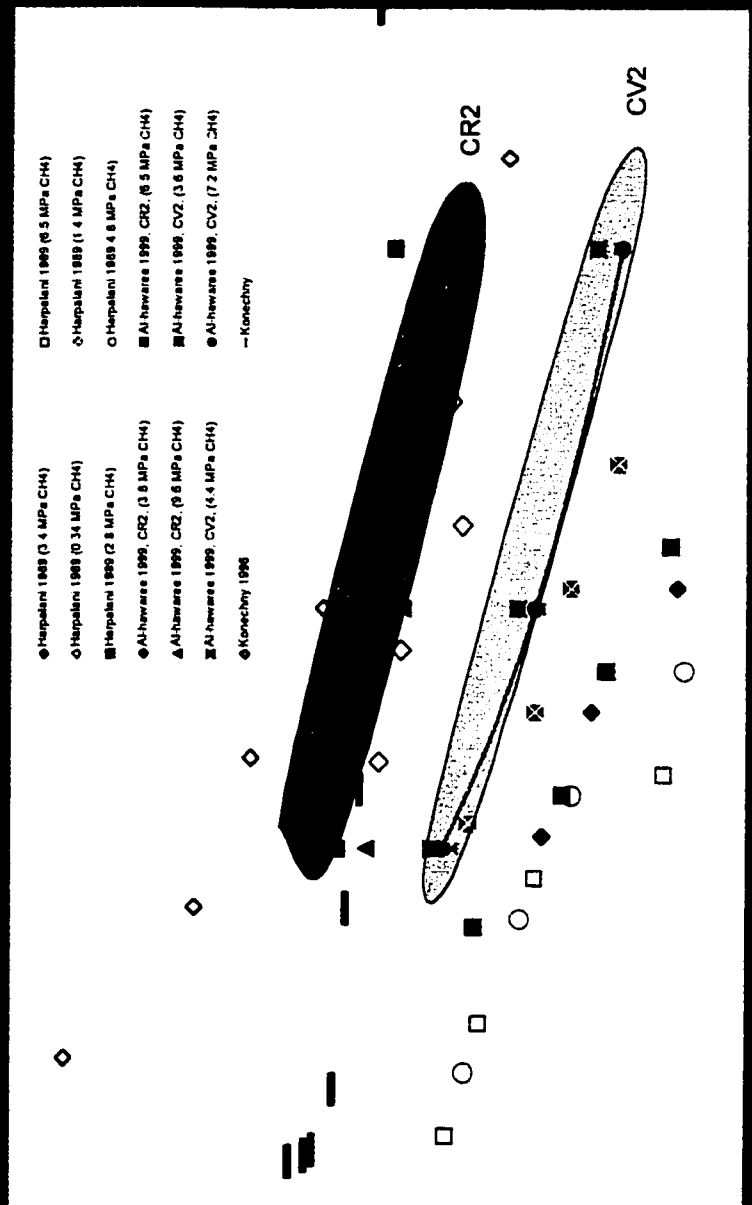Figure 6-3 Permeability vs effective isotropic confining stress (CO₂)

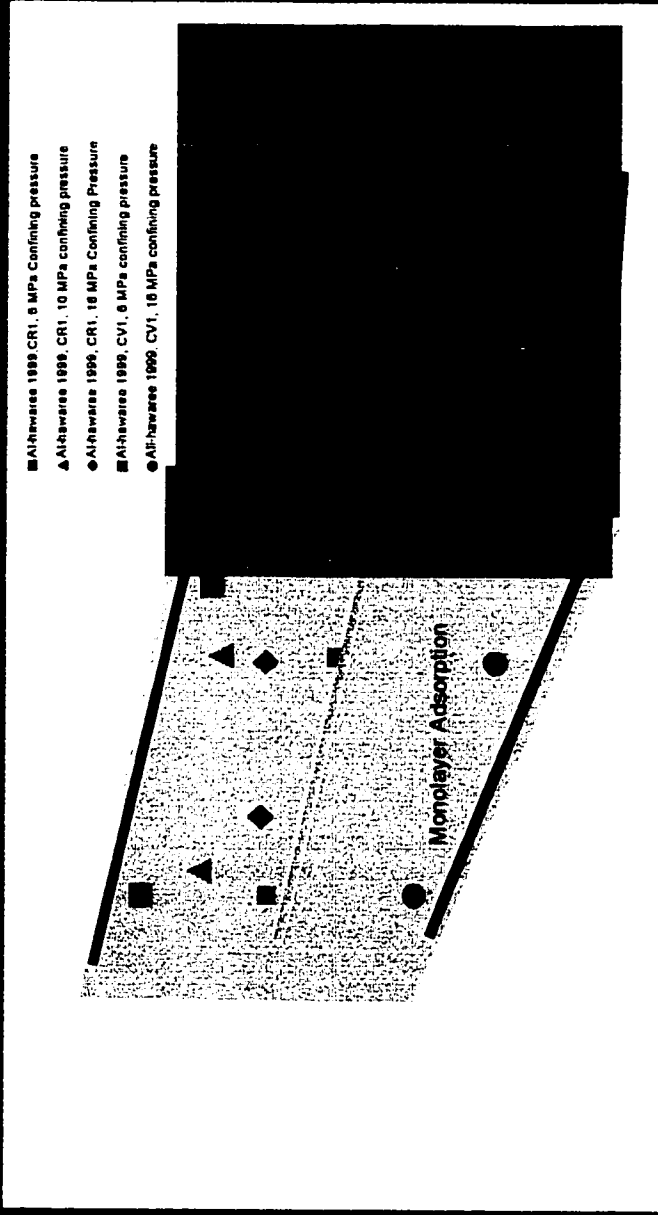Figure 6-4 Permeability vs effective isotropic confining stress (CH₄)

119

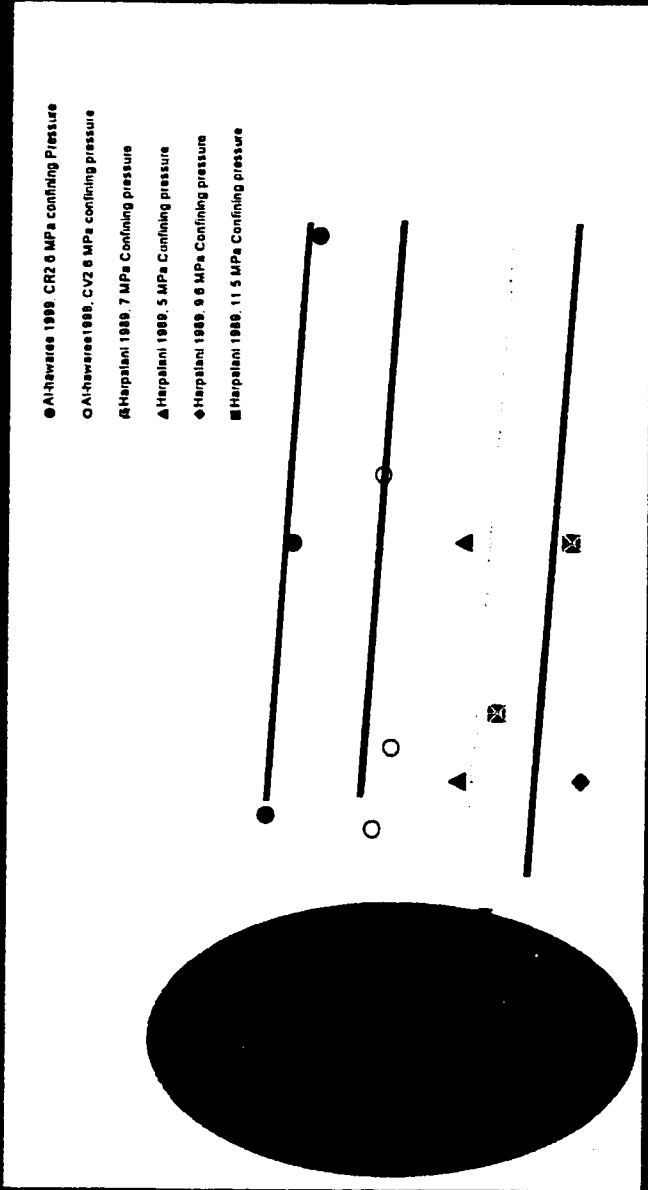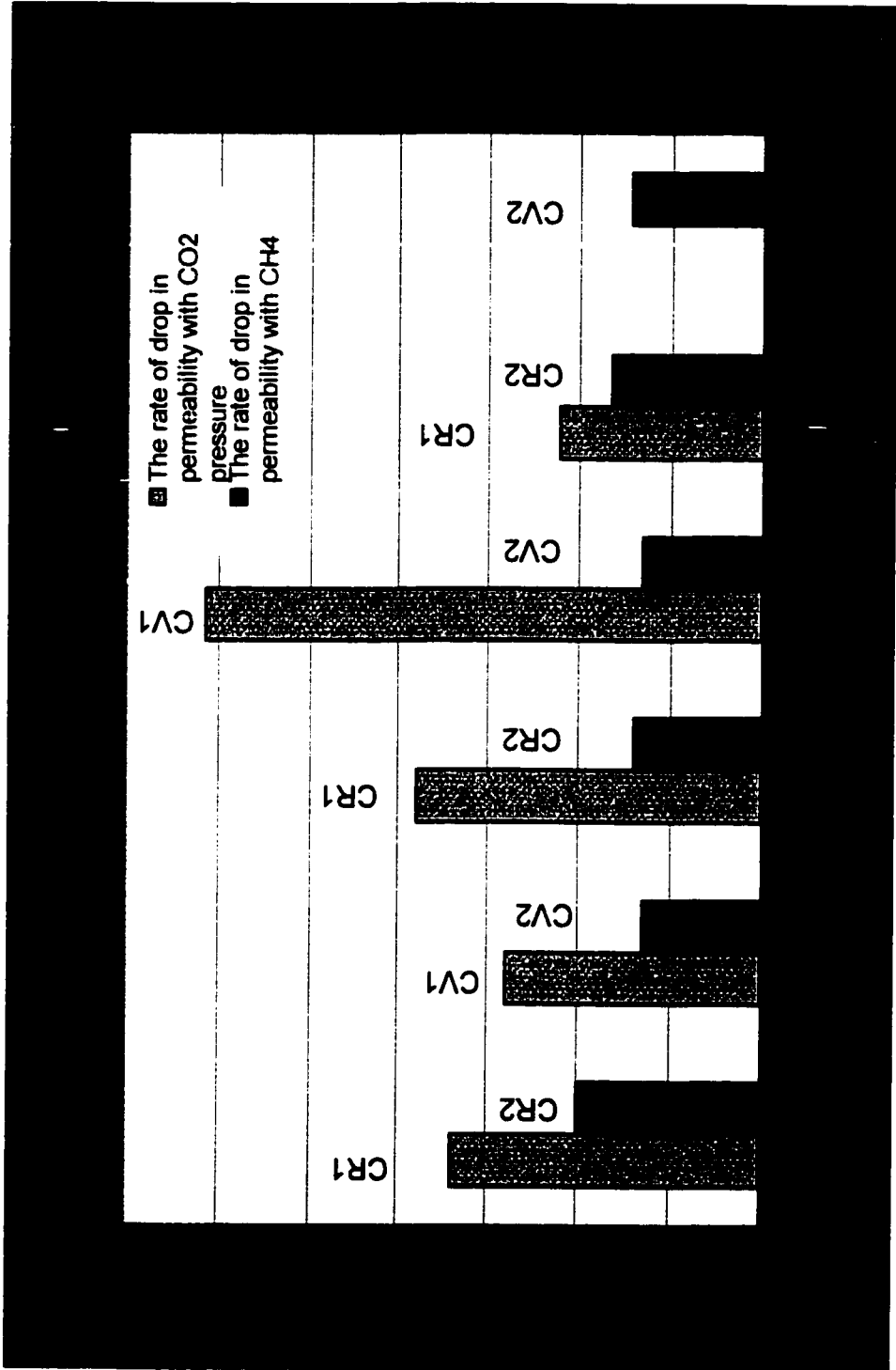Figure 6-5 Permeability versus CO₂ pressure

Figure 6-6 Permeability vs CH$_4$ pressure

Figure 6-7 Change in k_o for CO_2 and CH_4

CHAPTER 7 CONCLUSIONS AND RECOMMENDATIONS

7.1 CONCLUSIONS

7.1.1 Characterization Test Results

The characterization tests revealed that Cardinal River coal is a medium volatile bituminous coal composed of 85% carbon, 5.3% hydrogen, 1.5% nitrogen and 0.21% sulfur with a 1.013 reflectance index. Moisture content is 0.77% and the porosity is 3%. Coal Valley coal (CV) is a high volatile bituminous coal containing 68% carbon, 5% hydrogen, 1% nitrogen and 0.3% sulfur with a reflectance index of 0.58. The moisture content is around 6% and porosity is 2%.

Different sampling and coring techniques were used to obtain high quality samples. A freezing technique was one of the tools used to obtain high quality coal samples. Even though the frozen samples were never used in this research, the freezing technique proved to work well in coal sampling.

7.1.2 Adsorption Test Results

Rank impacted adsorption capacity of Cardinal River coal showed higher adsorption than Coal Valley coal. The isotherm for CO_2 clearly shows the increased adsorption capacity of CO_2 above CH_4. CO_2 exhibited a transition pressure of approximately 8.5 MPa where monolayer adsorption ended and multilayer adsorption began. More CO_2 has been adsorbed at the same gas pressure than CH_4. For instance, at 4 MPa gas pressure 12 cc/g of CH_4 was adsorbed compared to 30 cc/g of CO_2.

7.1.3 Permeability Results

CO_2 adsorption resulted in a dramatic reduction in intrinsic permeability. A 75% reduction in the intrinsic permeability (from 144 to 42 micro darcy) was measured over a CO_2 pressure range of 3.5 and 12 MPa. CH_4 showed much less impact on permeability reduction.

The permeability was reduced dramatically for increasing levels of isotropic effective stress. Permeability reductions between 51% and 90% were measured over the isotropic effective stress range of 6 to 16 MPa. For instance intrinsic permeability for CV1 at 10 MPa was reduced from 5.5 micro darcy to 0.5 micro darcy when effective confining stresses was increased from 6 to 16 MPa.

Testing showed that permeability versus effective confining stress was not a single relationship but depended on gas type and pressure. At any effective confining stress level, the magnitude of gas pressure influenced the intrinsic permeability. CO_2 had a much larger influence than CH_4. At $\sigma_m = 10$ MPa, an increase in CO_2 pressure from 3.5 MPa to 10 MPa resulted in a 10 fold reduction in intrinsic permeability. For the same σ_m, an increase in CH_4 pressure from 3.5 MPa to 10 MPa results in only a 2 to 3 fold reduction in intrinsic permeability.

Variation in permeability due to CO_2 gas pressure displayed a bi-linear relationship. At CO_2 gas pressures below the transition pressure of approximately 8.5 MPa, a relatively rapid decrease in permeability occurs as the gas pressure approaches 8.5 MPa. Beyond this transition pressure, permeability reductions become less dramatic. This bilinear response was not found for CH_4. It is believed the transition pressure for CH_4 is much greater than the maximum gas pressure used in this testing program.

7.1.4 Practical Application of Research

The major practical application of this research is the determination of fundamental permeability relationships to aid in the interpretation of production and injection field tests. During the sequestration process there will be increase in pore pressure and reduction in the effective stresses. By applying the results of this research one could predict the reduction in intrinsic permeability due to gas adsorption and the increase in the intrinsic permeability due to effective stress reduction.

7.2 RECOMMENDATIONS FOR FUTURE RESEARCH

The following recommendations may be useful for future geomechanical studies of the sequestration process of CO_2 in coalbeds:

7.2.1 Experimental Procedure

Due to leakage in the pressure systems, limited methane tests were performed. It is recommended that adsorption and permeability tests using methane be conducted.

Volume change measurements are important for understanding the shrinkage and swelling phenomena in coals. Owing to problems with the mercury double wall system, this could be achieved by modifying the triaxial cell to test 2 inch diameter samples. Sealing could then be achieved by using a latex membrane and liquid silicon cell fluid. Volume changes are obtained by using volume change devices capable of measuring the amount of pumped liquid in and out the cell when there is a change in the specimen volume.

7.2.2 Scale Effects

This research was performed on intact coal samples. Further research should include complete constitutive testing to examine the impacts of coal structure specially the coal fracture system. Samples in future research should cleats and bedding features. Testing larger samples will also improve volume change response during adsorption and permeability tests.

7.2.3 Sequestration Path

Stress history will have a dominating effect on the constitutive behavior of coal. For CO_2 enhanced gas recovery schemes, it is anticipated that the that the CO_2 injection CH_4 desorption history will also influence the constituent response of the coal. It is recommended that further testing be conducted following this sequestration path.

7.2.4 Risk Assessment

It is important to quantify the risk of different geological disposal methods for greenhouse gases and their impact on the environment. Additional research should be conducted to identify risk events and their consequences as well as the probability of their occurrence. For the options available within the province of Alberta the risk associated with the following methods should be examined:

- Risk of CO_2 Disposal in Depleted Oil Wells.
- Risk of CO_2 Disposal in Deep Aquifers.
- Risk of CO_2 Disposal in Coalbeds.

REFERENCES

ASTM. 1992. Standard Test Method for Determination of Pore Volume and Pore Volume Distribution of Soil and Rock by Mercury Intrusion Porosimetry (D4404-84 In 1997 Annual Book of ASTM Standards. ASTM, Philadelphia. Sect. 04. Vol. 08. pp. 582-586.

ASTM. 1990. Standard Test Methods for Proximate Analysis of the Analysis Sample of Coal and Coke by Instrumental Procedure (D 5142-90). In 1990 Annual Book of ASTM Standards. ASTM, Philadelphia. Sect. 05. Vol. 05. pp. 444-448.

ASTM. 1992. Standard Test Method for Surface Area of Catalysts (D3663-92). In 1992 Annual Book of ASTM Standards. ASTM, Philadelphia. Sect. 05. Vol. 03. pp. 642-645.

ASTM. 1993. Standard Test Methods for Instrumental Determination of Carbon, Hydrogen, and Nitrogen in Laboratory Sample of Coal and Coke (D5373-93). In 1993 Annual Book of ASTM Standards. ASTM, Philadelphia. Sect. 05. Vol. 05. pp. 459-462.

ASTM. 1997. Standard Test Methods for Specific Gravity of Soils (D 854-92). In 1997 Annual Book of ASTM Standards. ASTM, Philadelphia. Sect. 04. Vol. 08. pp. 88-91.

ASTM. 1997. Standard Test Methods for Sulfur in the Analysis Sample of Coal and Coke Using High Temperature Tube Furnace Combustion Methods (D4239-97). In 1997 Annual Book of ASTM Standards. ASTM, Philadelphia. Sect. 05. Vol. 05. pp. 366-374.

Angus, S., Armstrong, B., and deReuck, K.M. 1973. Carbon Dioxide, International Thermodynamic Tables of the Fluid State-3. IUPAC Project Center Imperial Collage, London. Pergamon Press. 385p.

Angus, S., Armstrong, B., and deReuck, K.M. 1976. Methane, International Thermodynamic Tables of the Fluid State-5. IUPAC Project Center Imperial Collage, London. Pergamon Press. 351p.

Ayoub, A., Colson, L., Hinkel, J., Johnston, D., and Levine, J. January 1991. Learning to Produce Coalbed Methane. Oilfield Review. pp. 27-40.

Adams, E.E., Golomb, D.S., and Herzog, H.J. 1995. Ocean Disposal of CO_2 at Intermediate Depths. Energy Convers. Mgmt. 1995. Vol. 36. No 6-9. pp 447-452.

Bell, G. J. 1989, Report prepared by Terra Tek, TR 89-54.

Bailey, R.T., and McDonald, M.M. 1993. Carbon Dioxide Capture and Use for EOR in Western Canada1. General overview. Energy Convers. Mgmt. 34, pp 269-279.

Bell, G.J., and Rakop, K.C. 1986. Hysteresis of Methane/Coal Sorption Isotherms. SPE 15454, paper presented at the 61st Annual Technical Conference and Exhibition of the SPE, New Orleans, LA., 1986. pp. 1-10.

Bise, C.J., and Sheetz, R.S. 1989. Effect of Coal Seam Permeability on the Selection of a Degasification Scheme. Mining Engineering, Littleton, Colorado., 1989. pp. 1035-1040.

Brunnauer, S., Emmet, P.H., and, Teller, E. 1938. Adsorption of Gases in Multimolecular Layers. J. Am. Chem. Soc. 60.

Cobleigh, H.R., 1953. ASME Screw Thread Manual. The American Society of Mechanical Engineers. 1953. pp. 5-7.

Crank, J. 1975. The Mathematics of Diffusion, Second Edition, Oxford Press.

Carmichael, R.S. 1986. Handbook of Physical Properties of Rocks. Volume 1 CRC Press, Inc. Boca Raton, Florida.

Carmichael, L.T., Berry, V., and Sage, B.H. 1965. Viscosity of Hydrocarbons. Methane. Journal of Chemical and Engineering Data. Vol. 10, No. 1. pp. 57-61.

Darcy, H. 1865. Les Fontaines Publiques de la Ville de Dijon (the water supply of the city of Dijon). Dalmount, Paris, 674pp.

Dowson, F.M. 1995. Coalbed Methane: A Comparison between Canada and the United States. Geological Survey of Canada., 1995. Bulletin 489, 60 pp.

Ettinger, I.L. 1958. Systematic handbook for the determination of the methane content of coal seams from the seam pressure of the gas and the methane capacity of coal: National Coal Board, Moscow, Translation No. A1606/SEH.

Francis, D. Extreme Weather and Climate Change. Climate Change Digest, Environment Canada, 1998.

Freund, P. 1998. International Collaboration on Technologies for Reducing

Greenhouse Gas Emissions. Greenhouse Gas Mitigation Edited by Riemer, P. W. F., Smith, A. Y. and Thambimuthu, K. V. 1998. pp 41-46.

Frederick, L.H., and Steinberg, M. 1981. Control of Carbon Dioxide Emissions from a Power Plant (and Use in Enhanced Oil Recovery). 1981.

Gregg, S.J. 1961. The Surface Chemistry of Solids. Reinhold, New York. pp. 830-839.

Gray, I. 1987. Reservoir Engineering in Coal Seams: part I – The physical process of gas storage and movement in coal seams. SPE Reservoir Engineering., pp. 28-34

Green, T.K. Am. Chem. Soc. Div. Fuel Chem. Preprints 1985, 30(4), 488

Gunter, W.D., Gentzis, T., Rottenfusser, B.A., and Richardson, R.J.H. 1996. A Fuel Resource with the Potential of Zero Greenhouse Gas Emissions. Preprint of paper presented at the Third International Conference on Carbon Dioxide Removal, Massachusetts Institute of Technology, September 9-11, 1996. pp. S217-s222.

Gunter, W.D., Gentzis, T., Rottenfusser, B.A., and Richardson, R.J.H. 1997. Deep Coalbed Methane in Alberta, Canada: A Fuel Resource with A Potential of Zero Greenhouse Gas Emissions. Energy Convers. Mgmt. 1997. Vol. 38. pp 217-222.

Guntrer, W.D., Wiwchar, B., and Perkins, E. H. 1997. Aquifer Disposal of CO_2 Rich Greenhouse Gases: Extension of the Time Scale of Experiment for CO_2 Sequestration Reactions by Geomechanical Modelling. Mineralogy and

Petrology. 1997. Vol. 59. pp 121-140.

Gunter, W.D., Bachu, S., Law, D., Marwaha, V., Drysdale, D.L., Macdonald, D.E., and McCann, T.J. 1995. Technical and economic feasibility of CO_2 disposal in aquifers within Alberta Sedimentary Basin. Canada. Energy Convers. 1995. Mgmt. 37. pp. 1135-1142.

Houpeupt, A.H. 1976. The Future Supply of Nature-Made Petroleum and Gas, (Ed. R. F. Meyer), First UNITAR Conference on Energy and Future, 1976, Chap. 28, p. 449.

Hitchon, B. (Editor). 1996. Aquifers Disposal of Carbon Dioxide: hydrodynamic and mineral trapping proof of concept. Geosience Publishing Ltd. (Box 79088, 1020 Sherwood Drive, Sherwood Park, Alberta T8A 5S3, Canada) 165 pp.

Houghton, J.T. 1996. Climate Change − The IPCC Scientific Assessment. Cambridge University Press, Cambridge, UK.

Horn, F.L., and Steinberg, M. 1981. Control of Carbon Dioxide Emission from a Power Plant (and Use in Enhanced Oil Recoovery). Process Sciences Divisions, Department of Energy and Environment, Brookhaven National Laboratory, Upton, NY 19973, USA. 1981.

Holditch, S.A., Ely, J.W., Semmelbeck, M.E., Carter, R.H., Hinkel. J., and Jeffrey, R.G. 1988. Enhanced Recovery of Coalbed Methane Through Hydraulic Fracturing. Proceedings SPE Joint Rocky Mountain Regional Low Permeability Reservoirs, Symposium and Exhibition. Society of Petroleum

Engineers of AIME, Richardson. TX, USA., 1988. SPE. 18250. pp. 43-51.

He, X., and Shining, Z. 1992. The Rheological Fracture Properties and Outburst Mechanism of Coal Containing Gas. Proceedings, 11th International Conference Ground Control mining. Australian Institute of Mining and Metallurgy. 1992. pp. 575-579.

Harpalani, S., and Chen, G. 1995. Estimation of changes in fracture porosity of coal with gas emission. Fuel, Volume 74, Number 10.

Harbalani, S., and McPherson, M.J. 1985. Effect of Stress on Permeability of Coal, Proceeding. 26th U. S. Symposium on Rock Mechanics, Rapid City., 1985. pp.830-839.

Harpalani, S., and McPherson, M..J. 1986. Retention and Release of Methane in Underground Coal Working. International Journal of Mining and Geological Engineering. 4; 3, pp. 217-233.

Harpalani, S., and Pariti, U.M. 1993. Study of Coal Sorption Isotherms Using a Multicomponent Gas Mixture. Proceedings, International Coalbed Methane Symposium. 1993. pp. 151-160.

Harpalani, S., and Schraufnagel, R. 1990. Shrinkage of Coal Matrix with Release of Gas and its Impact on Permeability of Coal. Fuel, vol. 69. pp. 551-556.

Harpalani, S., and Zhao, X. 1989. An Investigation of the Effect of Gas Desorption on Coal Permeability. Proceeding of the 1989 Coalbed Methane Symposium, The University of Alabama, Tuscaloosa. pp. 57-63.

Joubert, J.I. 1973. Sorption of Methane in Moist Coal. Fuel, vol. 52, pp. 181-185.

Joubert, J.I. 1974. Effect of Moisture on the Methane Capacity of American Coals. Fuel, Vol. 53, pp. 186-191.

Kim, A.G. 1977. Estimating Methane Content of Bitiminous Coalbeds from Adsorption Data. US Bureau of Mines Reptort of Investigation RI 8245, 1977 22p.

Kaiser, P.K. 1979. Time Dependent Behaviour of Tunnels in Jointed Rock Masses. Ph.D. thesis, Department of Civil Engineering, University of Alberta, Edmonton, Alberta.

King, J.G., and Wilkings, E.T. 1944. Proceedings of the conference on ultrafine structures of coals and cokes. p.46. BCURA, London, 1944.

Konechny, P., and Kozusnikova, A. 1996. Measurement of Gas Permeability of Coal and Clastic Sedimentary Rocks Under Triaxial stress conditions. Coalbed Methane and Coal Geology; Geological Society Special Publication No 109, PP 227-229.

Langmuir, I. 1916. The Constitution and Fundamental Properties of Solids and Liquids. Journal of Am. Chem. Soc., 38. p. 221.

Levine, R.L. 1996. Model Study of the Influence of Matrix Shrinkage on Absolute Permeability of Coalbed Reservoir. Coalbed Methane and Coal Geology, Geological Society Special Publication. No. 109. pp. 197-212.

Mckee, C.R., Bumb, A.C., and Koeng, R.A. 1988. Stress-Dependent Permeability

and Porosity of Coal. Geology and Coalbed Methane Resources of Northern San Juan Basin, Colorado and New Mexico., 1988. pp 143-153.

McElhiney, J.E., Koenig. R.A., and Schraufnagel, R.A. 1989. Evaluation of Coalbed-Methane Reserves Involves Different Techniques. Oil and Gas Journal. pp. 63-72.

Mavor, J.M., and Vaughn, J.E. 1998. Increasing Coal Absolute Permeability in the San Juan Basin Fruitland Formation. Society of Petroleum Engineers., pp. 201-206.

Moffat, D.H., and Weal, K. E. 1955. Sorption by Coal of Methane at High Pressures Fuel, 1955. Vol. 34. pp. 449-462.

Noonan, D.K.J. 1972. Fractured Rock Subjected to Direct Shear. M.Sc. thesis, Department of Civil Engineering, University of Alberta, Edmonton, Alberta.

Nikols, D.J. and Rottenfusser, B.A. 1991. Coalbed Methane –A Canadian Resources for the 1990's. Coalbed Methane – 1991, Rocky Mountains Association of Geologists., 1991. pp 249-253.

Oberg, E., Jones, F.D., and Horton, H.L. Machinery's Hand Book, 23rd Edition. Industrial Press Inc. New York. 2511p.

Perkins, E.H., and Gunter, W.D. 1995a. Aquifer Disposal of CO_2 Rich Greenhouse Gases: Modelling of Water-Rock Reaction Paths in a Siliciclastic Aquifer. In: Kharaka Y K, Chudaev OV (eds) VIII International Symposium on Water-Rock Interaction. Balkema, Rotterdam., 1995. pp 895-898.

Ruppel, T.C. 1972. Adsorption of Methane/Ethane Mixtures on Dry Coal at Elevated Pressure. Fuel, Vol. 51. pp. 297-303.

Reucroft, P. J. 1986. Gas Induced Swelling in Coal. Fuel, 1986. Vol. 65. pp. 816-820.

Robinson Jr, R.L., Hall, F.E., Chunhe, Z., Gasem, K. A.M., and Yee, D. 1994. Adsorption of Pure Methane, Nitrogen, and Carbon Dioxide and their Binary Mixture on Wet Fruitland Coal. SPE 29194, Eastern Regional Conference and Exhibition. 1994. pp. 329-344.

Rotty, R.M., and Marland, G. 1980. Interaction of Energy and Climate, (Ed. W. Balk), Proceedings, International Workshop Munster, Germany., 1980. p. 204.

Sethuraman, A. R. 1987. Gas and Vapor Induced Coal Swelling. American Society Division of Fuel Chemistry Preprints. Vol. 32, no. 1. pp. 259-264.

Singh, A.K. 1968. Desorption Studies of Gases from Coal. M.Sc. thesis, University of Alberta. Edmonton, Alberta.

Stefanska, C.G. 1990. Influence of Carbon Dioxide and Methane on Changes of Sorption , and Dilatometric Properties of Bituminous Coals, Archiwum Gornictwa. Vol. 35, no. pp 105-113.

Stevenson, M.D., Pinczewski, W.V., Somers, M.L., and Bagio, S.E. 1991 Adsorption/desorption of multicomponent gas mixtures at in-seam conditions. Society of petroleum Engineers, 23026. Proceedings of the SPE Asia-Pacific conference in Perth, Western Australia., 1991. pp. 741-756.

Sawyer, W.K., Zuber, M.D., Kuuskraa, V.A., and Horner, D.M. 1987. Using Reservoir Simulations and Field Data to Define Mechanisms Controlling Coalbed Methane Production. Coalbed Methane Symposium, Tuscaloosa, Ala., November 16-19, 1987.

Van Krevden, D.W. 1981. Coal: Typology – chemistry – Physics – Constitution. Elsvier Sci. Pub. Co. New York, 1981.

Vaziri, H.H., Wang, X., Palmer, I.D., Khodaverdian, M., and McLennan, J. 1997. Back Analysis of Coalbed Strength Properties from Field Measurements of Wellbore Cavitation and Methane Production. International Rock Mechanics, Mining Science, and Geomechanics Abstracts.

Vesovic, V., Wakeham, W.A., Olchowy, G.A., Sengers, J.V., Watson, J.T.R., and Millat, J. 1990. The Transport Properties of Carbon Dioxide. Journal of Physical and Chemical Reference Data. Vol. 19., No. 3. 1990. pp. 763-779.

Turkenburg, C.W. 1997. Sustainable Development, Climate Change and Carbon Dioxide Removal (CDR), Energy Convers. Mgmt Vol. 38 Suppl., pp. S3-S12.

Webster, I. 1998. Case Study of Potential AIJ Within Canada. Greenhouse Gas Mitigation (Edited by Riemer, P. W. F., Smith, A.Y. and Thambimuthu, K.V., 1998. pp 137-142.

Young, D.M., and Crowell, A.D. 1962. Physical adsorption of gases. Page 1, London Butterworth.

Yang, R.T., and Saunders, J.T. 1985. Adsorption of Gases on Coal and heat

treated Coals at Elevated Temperature and Pressure: Adsorption from Hydrogen and Methane as Single Gases. Fuel, Vol.64. pp. 616-620.

APPENDIX A CHARACTERIZING TEST RESULTS

This Appendix contains the detailed results of characterization tests. Results of specific gravity tests, porosity, moisture content and reflectance tests are presented in the following tables and figures.

Test no.	LUSCAR COAL			CARDINAL RIVER COAL		
	1	2	3	1	2	3
Vol of flask at 20 C	500 ml	500 ml	500 ml	500 ml	500 ml	500 ml
Method of air removal	Vacuum	Vacuum	Vacuum	Vacuum	Vacuum	Vacuum
Mass fl + water + Soil = Mbws	689.84	690.18	690.24	692.58	688.08	688.05
Temperature, C	24	24	24.5	23	25	25
Mass fl + water = Mbw	675.24	675.3	675.25	675.45	671.04	671.12
Dish no.	A2	TC1	A1	A2	TC1	GC2
Mass dish + dry soil	909.08	766.73	893.8	890.74	768	910.15
Mass of dish	860.73	718.3	845.23	840.73	718.26	860.78
Mass of dry soil = Ms	48.35	48.43	48.57	50	49.74	49.37
Mw = Ms + Mbw - Mbws	33.75	33.55	33.58	32.87	32.7	32.44
Alpha = ROHt/ROH 20C	0.9986	0.9991	0.9991	0.9994	0.9988	0.9988
Gs = Alpha *Ms/Mw	1.43	1.442	1.445	1.52	1.519	1.52

Table A-1 Specific Gravity Test Results

COAL	Container No.	Weight	Cont+wet Sample	Cont+Dry Sample	W%
LUSCAR	1H	1.02	52.95	49.32	7.50%
	2H	1.01	35.14	32.78	7.42%
	3H	1.01	73.87	69.37	6.60%
CARDINAL RIVER	1M	1	8.69	8.63	0.78%
	2M	0.98	10.41	10.34	0.75%

Table A-2 Moisture Content Results

140

COAL	SAMPLE	Weight of Sample (g)	Volume of Sample (cc)	Weight of Sample +Mercury (g)	Unit WEIGHT (g/cc)	Porosity (%)
LUSCAR	1	17.74	12.945	21.47	1.3704	3.1
	2	11.58	8.386	13.84	1.38	2
	3	19.79	14.396	21.97	1.374	1.6
	4	19.76	14.62	24.43	1.35	2.5
	5	25.88	18.201	28.26	1.42	1.2
CARDINAL	1	6.34	5.055	7.19	1.254	4
	2	9.74	7.739	12.33	1.258	3.2
	3	4.2	3.671	4.7	1.144	2

Table A-3 Porosity Tests Results (Mercury Intrusion)

141

Sample							
39-98		40-98		41-98		42-98	
Measurement No	Reflectance	Measurement No	Reflectance	Measurement No	Reflectance	Measurement No	Reflectance
1	0.997	1	0.977	1	0.566	1	0.569
2	0.982	2	1.033	2	0.564	2	0.565
3	1.011	3	1.029	3	0.556	3	0.592
4	1.058	4	1.017	4	0.56	4	0.588
5	1.017	5	1.076	5	0.613	5	0.575
6	1.01	6	1.017	6	0.593	6	0.552
7	0.962	7	1.019	7	0.547	7	0.558
8	0.993	8	1.026	8	0.609	8	0.552
9	1.026	9	1.014	9	0.615	9	0.598
10	0.942	10	1.001	10	0.563	10	0.553
11	0.955	11	1.007	11	0.559	11	0.581
12	0.937	12	1.038	12	0.573	12	0.598
13	1.027	13	0.983	13	0.565	13	0.572
14	1.007	14	0.996	14	0.573	14	0.575
15	1.017	15	0.994	15	0.585	15	0.605
16	1.06	16	1.048	16	0.608	16	0.598
17	1.028	17	1.069	17	0.568	17	0.604
18	0.981	18	1.045	18	0.588	18	0.576
19	1.028	19	0.994	19	0.576	19	0.618
20	1.018	20	1.011	20	0.596	20	0.554
21	1.078	21	0.99	21	0.605	21	0.557
22	1.023	22	1.023	22	0.549	22	0.56
23	1.003	23	1.013	23	0.596	23	0.577
24	1.028	24	0.997	24	0.604	24	0.575
25	1.016	25	0.98	25	0.586	25	0.57
26	0.996	26	1.05	26	0.606	26	0.566
27	1.02	27	0.977	27	0.543	27	0.548
28	1.058	28	1.004	28	0.552	28	0.581
29	1.085	29	0.974	29	0.576	29	0.584
30	1.003	30	1.001	30	0.563	30	0.589
31	0.979	31	0.984	31	0.558	31	0.541
32	1.032	32	1.025	32	0.559	32	0.563
33	1.045	33	0.967	33	0.578	33	0.621
34	1.05	34	1.031	34	0.568	34	0.54
35	1.013	35	1.029	35	0.598	35	0.59
36	1.07	36	0.978	36	0.577	36	0.576
37	1.058	37	1.059	37	0.582	37	0.563
38	1.095	38	1.007	38	0.589	38	0.596
39	1.046	39	1.076	39	0.602	39	0.645
40	1.057	40	1.005	40	0.562	40	0.61
41	1.035	41	0.977	41	0.639	41	0.592
42	0.945	42	0.986	42	0.626	42	0.627
43	0.997	43	0.977	43	0.635	43	0.541
44	0.989	44	1.017	44	0.617	44	0.589
45	1.022	45	0.94	45	0.61	45	0.572
46	1.008	46	1.02	46	0.609	46	0.587
47	0.959	47	1.004	47	0.641	47	0.561
48	0.971	48	1.006	48	0.563	48	0.588
49	1.008	49	0.996	49	0.566	49	0.558
50	1.009	50	0.977	50	0.562	50	0.625
51	0.998	51	0.966	51	0.571	51	0.601
52	0.981	52	0.99	52	0.53	52	0.626
53	0.965	53	0.979	53	0.586	53	0.625
54	1.087	54	0.961	54	0.542	54	0.636
55	1.025	55	0.973	55	0.537	55	0.615
56	1.024	56	0.97	56	0.566	56	0.547
57	1.023	57	0.965	57	0.562	57	0.591
58	1.003	58	1.017	58	0.617	58	0.607
59	0.949	59	0.993	59	0.598	59	0.656
60	0.983	60	1.023	60	0.613	60	0.613
61	0.981	61	1.032	61	0.563	61	0.633
62	1.005	62	0.975	62	0.626	62	0.64
63	1.054	63	0.961	63	0.606	63	0.636
64	1.036	64	1.049	64	0.612	64	0.602
65	1.015	65	1.071	65	0.552	65	0.569
66	1.036	66	1.073	66	0.541	66	0.582
67	1.015	67	1.076	67	0.556	67	0.606
68	1.038	68	1.099	68	0.585	68	0.553
69	1.005	69	1.054	69	0.59	69	0.564
70	1	70	1.038	70	0.561	70	0.574
71	1	71	1.027	71	0.581	71	0.575

Table A-4 Reflectance Test Results
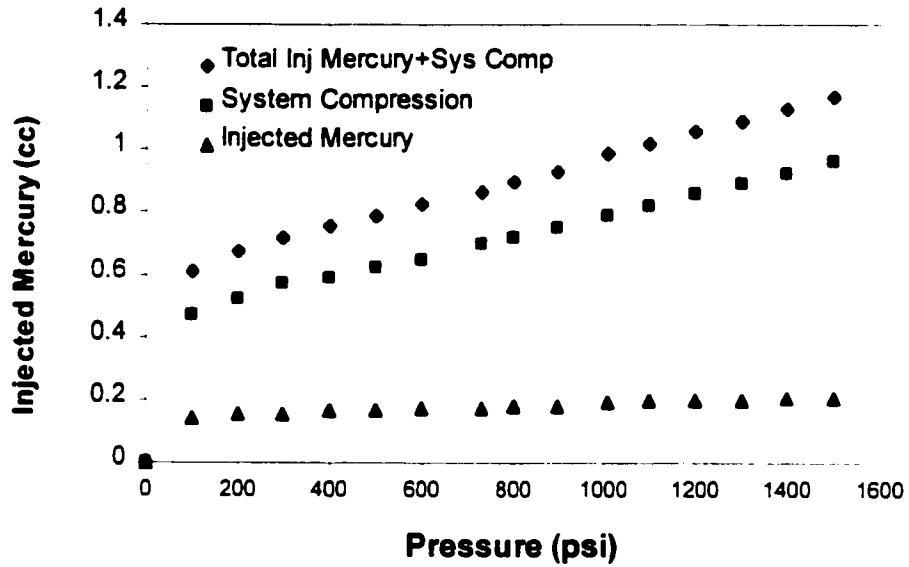
Figure A-1 Mercury Intrusion Test 1 on Cardinal River Coal
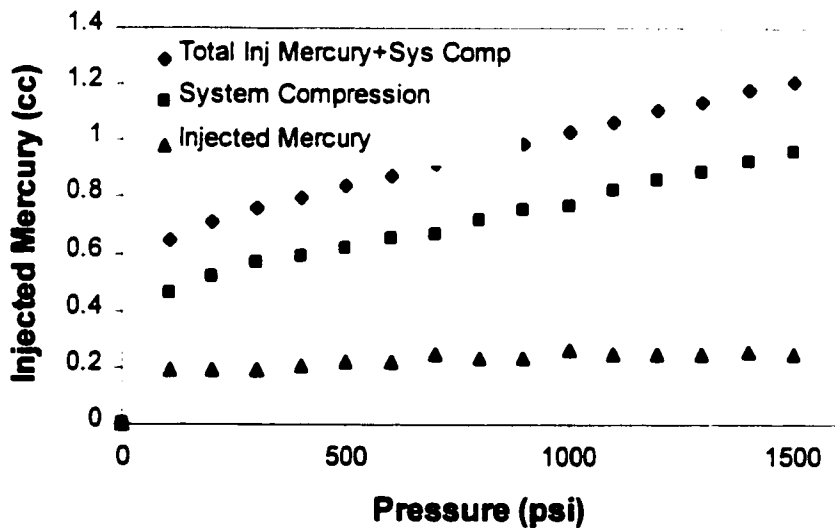
Figure A-2 Mercury Intrusion Test 2 on Cardinal River Coal
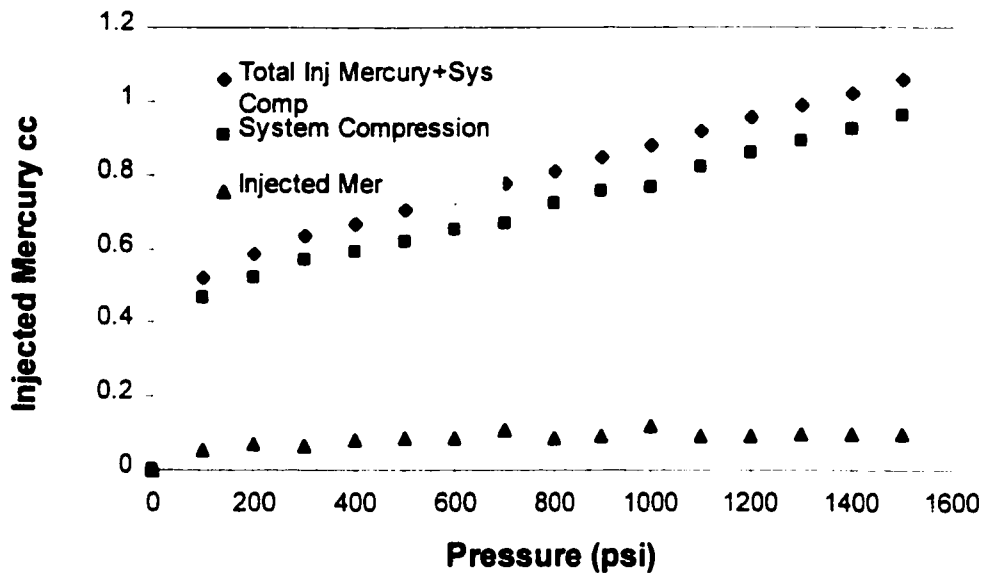
Figure A-3 Mercury Intrusion Test 3 on Cardinal River Coal
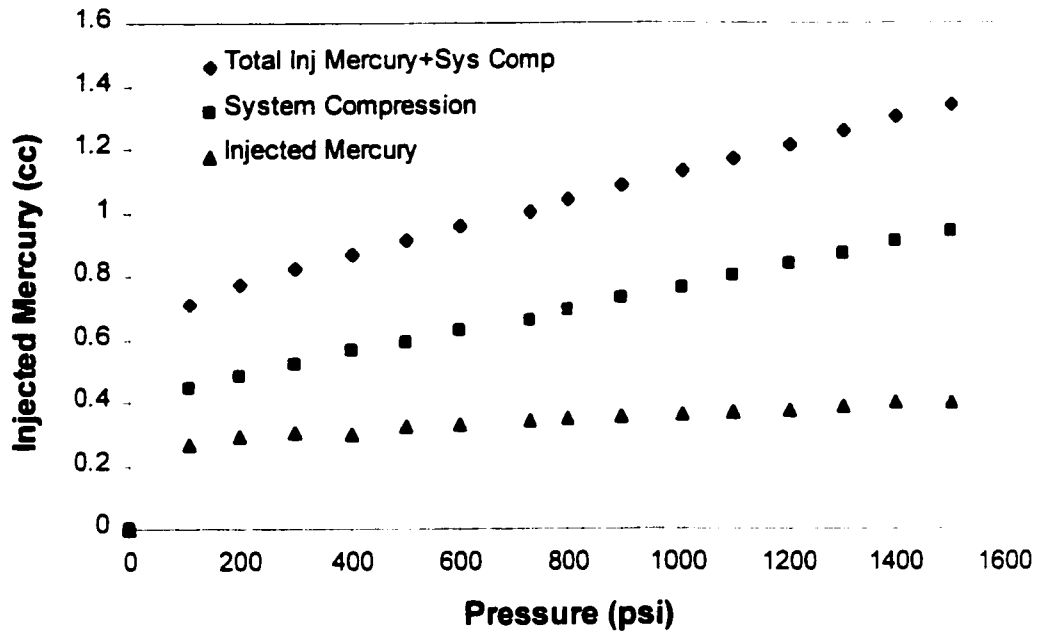
Figure A-4 Mercury intrusion test 1 on Luscar coal
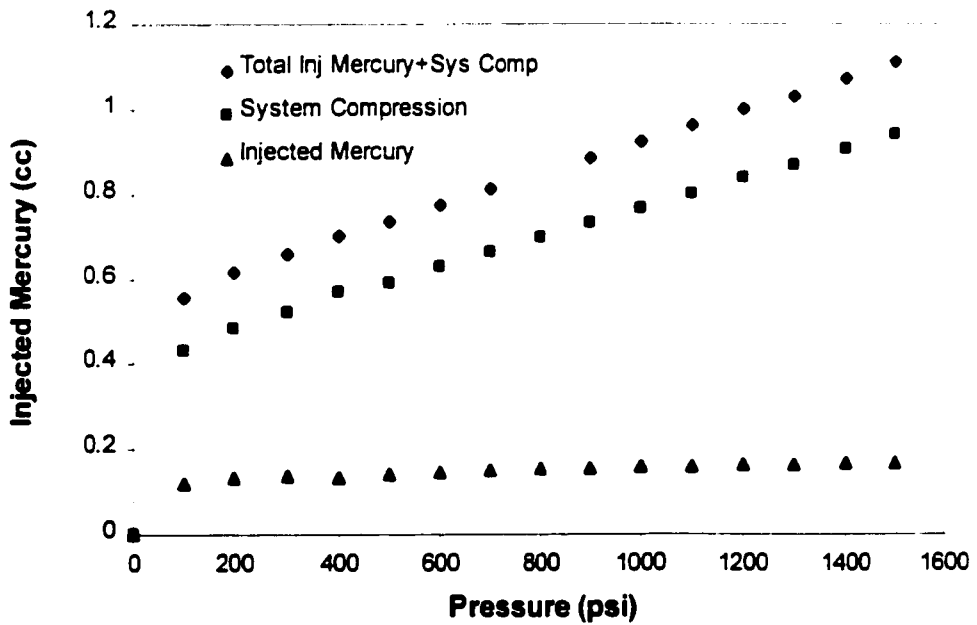
Figure A-5 Mercury Intrusion Test 2 on Luscar Coal
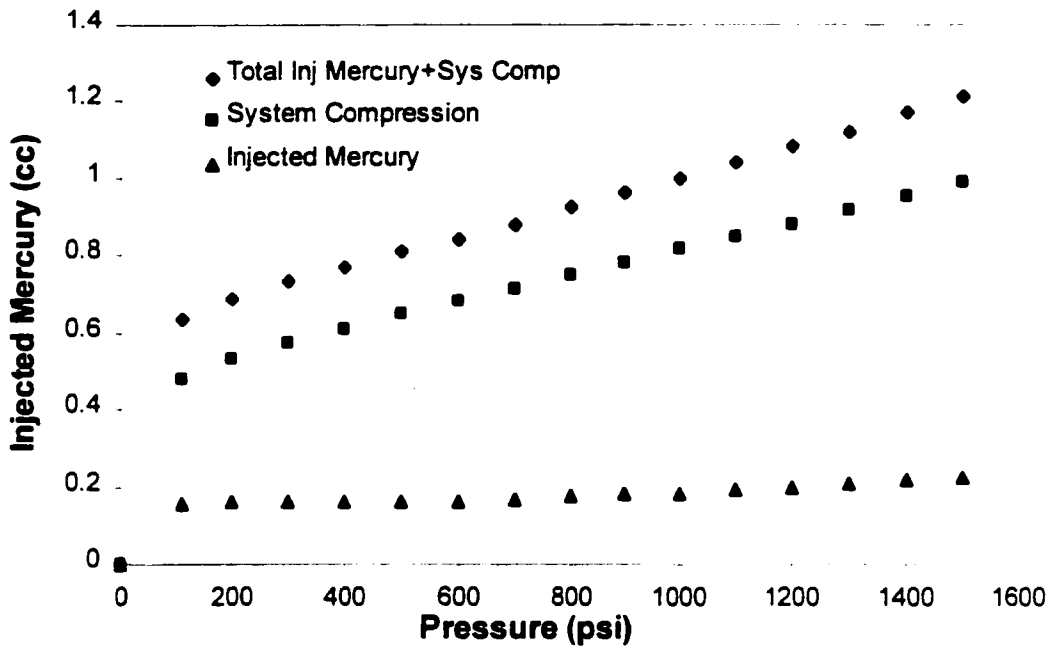
Figure A-6 Mercury Intrusion Test 3 on Luscar Coal
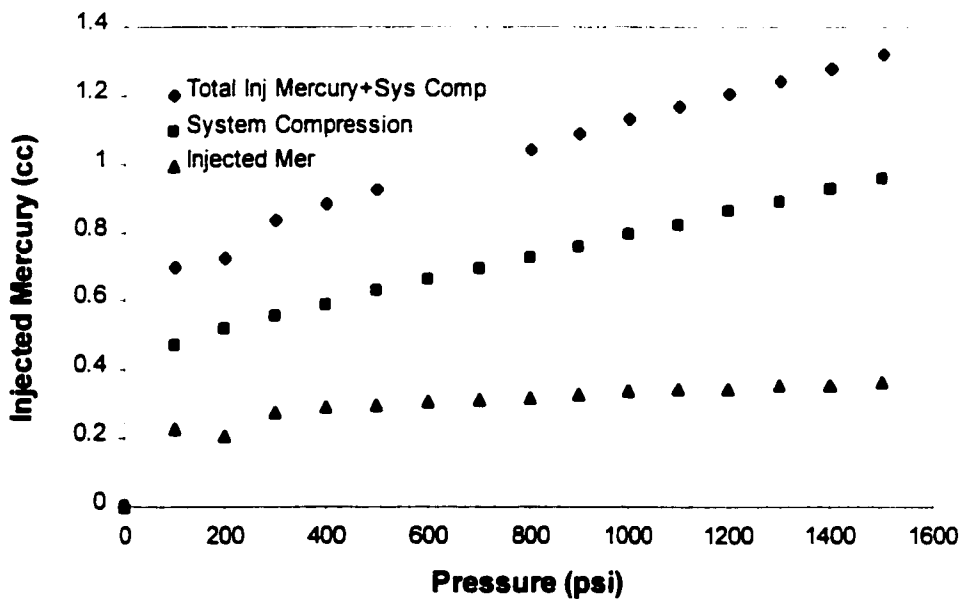
Figure A-7 Mercury Intrusion Test 4 on Luscar Coal

146
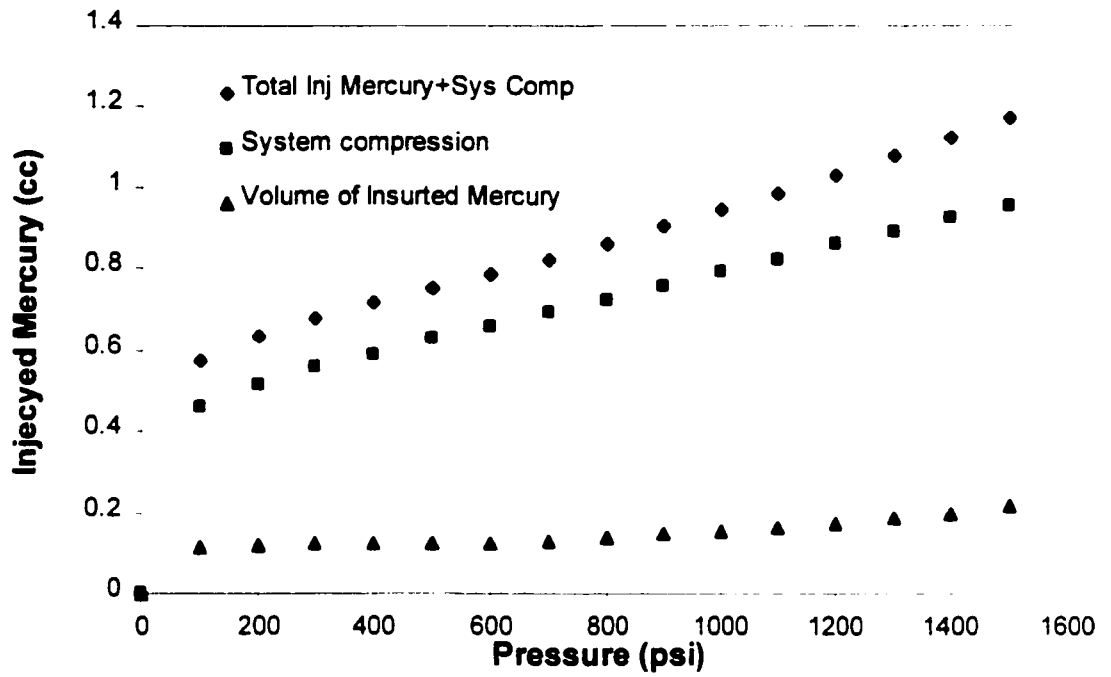
Figure A-8 Mercury Intrusion Test 5 on Luscar Coal

APPENDIX B TRIAXIAL CELL DE SIGN

This Appendix contains the detailed design procedure of the high pressure double wall triaxial cell.

Test Conditions for Cell

- Temperature: the temperature will range from ambient to around $99°$.

- Pore pressure will range from 0 to 20 MPa.

- The confining effective stress σ_3' will range from 0 to 25 MPa.

- Assuming $(\frac{\sigma_1'}{\sigma_3})= 3$ and $(\sigma_1 - \sigma_3) = 50MPa$, we find $\sigma_1 = 95MPa$.

- $\sigma_3 = 45MPa$.

The cell body was chosen to tolerate the previous confining pressure. The body is the same steel used in well casing, the steel properties are presented in the following table:

Size O.D.	Weight	Inside Diameter	Grade	Burst Pressure	Tensile Strength	Collaps Pressure
in	per foot pound	in		psi	Pounds	Psi
5 ½"	20	4.778	N - 80	9,190	382,000	7,540

Table B-1 Cell Body Properties

The threads for both end caps were designed according to ASME screw threads manual:

Load Calculation:

$$A = \frac{\pi * 12.136^2}{4} = 115.67cm^2 = 11.567 * 10^{-3} m^2$$

V_y = 45*1000*11.567*10^{-3} = 520.515KN

V_y = 520.515*224.81 = 117024 Pounds

149

The American National Standards Stub Acme Threads 4G was chosen for the design.

- D = 5.5"
- n = 10
- P = 0.1
- E = D – 0.3*P = 5.5 – 0.3 * 0.1 = 5.47"
- K = D – 0.6*P = 5.5 – 0.6 * 0.1 = 5.44"

External Threads (Screw)

1- Major diameter Max = D = 5.5"
2- Major diameter Min = D – 0.05*P = 5.5 – 0.05 * 0.1 = 5.4995"
3- Pitch diameter Max = E – 0.0091 = 5.47 – 0.0093 = 5.460619"
4- Pitch diameter Min = 5.460619 – 0.00785404 = 5.45276"
5- Minor diameter Max = K – 0.02 = 5.42"
6- Minor diameter Min = 5.42 – 0.0078504 = 5.41214"

Internal Threads (Nuts)

7- Major diameter Min = D + 0.02 = 5.5 + 0.02 = 5.52"
8- Major diameter Max = 5.52 + 0.0078504 = 5.5278504"
9- Pitch diameter min = E = 5.47"
10-Pitch diameter Max = 5.47 + 0.0078504 = 5.4778504"
11-Minor diameter Min = K = 5.44"
12-Minor diameter Max = 5.44 + 0.05 * P = 5.44 + 0.005 = 5.445"

- Pitch P = 1/10 = 0.1"
- Basic thread height h = 0.3 * P = 0.3 * 0.1 = 0.03"
- Basic thread thickness t = 0.5 * P = 0.5 * 0.1 = 0.05"

- Basic flat at crest F_{cn} = 0.4224 * P = 0.4224 * 0.1 = 0.04224" Internal threads.
- Basic flat at crest F_{cs} = 0.4224 * P = 0.4224 * 0.1 = 0.04224" External threads.

- Stress Area = $3.1416 * \left(\dfrac{Es + Ks}{4} \right)^2$ - the internal hole

Stress Area = $3.1416 * \left(\dfrac{5.45276 + 5.41214}{4} \right)^2 - \left(\dfrac{\pi * 4.778^2}{4} \right) = 5.2479 in^2$

- Shear Area = $3.1416 * K_n [0.5 + n * \tan 14.5 * (E_s - K_n)]$

Shear Area = $3.1416 * 5.445 * [0.5 + 10 * \tan 14.5 * (5.45276 - 5.445)] = 8.89$ in^2 per one inch length.

Threads Strength

The Tensile Strength = 382000/5.8282 = 65543.2 psi.

The Applied Stress = 117024/5.2479 = 22299.205 psi.

FS = 65543.2/22299.205 = 2.9

Length of engagement:

Assuming that the shear strength is 0.5 of the tensile strength

$$Le = \dfrac{2 * As}{\pi * n * Kn_{max} \left[\dfrac{1}{2n} + 0.57735(Es_{min} - Kn_{max}) \right]}$$

$$Le = \frac{2 * 5.4214}{\pi * 10 * 5.445 * \left[\dfrac{1}{2 * 10} + 0.57735(5.45276 - 5.445)\right]}$$

Le = 1.126 = 1.5 in

Shear Area = 1.5 * 8.89 = 13.335 in^2

Assuming the shear strength is 0.5 * the tensile strength:

Shear Strength = 0.5 * 65543 = 32771.5 psi

The Applied Shear stress = 117024/13.335 = 8775.7 psi

FS = 32771.5/8775.7 = 3.7

The Top Plate Strength

Using 15 mm thick steel plate with the same casing properties the shear area was calculated as follow:

Shear Area = π * 3.5968 * 0.59 = 6.673 in^2

The Applied Shear Stress = 117024/6.673 = 17537 psi

FS = 32771.5/17537 = 1.87
The plate will tolerate the applied stress.

APPENDIX C CALIBRATION

This Appendix presents the calibration plots of all transducers used during the permeability tests. This includes differential pressure transducer for permeability measurements, differential pressure transducer for volume change measurement, LVDT to measure the volume of adsorbed gas, pressure transducers to measure pressure in all the pumps used during the tests.

Differential Pressure Transducer Calibration
April 17 1999

(a)

$y = 2.0497x - 0.1903$
$R^2 = 0.9999$

Differential Pressure (psi) vs Output (Volt)
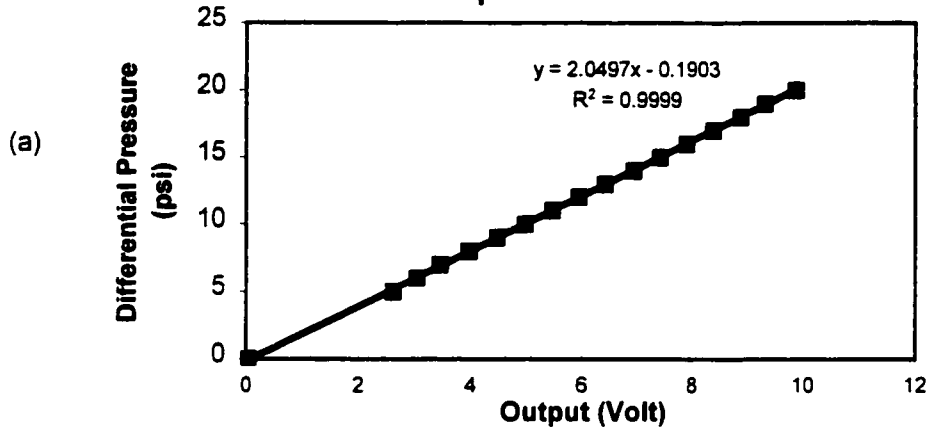
Differential Pressure Transducer Calibration
May 3 1999

(b)

$y = 10.948x + 4.8285$
$R^2 = 1$

Differential Pressure (psi) vs Output (Volt)
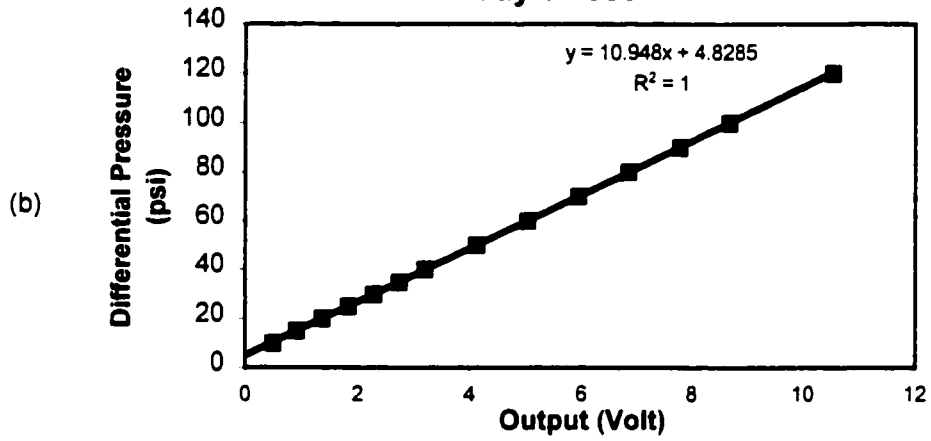
Differential Pressure Transducer Calibration
Jun 10 1999

(c)

$y = 20.032x - 3.7382$
$R^2 = 1$

Differential Pressure (psi) vs Output (Volt)
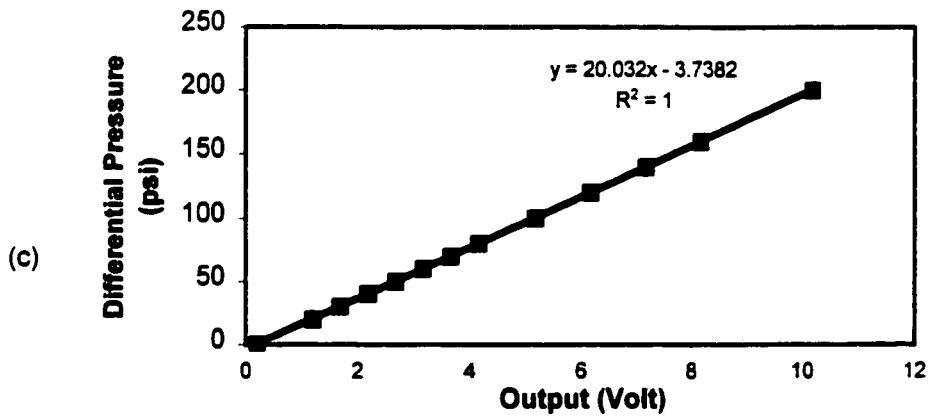
Figure C-1 Permeability Differential Pressure Transducer Calibrations

154
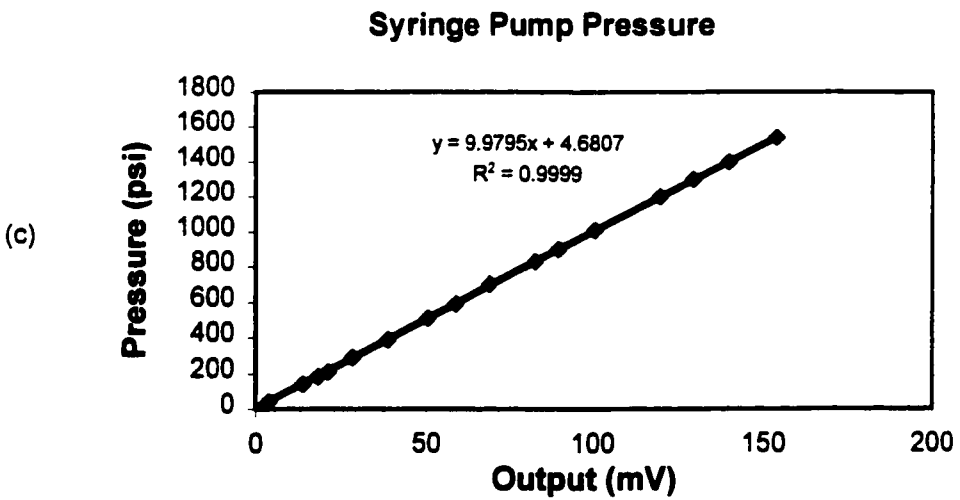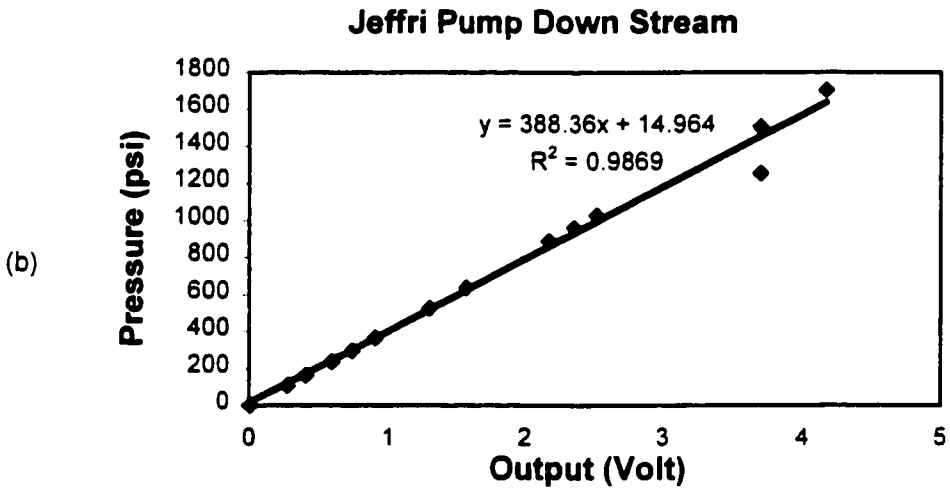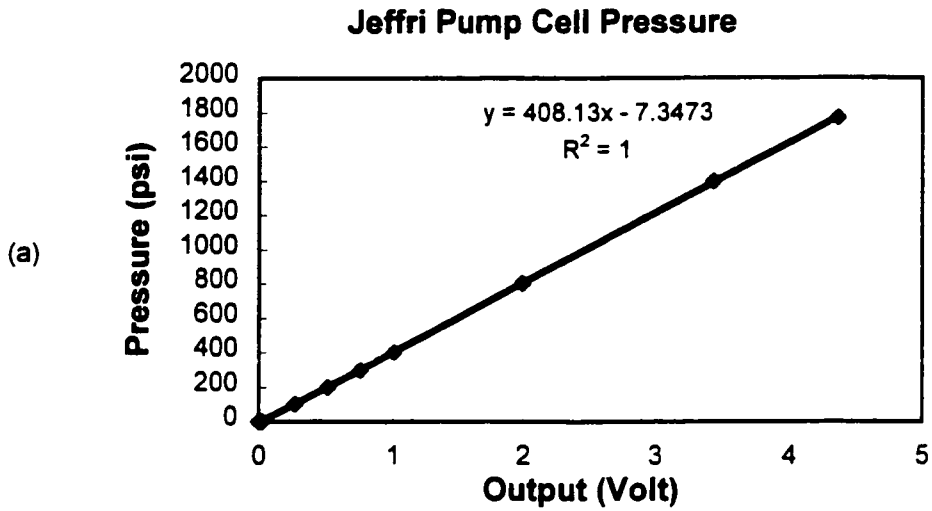
Figure C-2 Pressure Transducer Calibrations

DP volume change

$$y = 2.0211x + 0.0476$$
$$R^2 = 0.9996$$
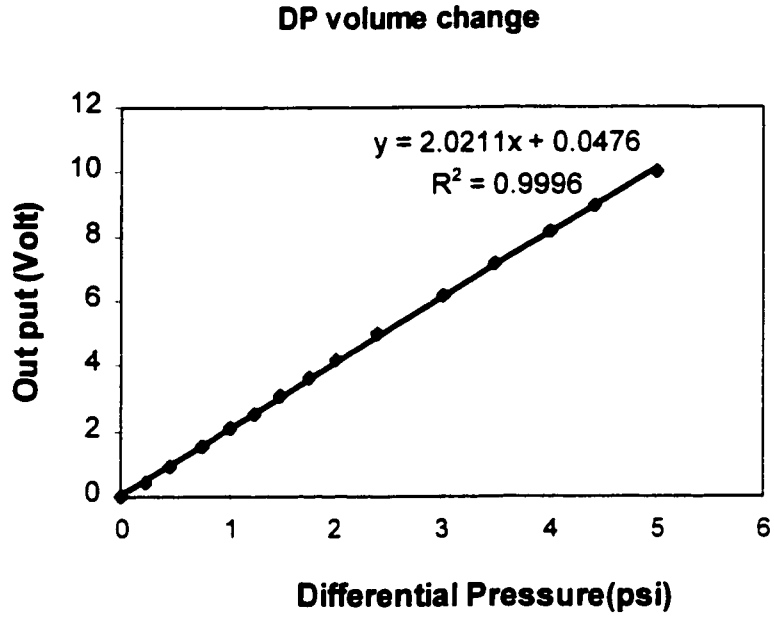
Figure C-3 Volume Change Differential Pressure Transducer Calibration

LVDT for Volume of Pumped Gas

$$y = -25.194x + 47.182$$
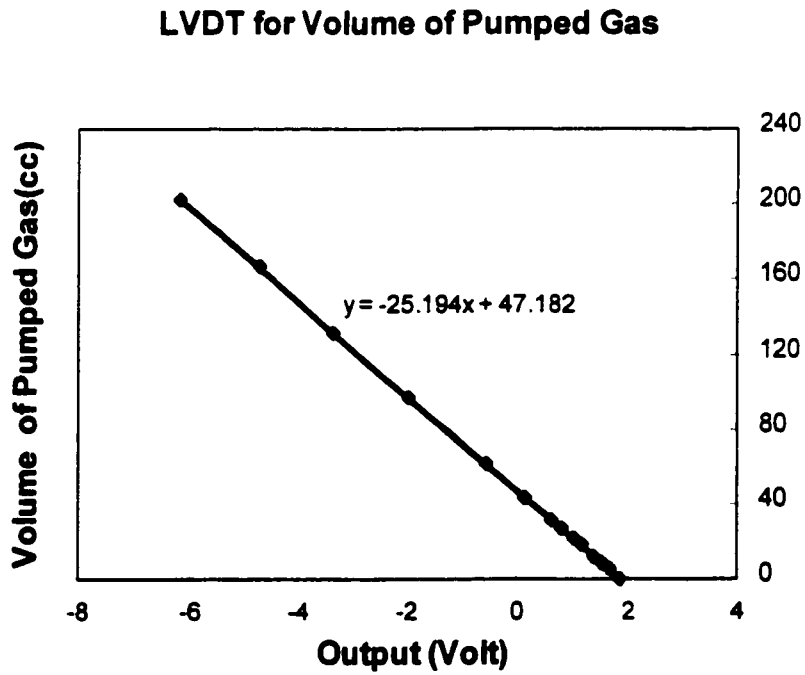
Figure C-4 LVDT Calibration

APPENDIX D ADSORPTION AND PERMEABILITY RESULTS

This Appendix contains all adsorption and permeability results for Cardinal River and Luscar Coals.

A total of four samples were used in the tests, two for testing using Methane and two samples for testing adsorption and permeability with CO_2 as the permeable fluid.

Samples have the same diameter (around 24 mm) but varied in length between 35 to 50 mm. All samples were cored using a diamond coring machine and the coring was perpendicular on the bedding planes.
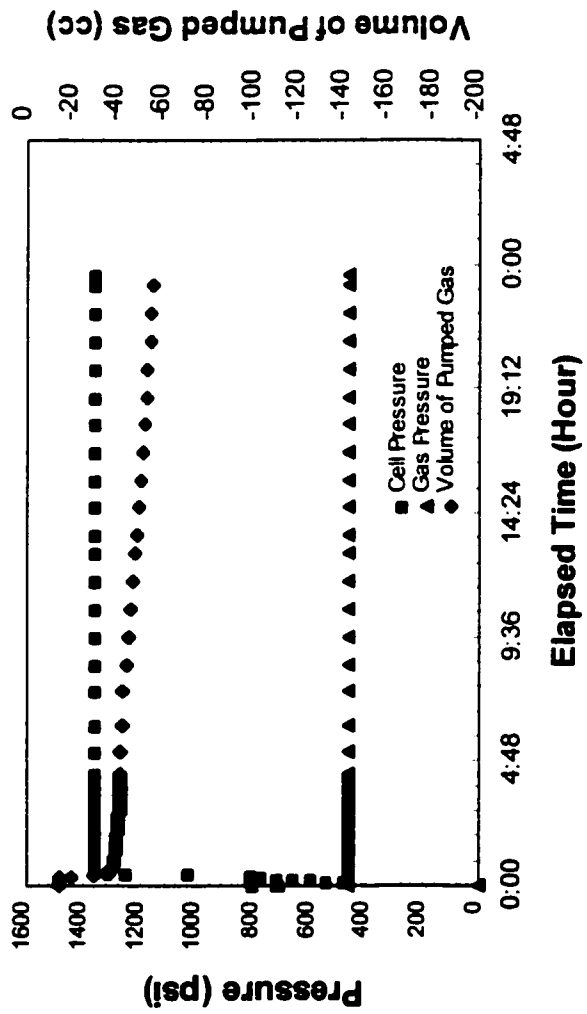
Figure D-1 Adsorption Test at 3.5 MPa, Cardinal River Coal, CR1 (CO₂)

158
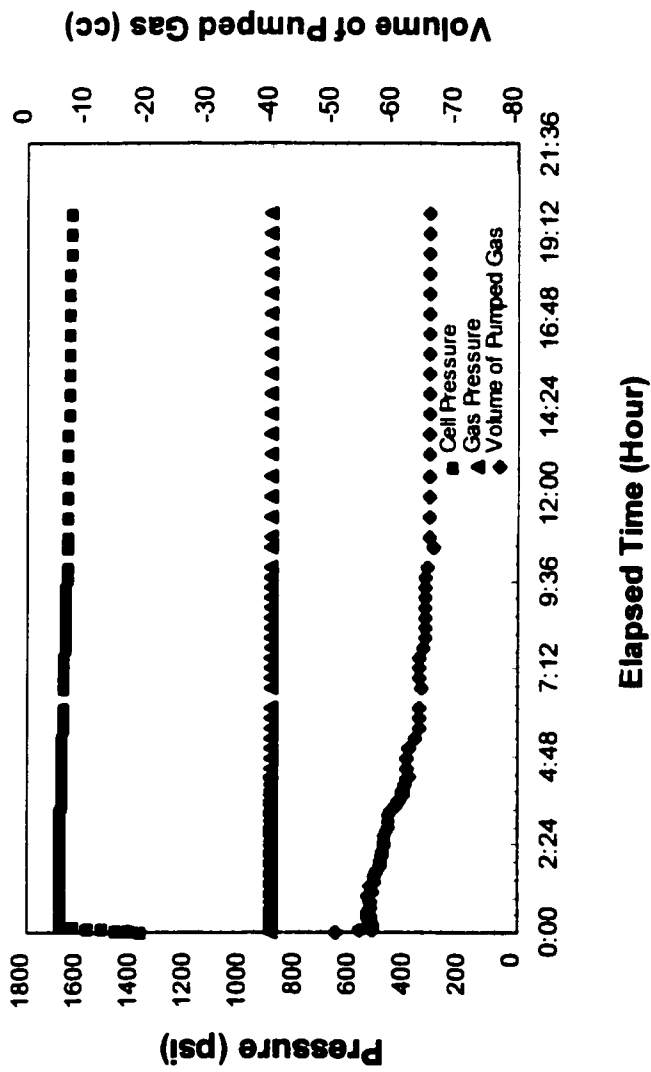
Figure D-2 Adsorption Test at 6.2 MPa, Cardinal River Coal, CR1 (CO_2)
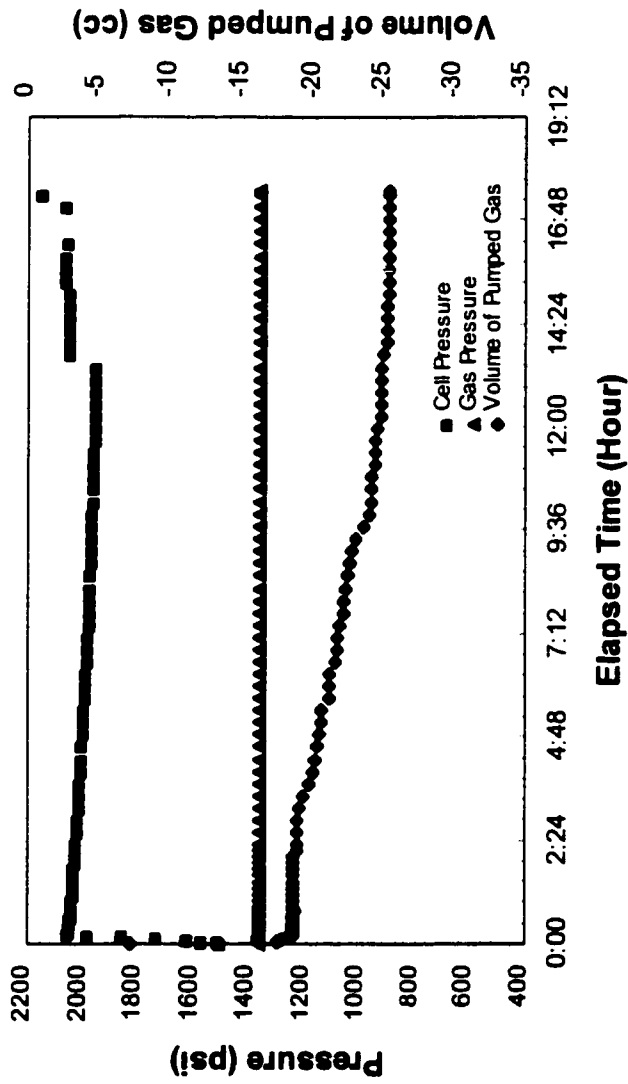
Figure D-3 Adsorption Test at 9.6 MPa, Cardinal River Coal, CR1 (CO₂)

160
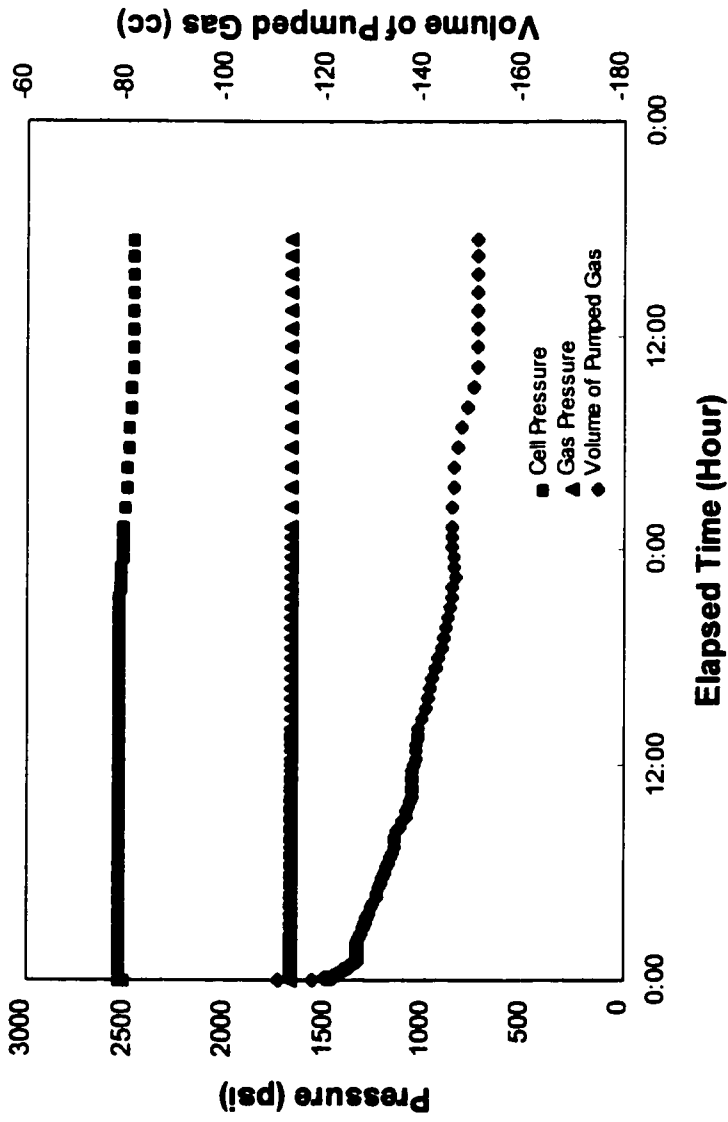
Figure D-4 Adsorption Test at 12 MPa, Cardinal River Coal, CR1 (CO₂)
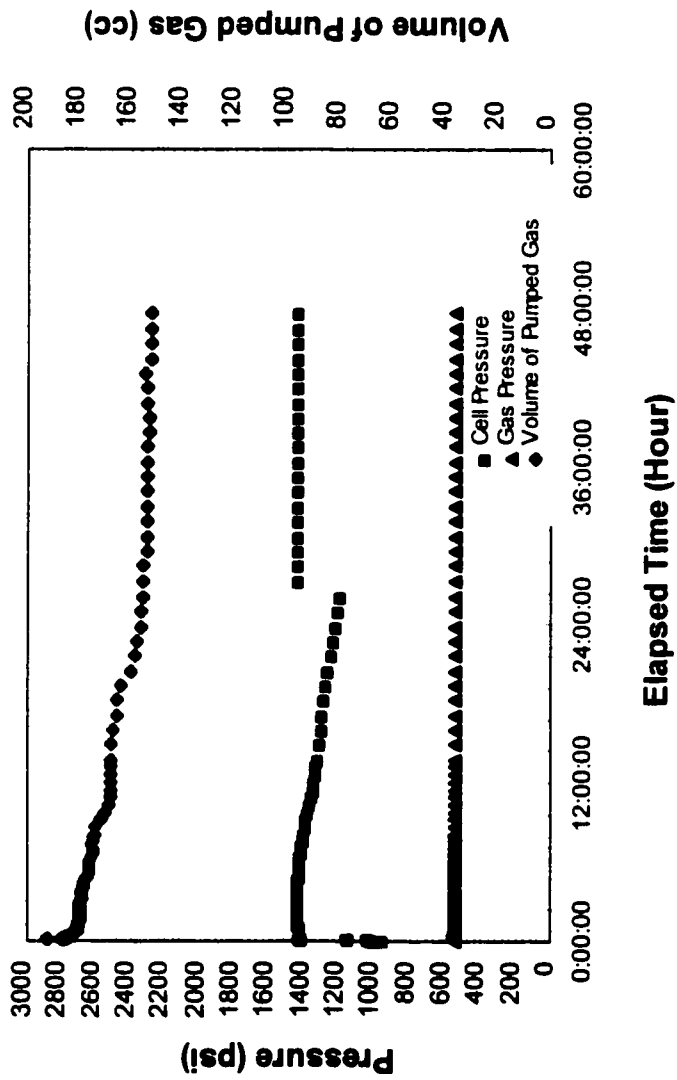
Figure D-5 Adsorption Test at 3.8 MPa, Luscar Coal, CV1 (CO₂)
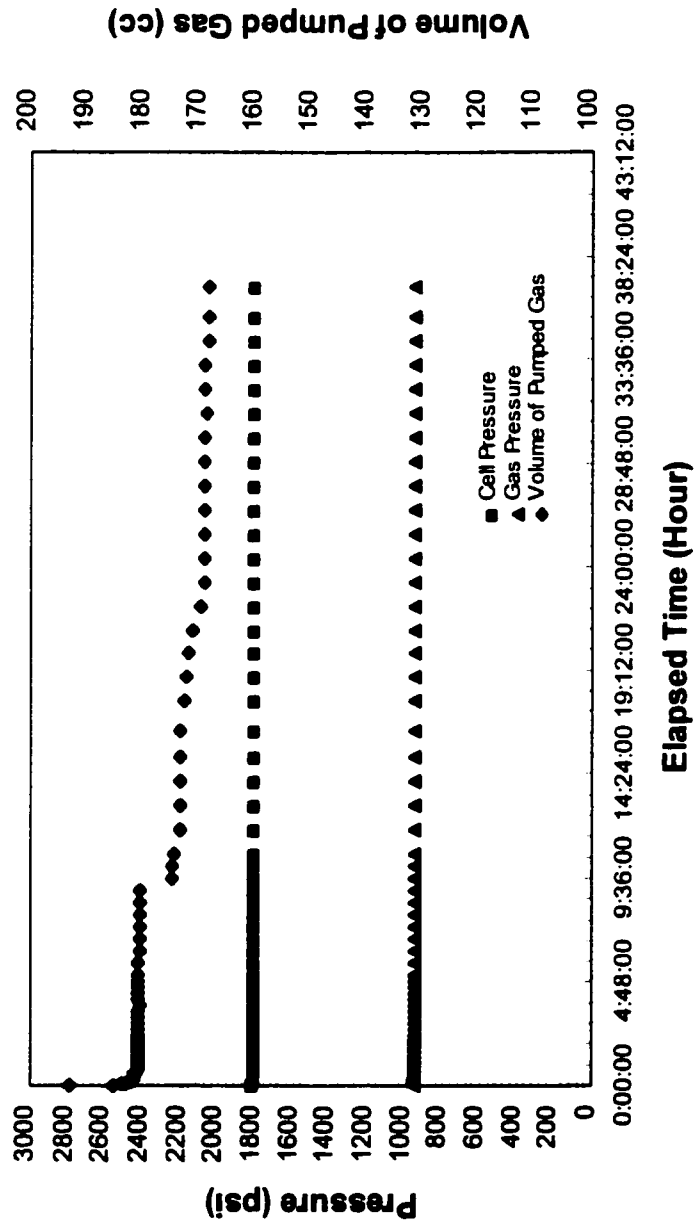
Figure D-6 Adsorption Test at 6.5 MPa, Luscar Coal, CV1 (CO₂)

163
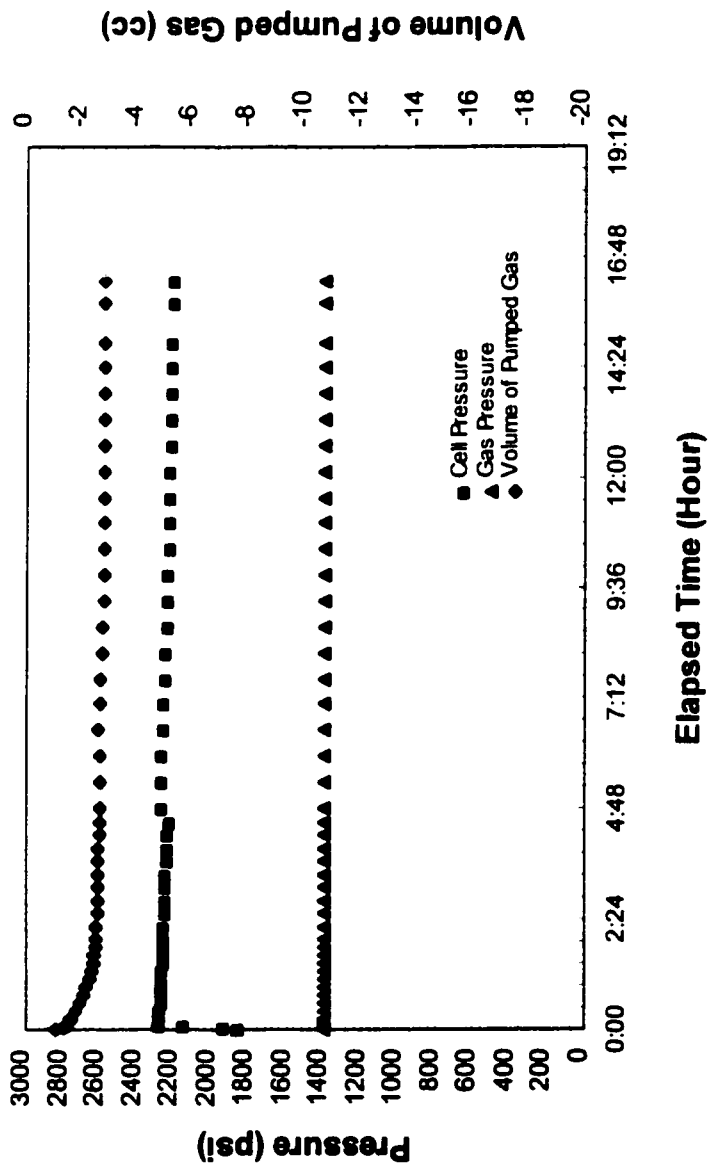
Figure D-7 Adsorption Test at 9.6 MPa, Luscar Coal, CV1 (CO₂)
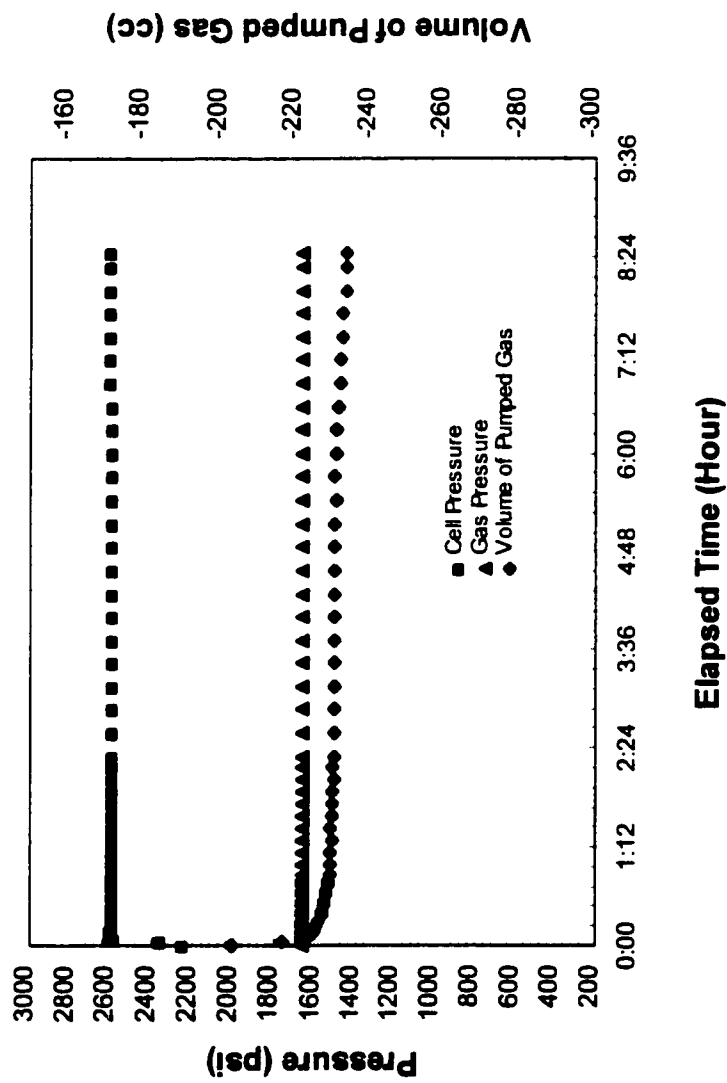
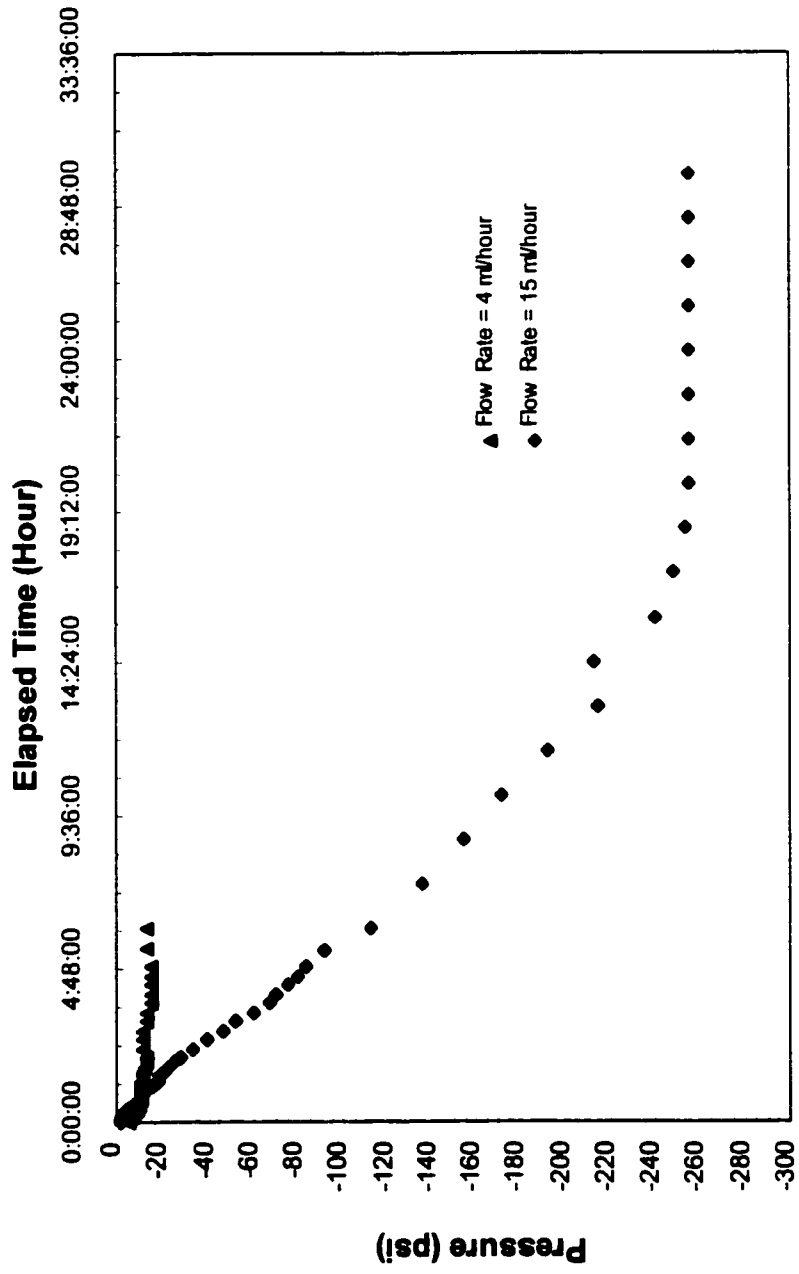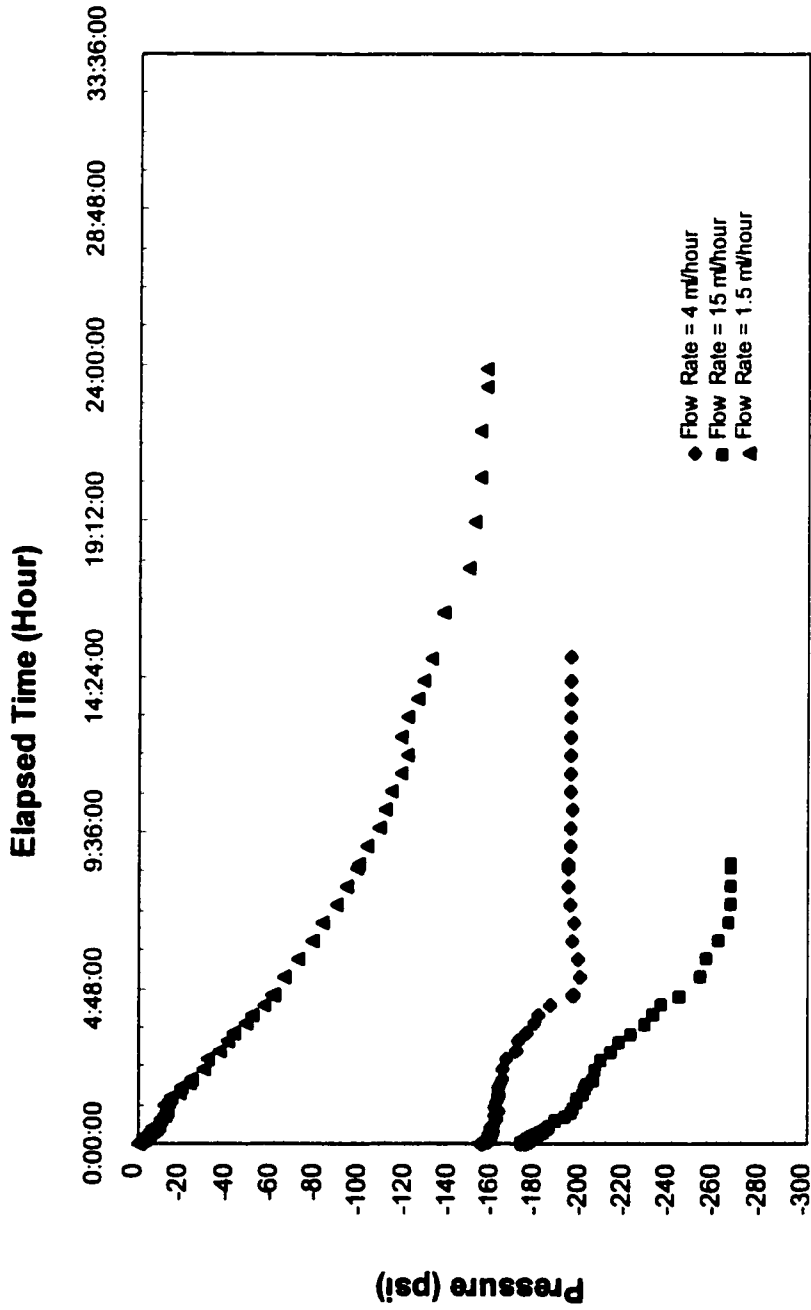**Figure D-8 Adsorption Test at 12 MPa, Luscar Coal, CV1 (CO₂)**
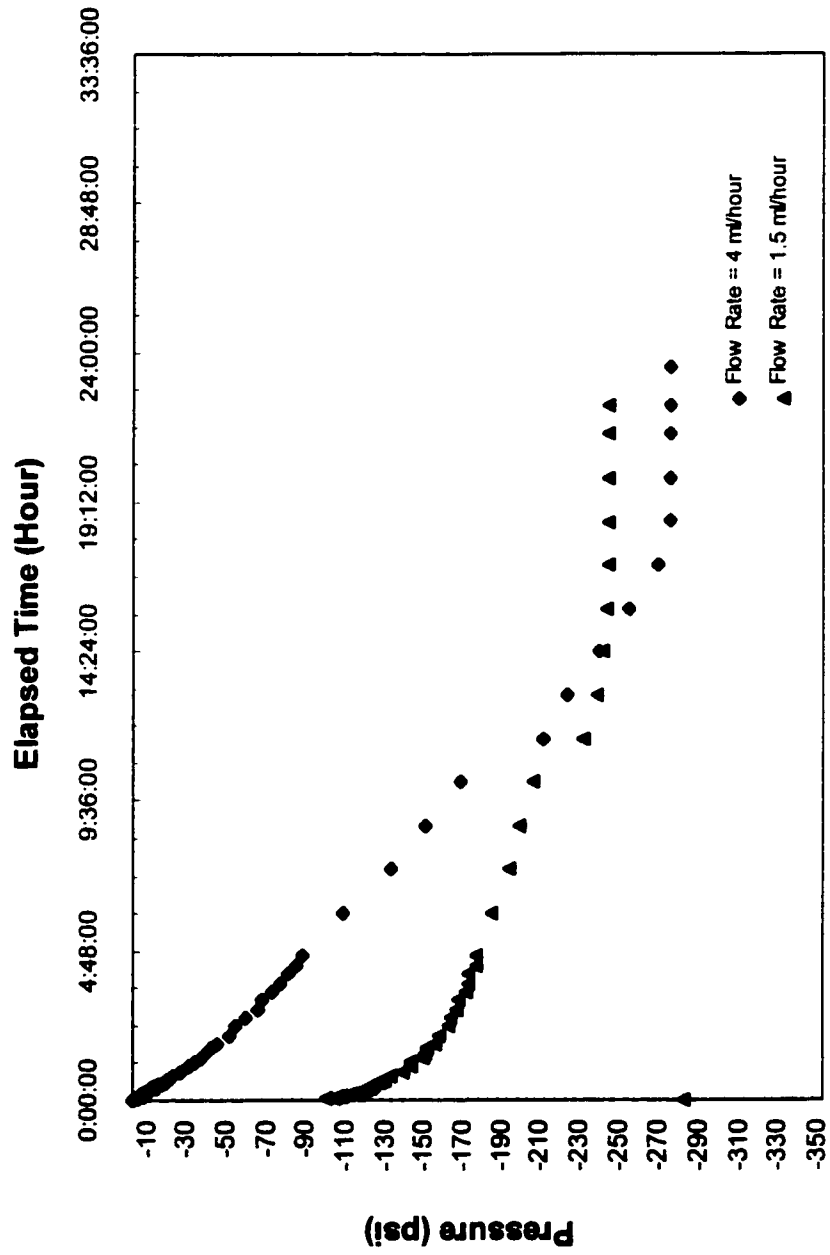
165
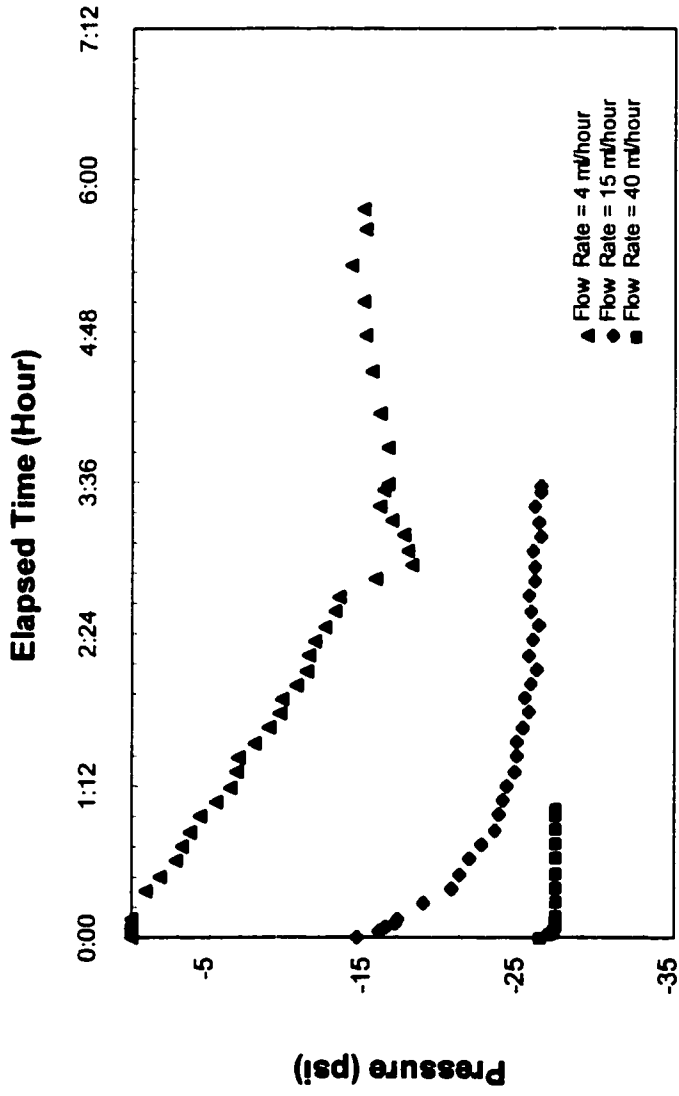
Figure D-9 Steady State Seepage at 3.8 MPa Gas Pressure and 6 MPa Effective Stress, CR1.
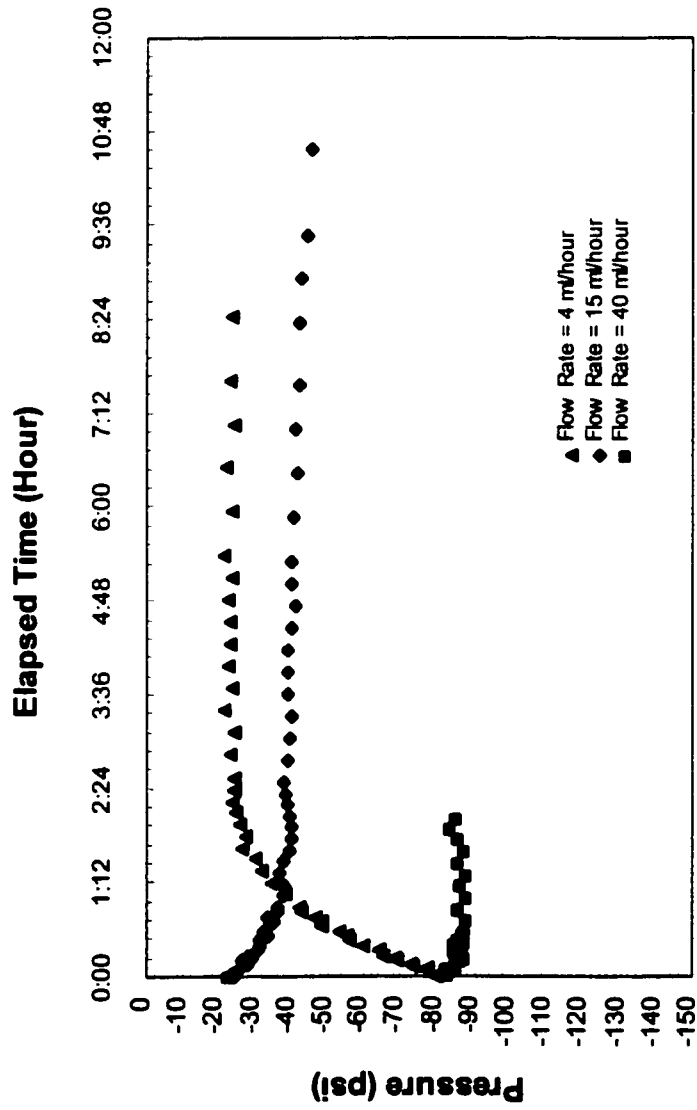
Figure D-10 Steady State Seepage at 9.6 MPa Gas Pressure and 6 MPa Effective Stress, CR1.
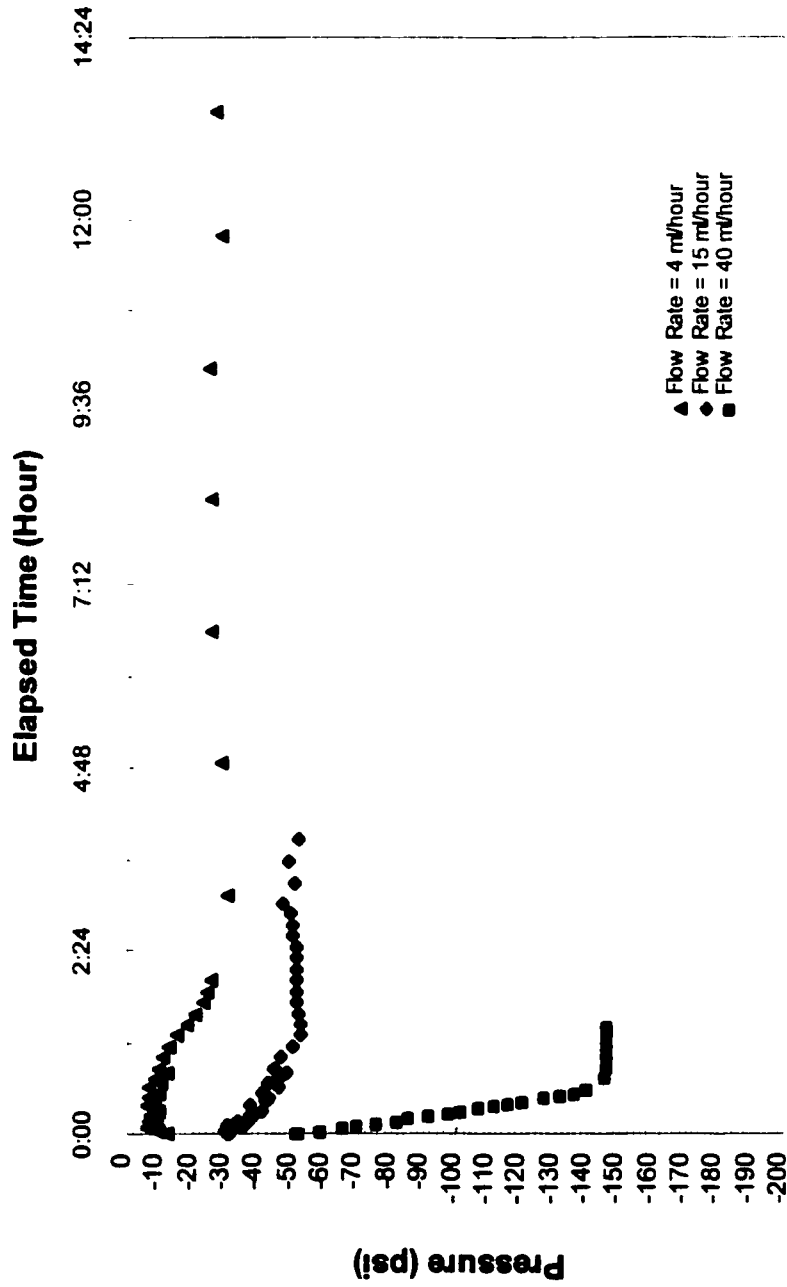
Figure D-11 Steady State Seepage at 12 MPa and 6 MPa Effective Stress, CR1
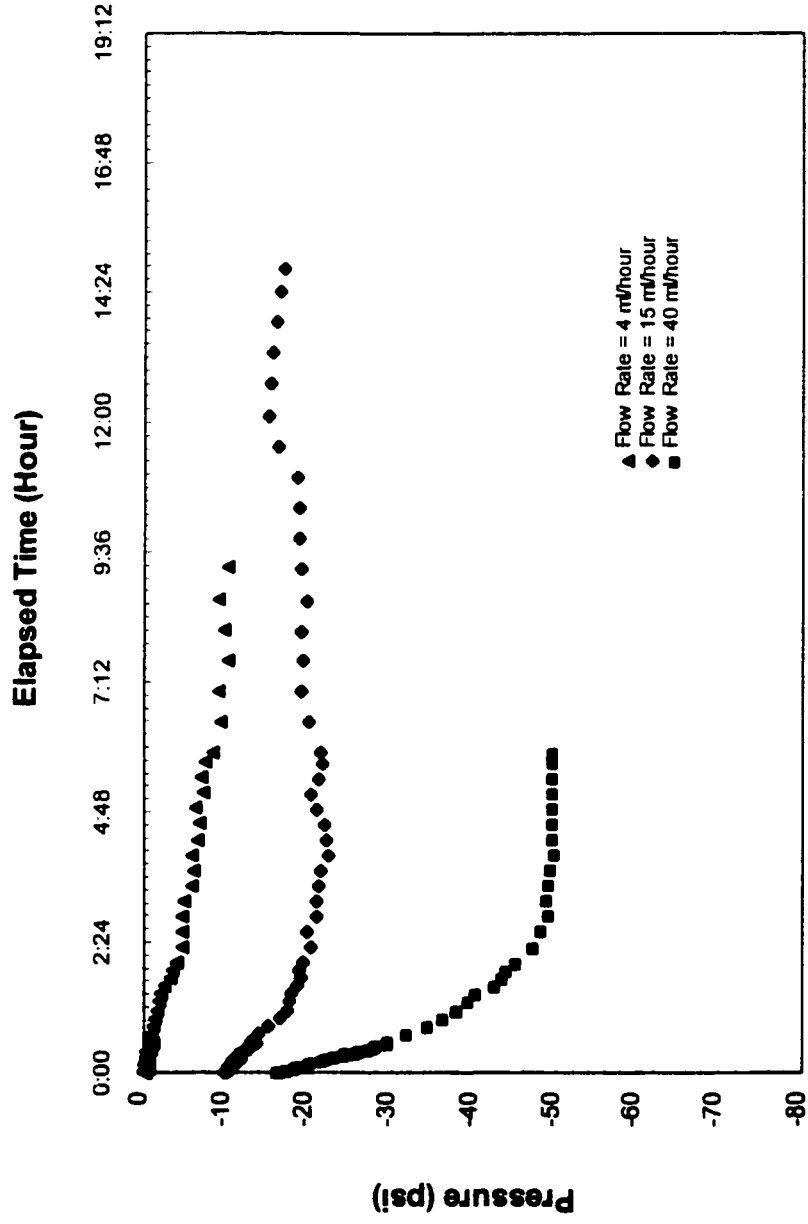
Figure D-12 Steady State Seepage at 3.5 MPa Gas Pressure and 10 MPa Effective Stress, CR1

169
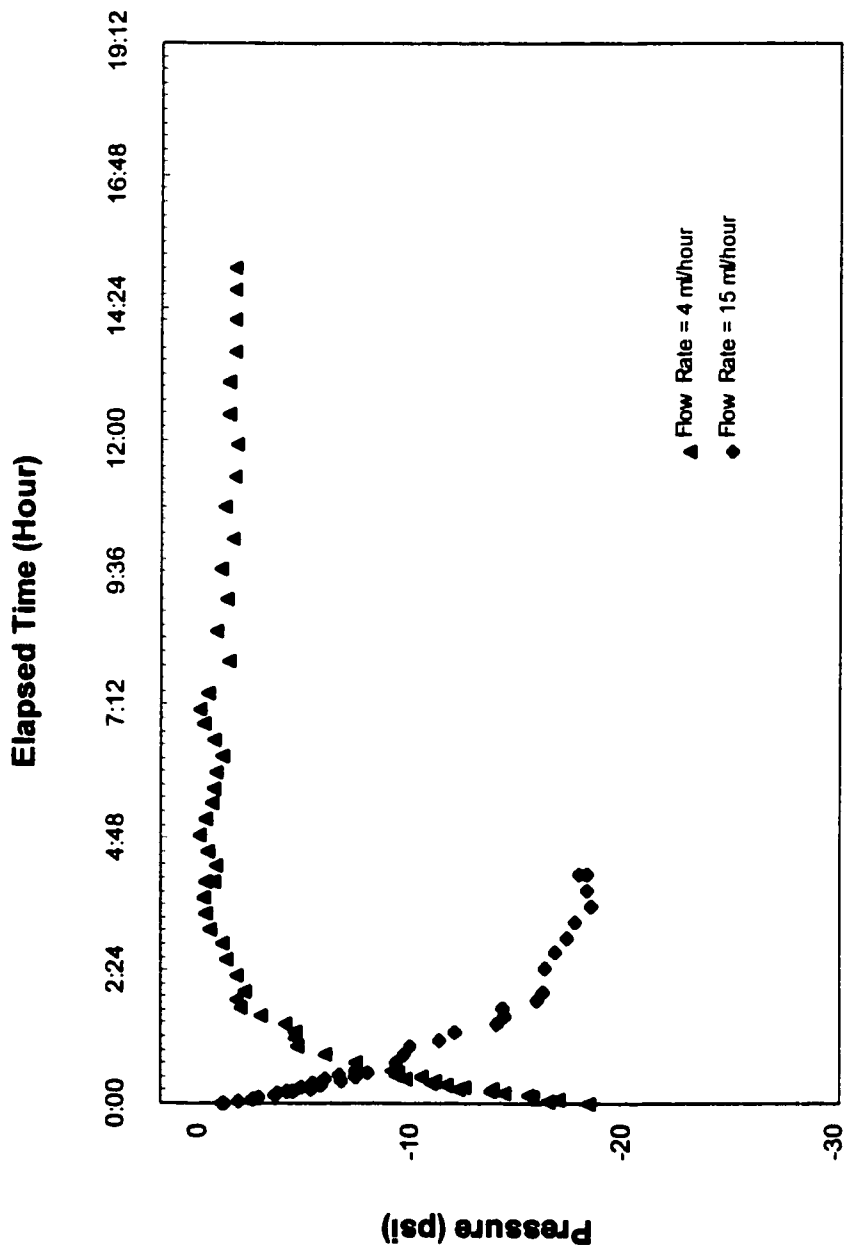
Figure D-13 Steady State Seepage at 5.5 MPa Gas Pressure and 10 MPa Effective Stress, CR1

170
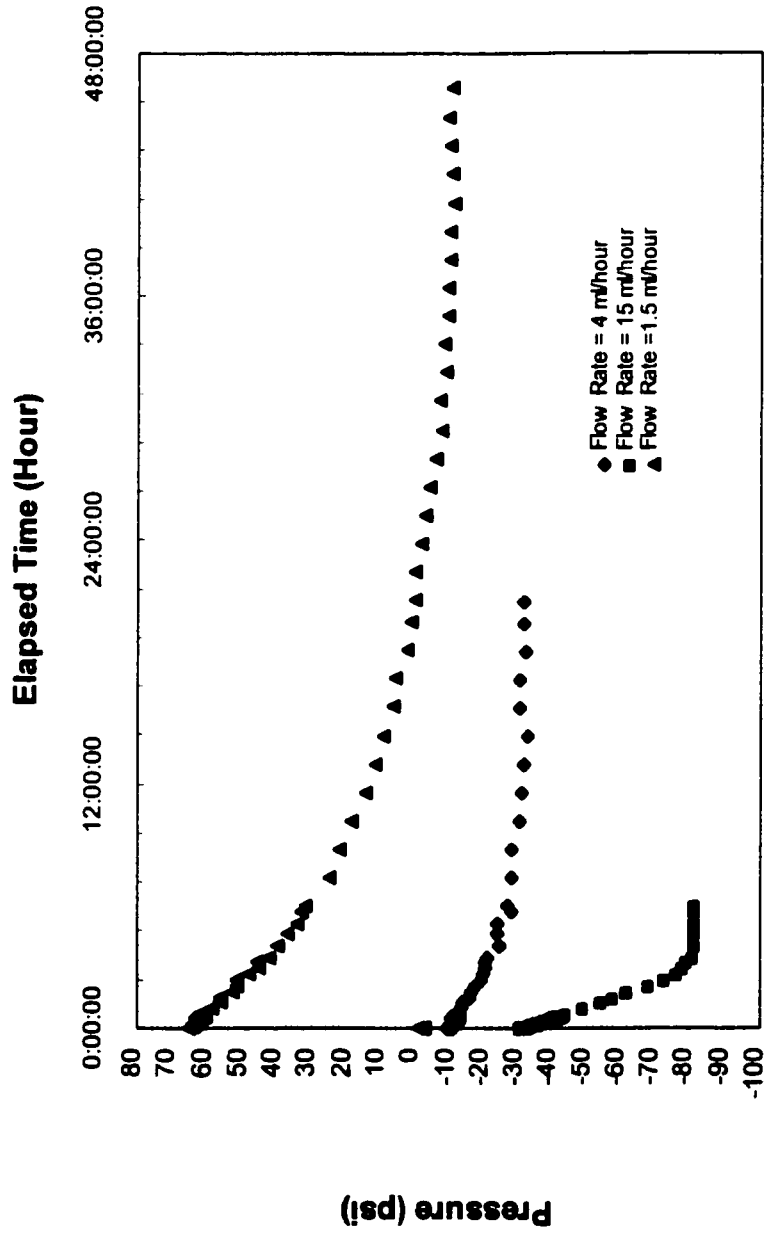
Figure D-14 Steady State Seepage at 8.3 MPa Gas Pressure and 10 MPa Effective Stress, CR1

171
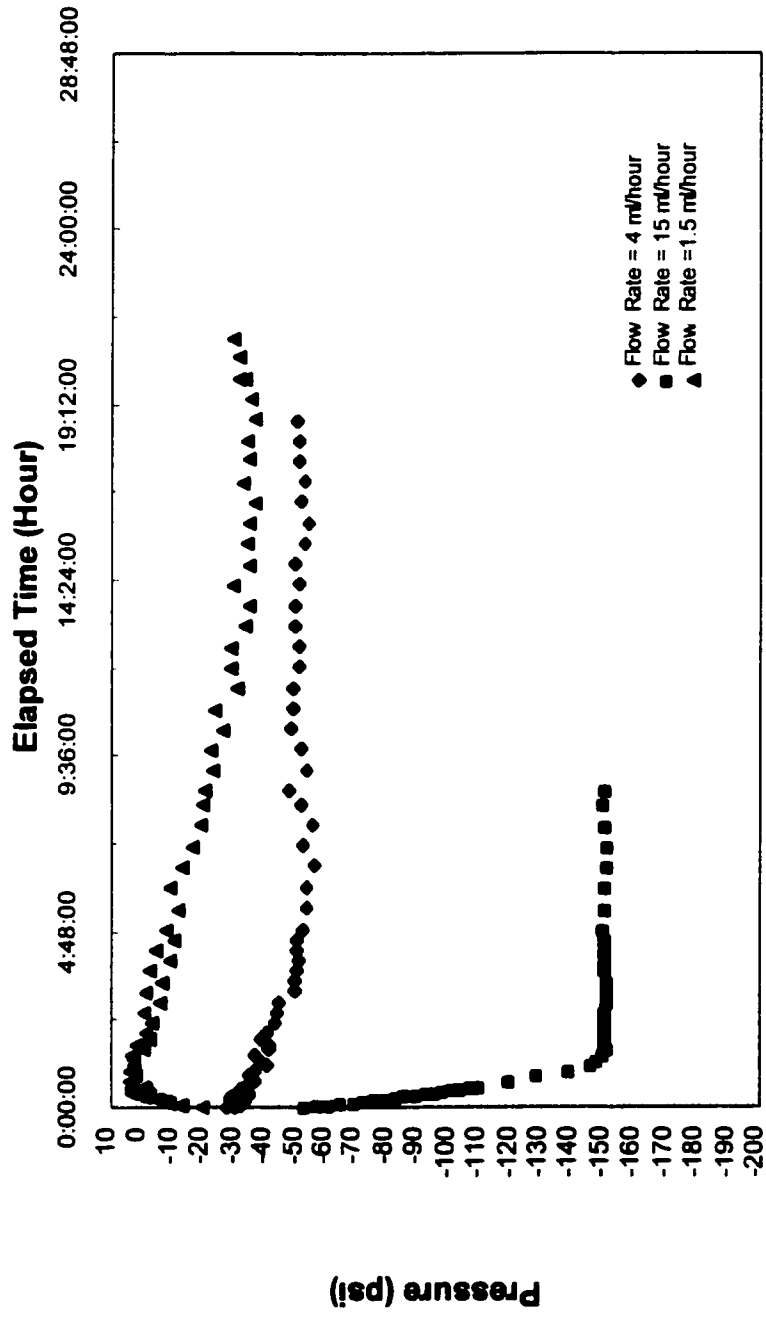
Figure D-15 Steady State Seepage at 12 MPa Gas Pressure and 10 MPa Effective Stress, CR1
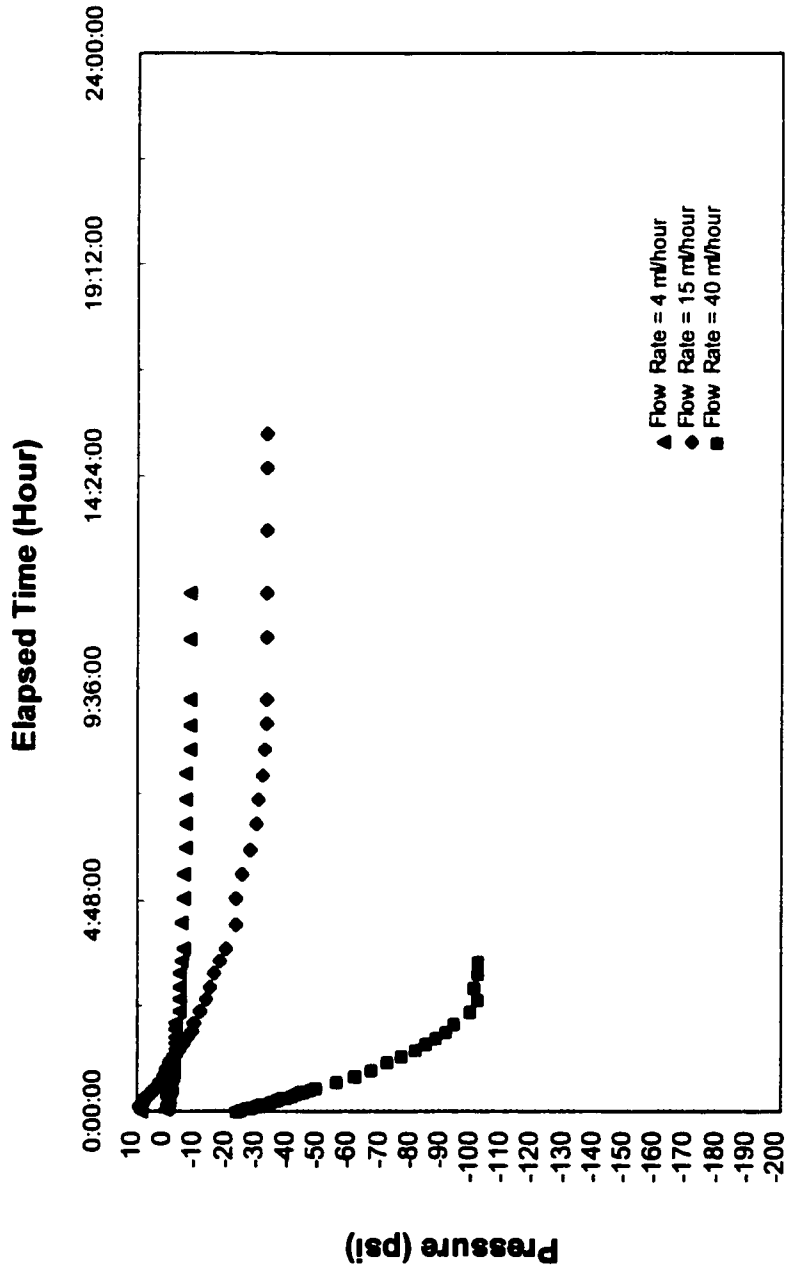
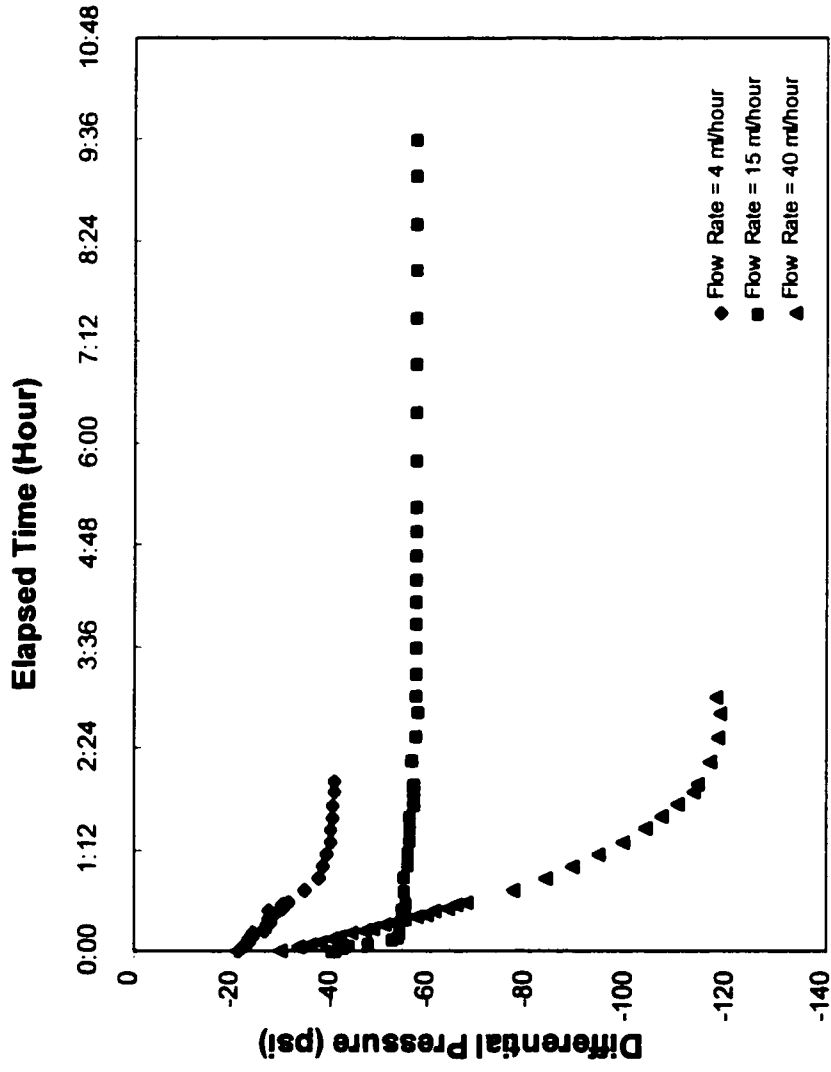**Figure D-16 Steady State Seepage at 4.5 MPa Gas Pressure and 16 MPa Effective Stress, CR1**
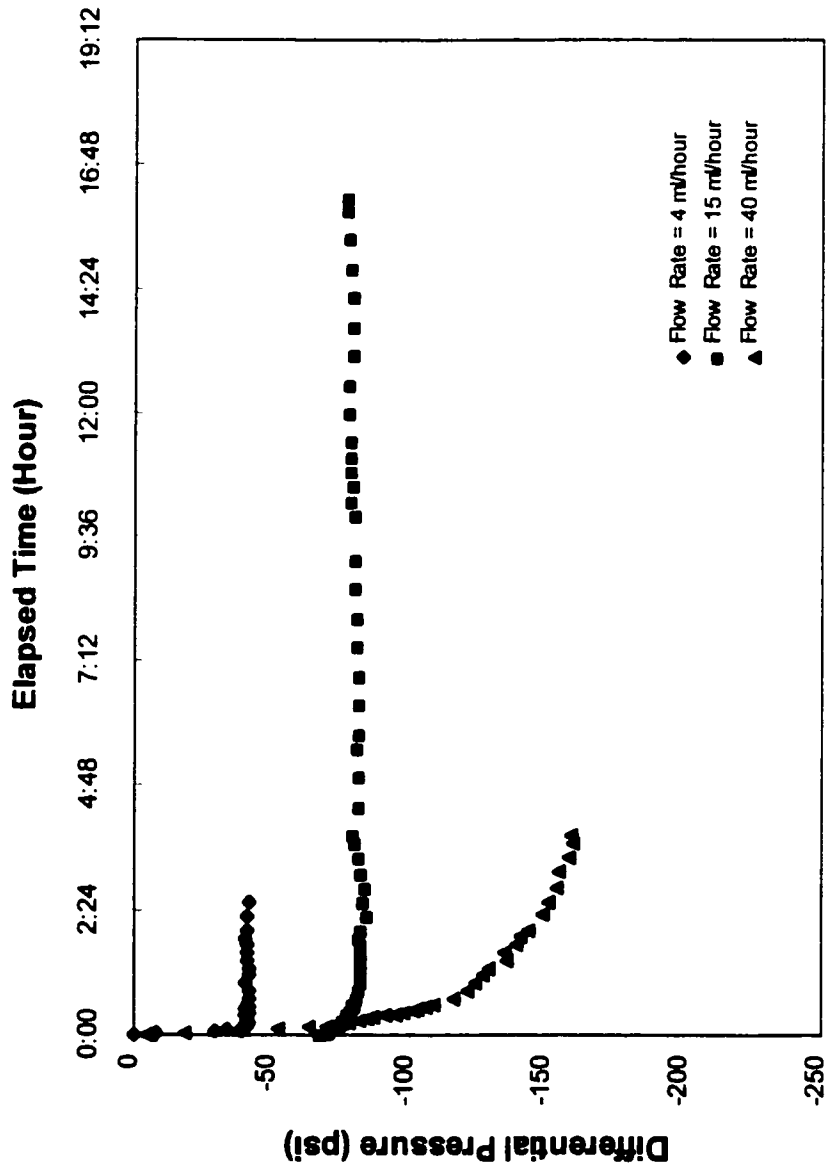
173
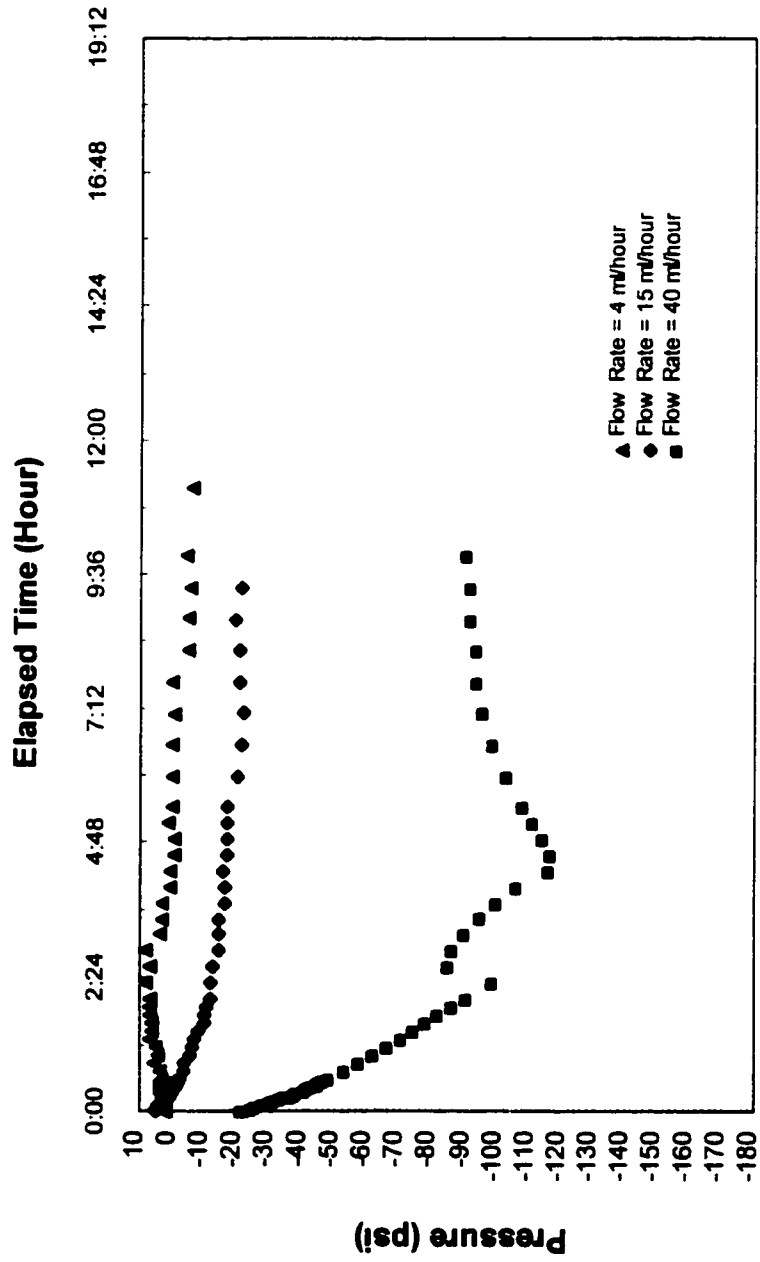
Figure D-17 Steady State Seepage at 6.3 MPa Gas Pressure and 16 MPa Effective Stress, CR1.

174
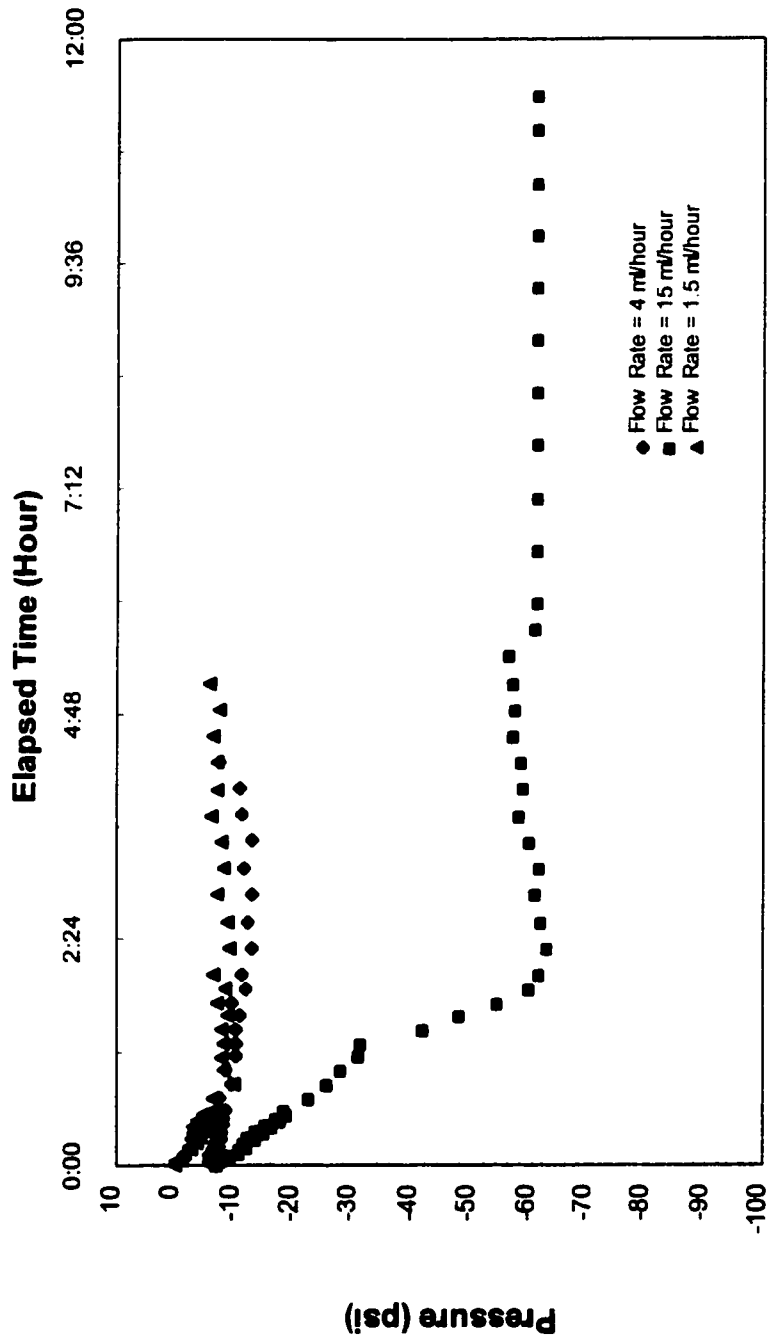
Figure D-18 Steady State Seepage at 8.3 MPa Gas Pressure and 16 MPa Effective Stress, CR1

175
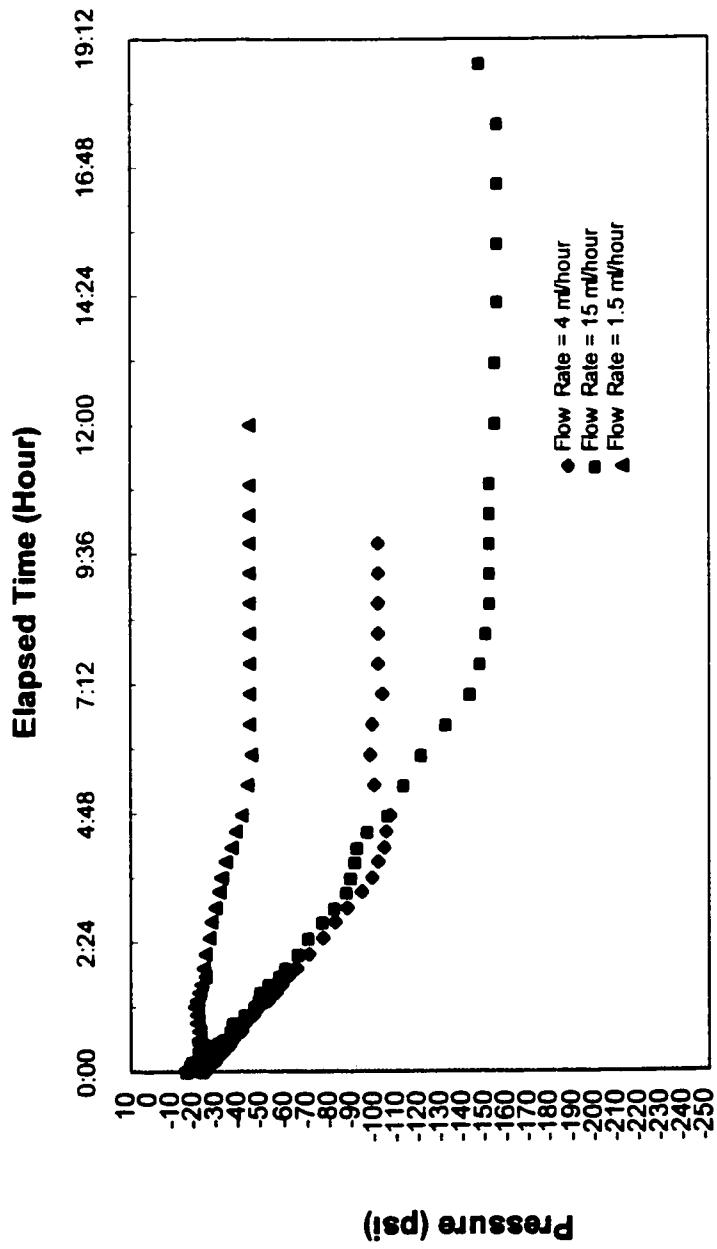
Figure D-19 Steady State Seepage at 10.3 MPa Gas Pressure and 16 MPa Effective Stress, CR1
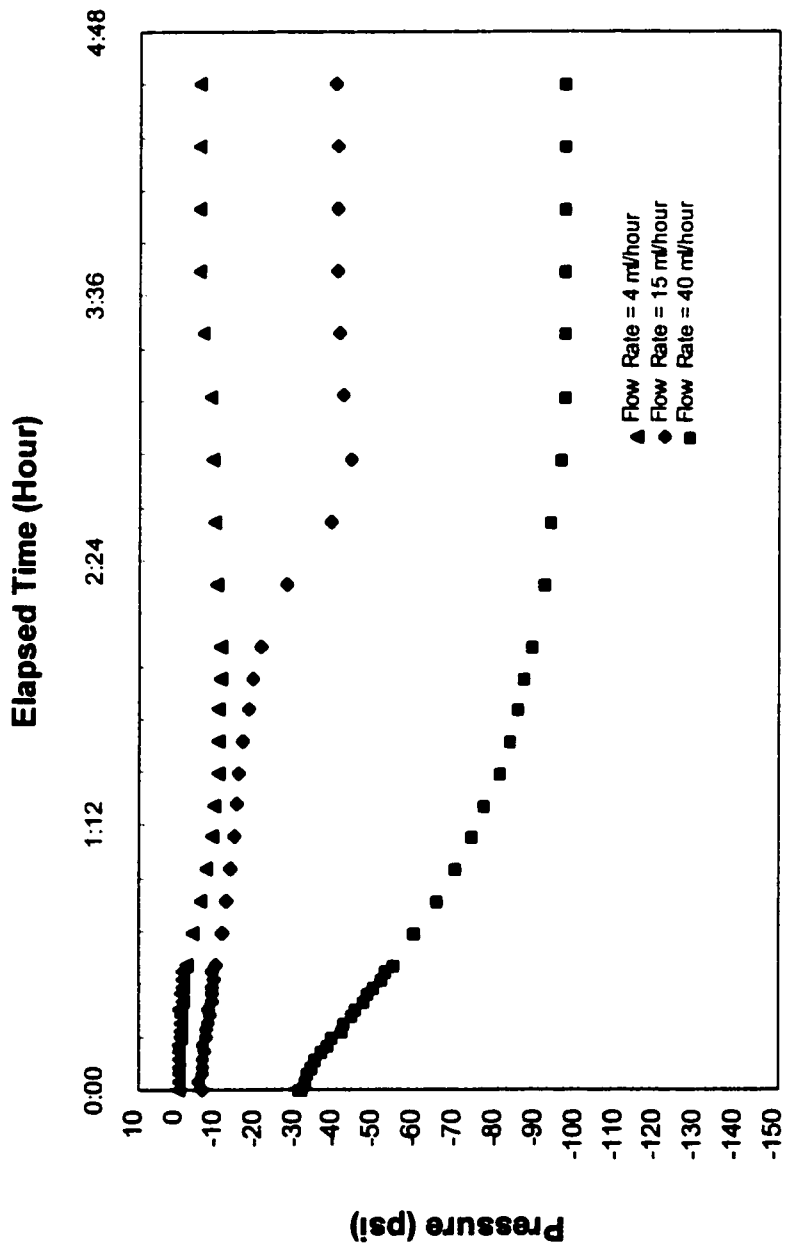
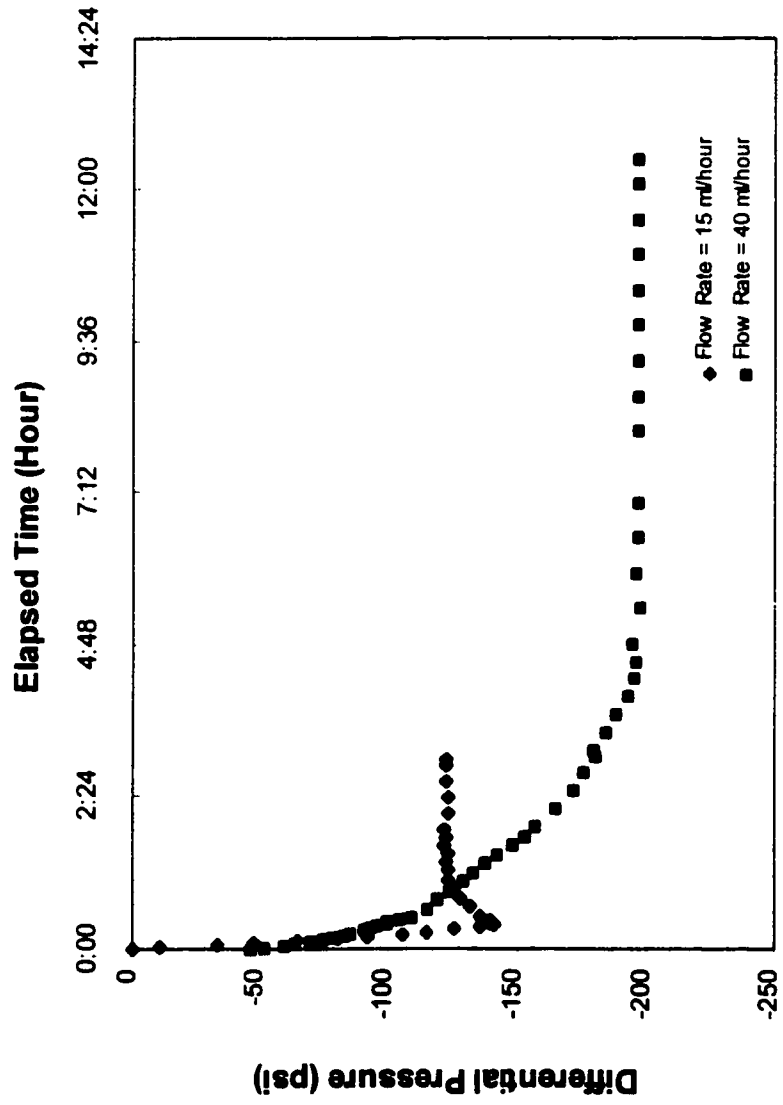Figure D-20 Steady State Seepage at 3.7 MPa Gas Pressure and 6 MPa Effective Stress, CV1
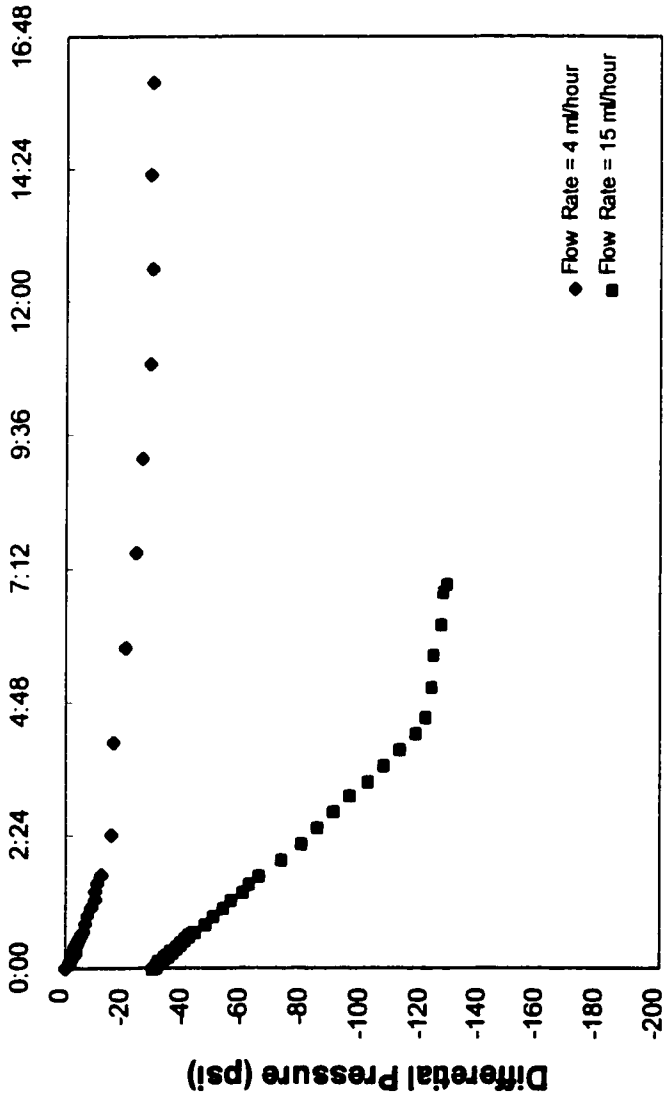
177
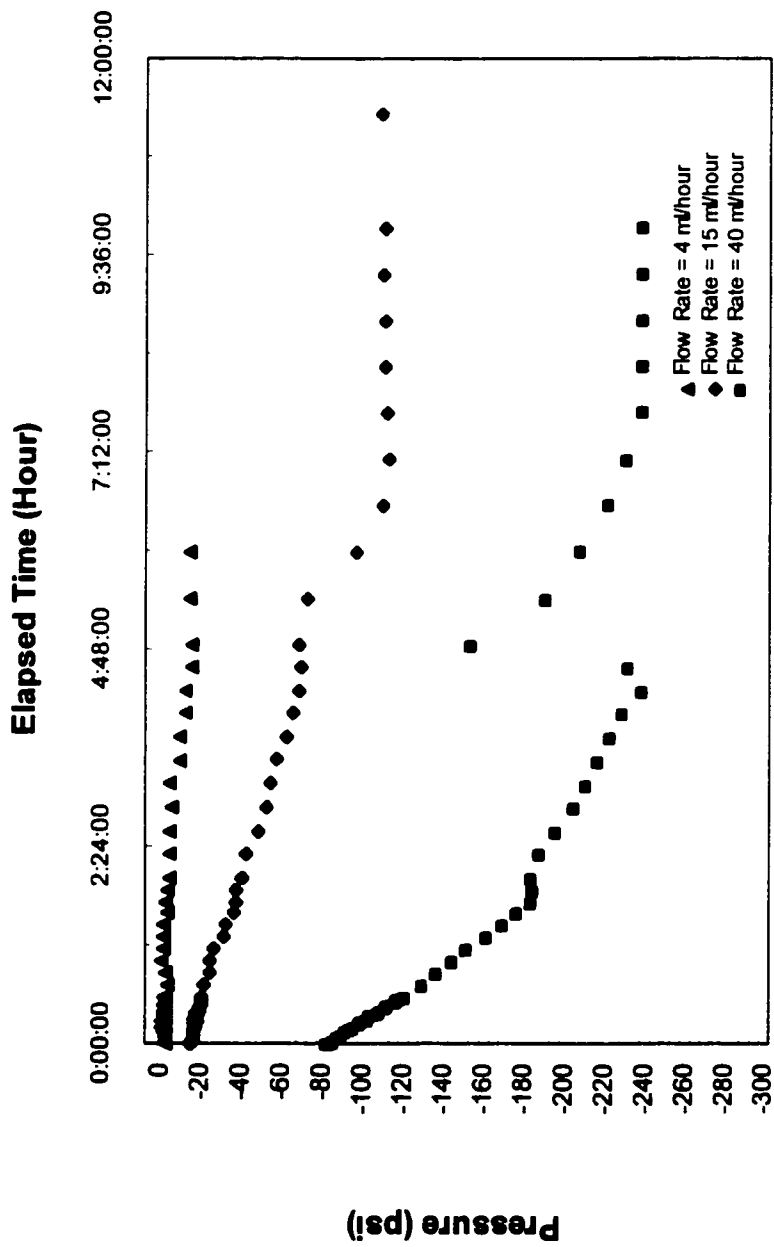
Figure D-21 Steady State Seepage at 6.4 MPa Gas Pressure and 6 MPa Effective Stress, CV1
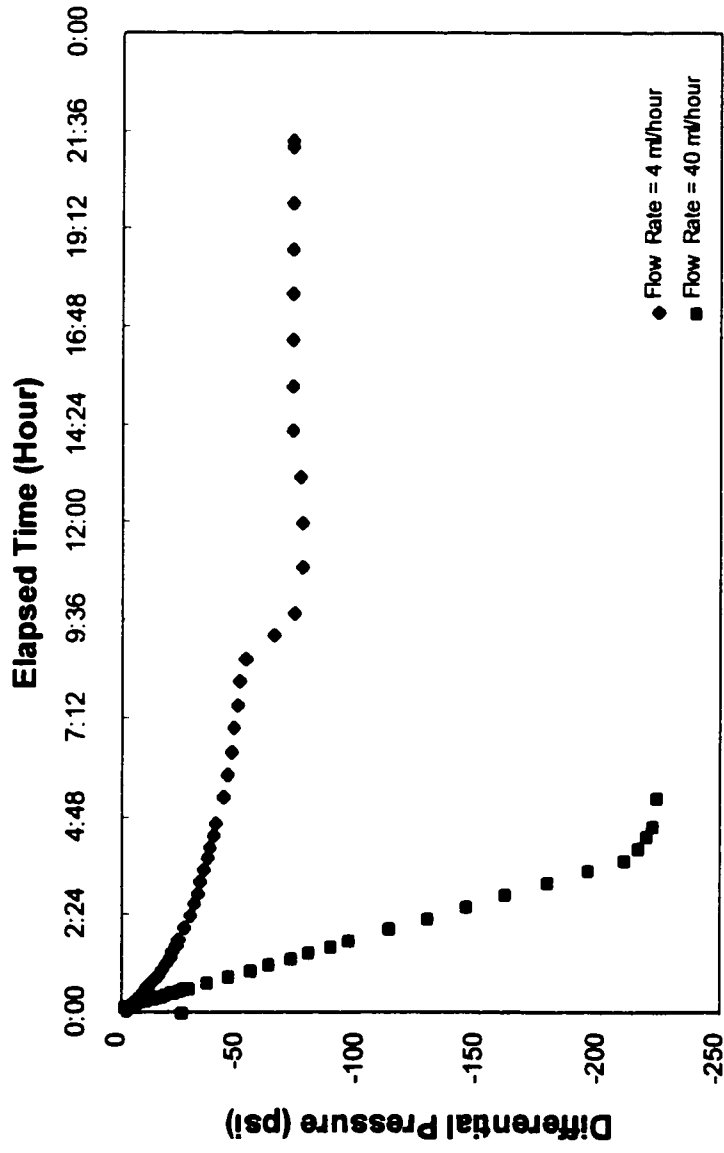
178
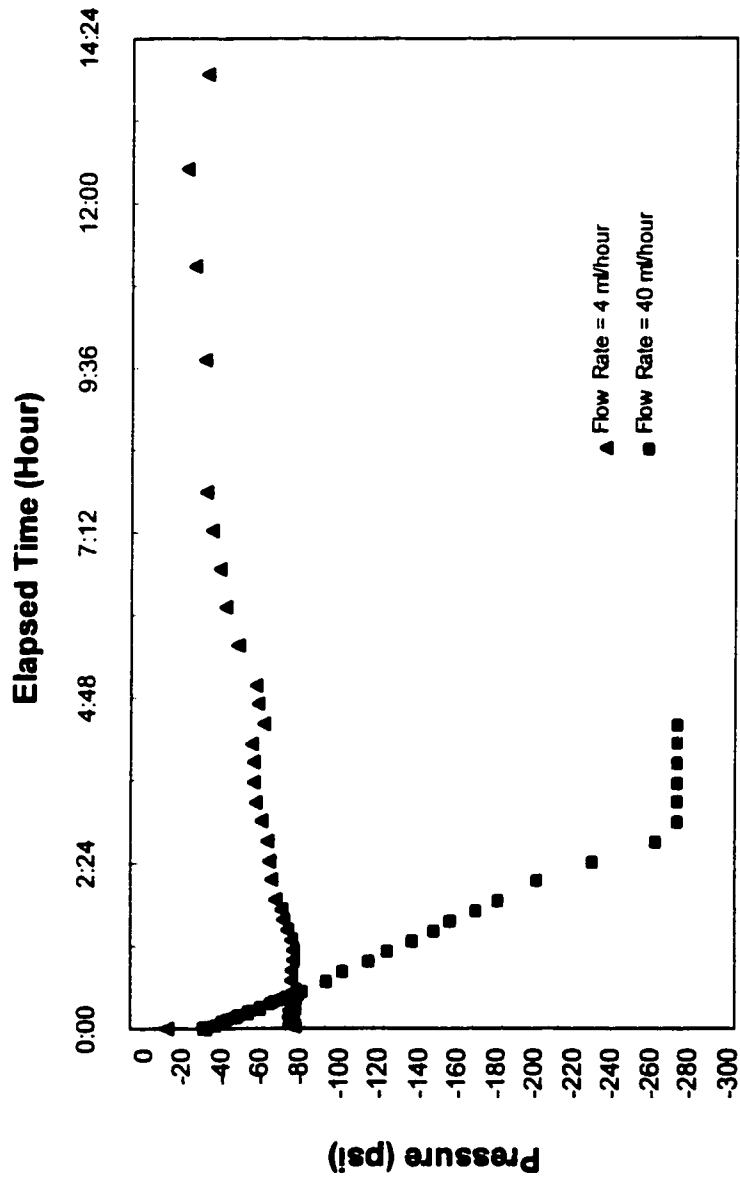
Figure D-22 Steady State Seepage at 9.6 MPa Gas Pressure and 6 MPa Effective Stress, CV1
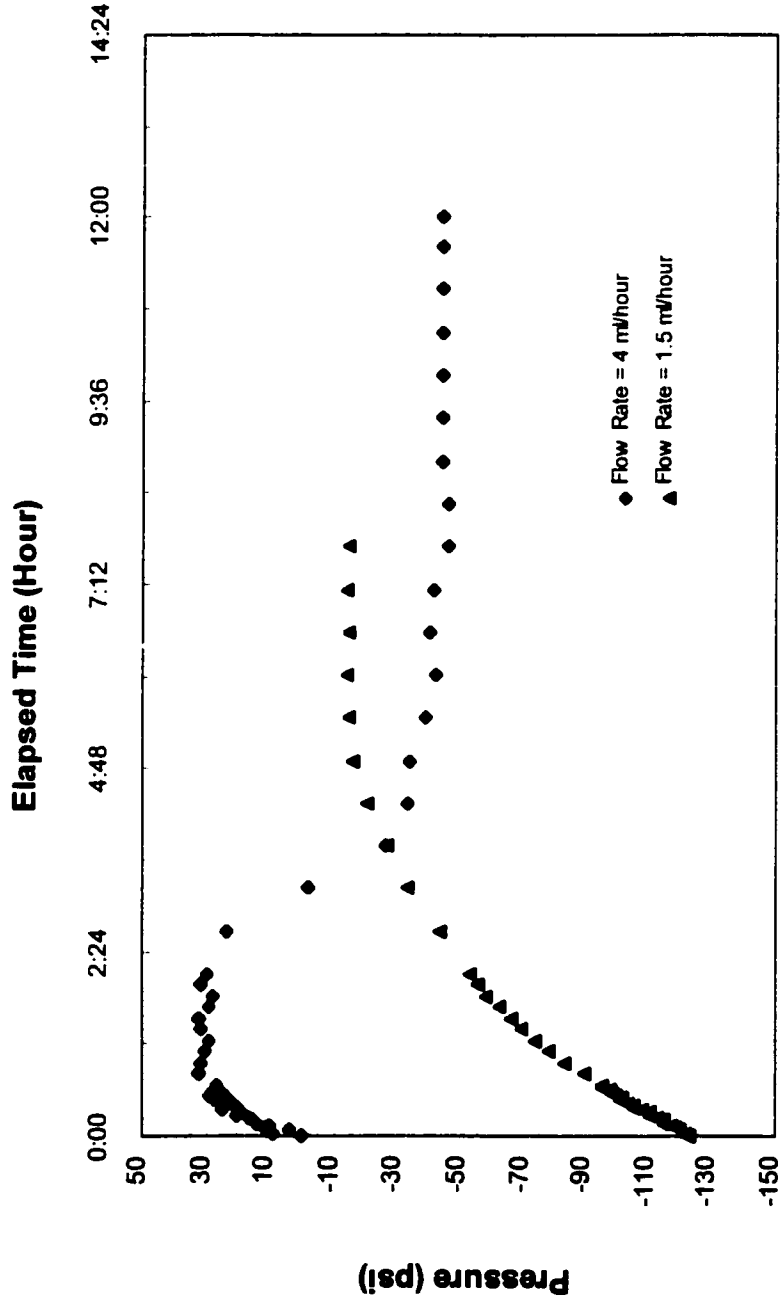
Figure D-23 Steady State Seepage at 12 MPa Gas Pressure and 6 MPa Effective Stress, CV1

Figure D-24 Steady State Seepage at 3.4 MPa Gas Pressure and 16 MPa Effective Stress, CV1

Figure D-25 Steadty State Seepage at 6.5 MPa Gas Pressure and 16 MPa Effective Stress, CV1

182

Figure D-26 Steady State Seepage at 9.6 MPa Gas Pressure and 16 MPa Effective Stress, CV1.

Figure D-27 Steady State Seepage at 3.8 MPa Gas Pressure and 6 MPa Effective Stress, CR2

Figure D-28 Steady State Seepage at 6.4 MPa Gas Pressure and 6 MPa Effective Stress, CR2
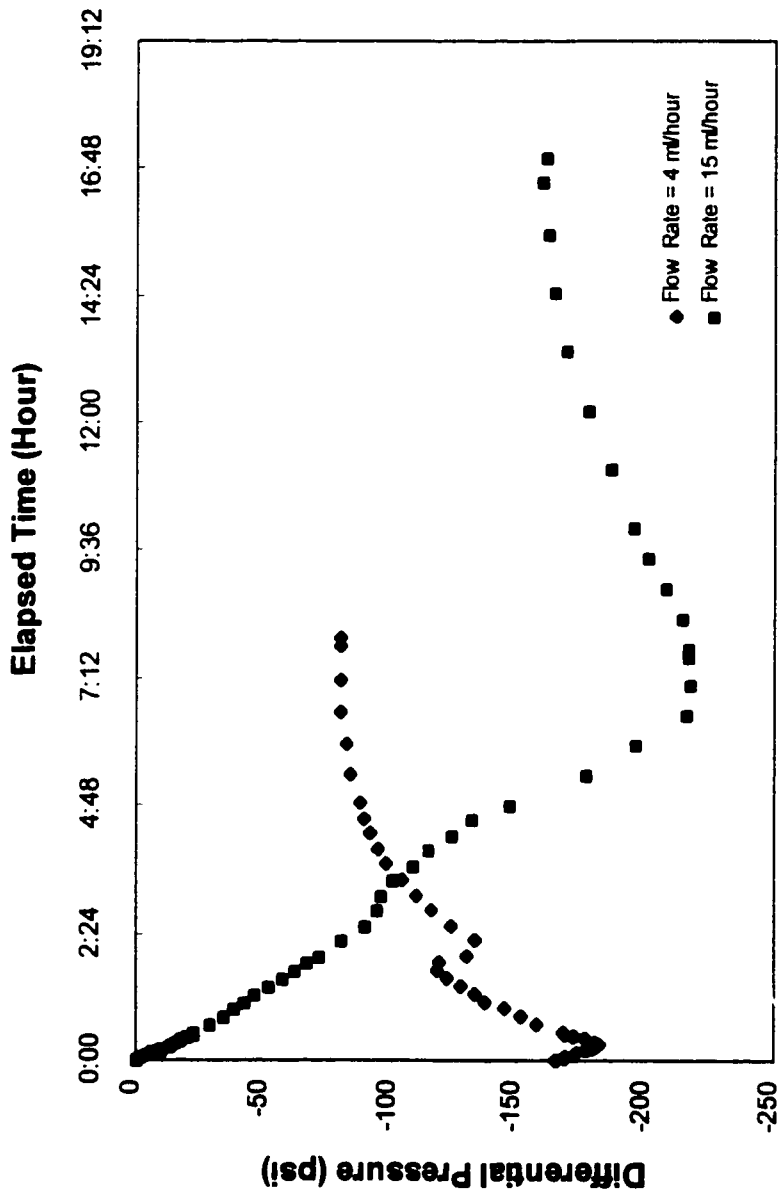
Figure D-29 Steady State Seepage at 9.6 MPa Gas Pressure and 6 MPa Effective Stress, CR2

Figure D-30 Steady State Seepage at 3.6 MPa Gas Pressure and 6 MPa Effective Stress, CV2

Figure D-31 Steady State Seepage at 4.5 MPa Gas Pressure and 6 MPa Effective Stress, CV2

Figure D-32 Steady State Seepage at 7.2 MPa Gas Pressure and 6 MPa Effective Stress, CV2
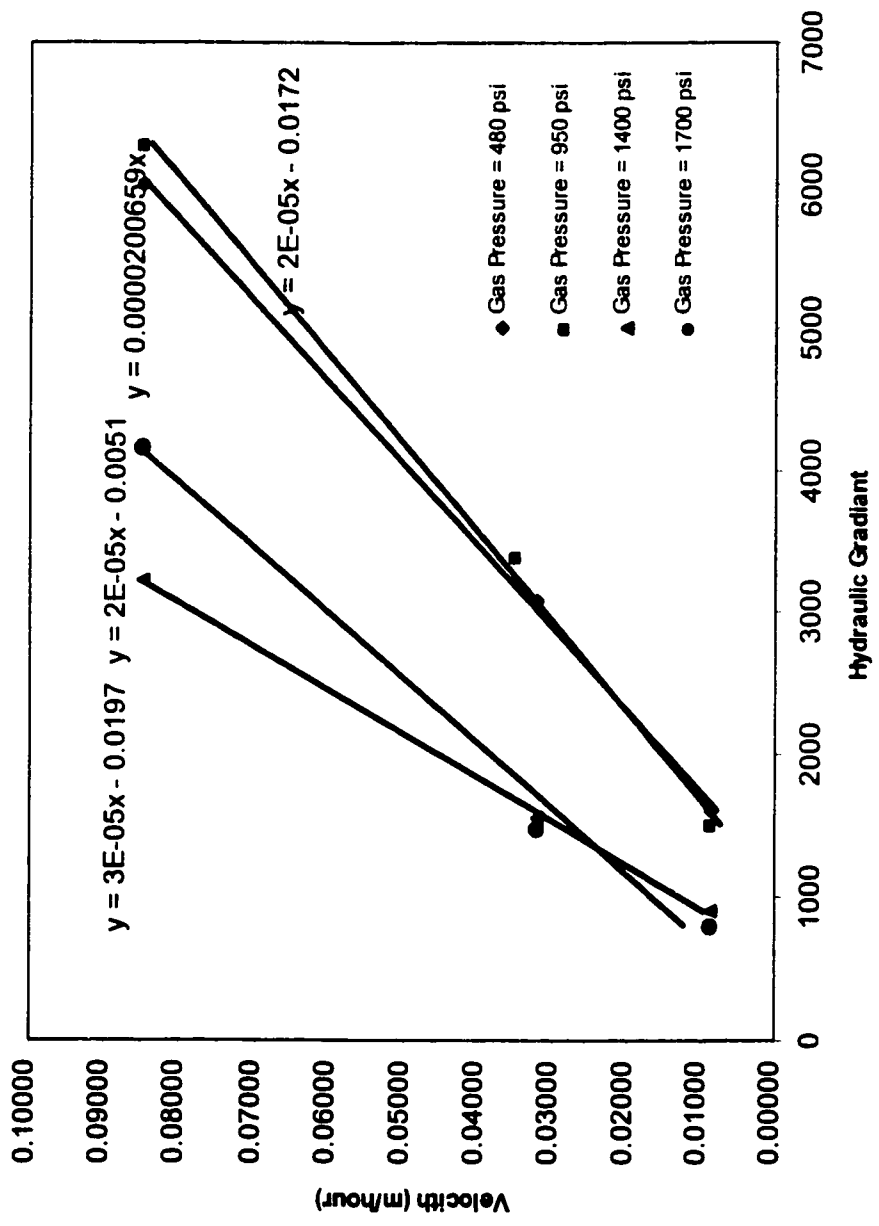
Figure D-33 Permeability at 6 MPa Effective Stress Using CO2 as a Permeable, CR1.
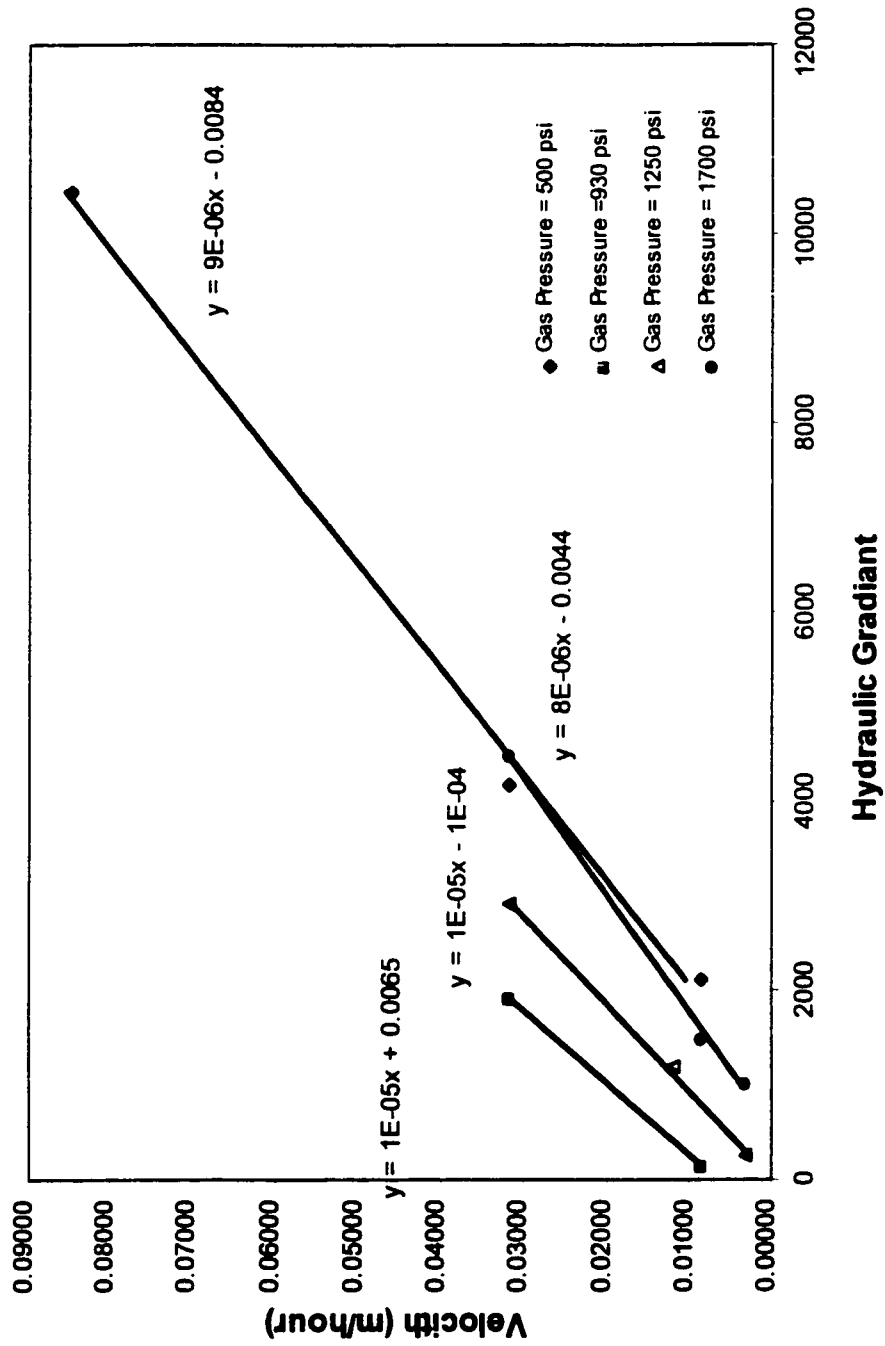
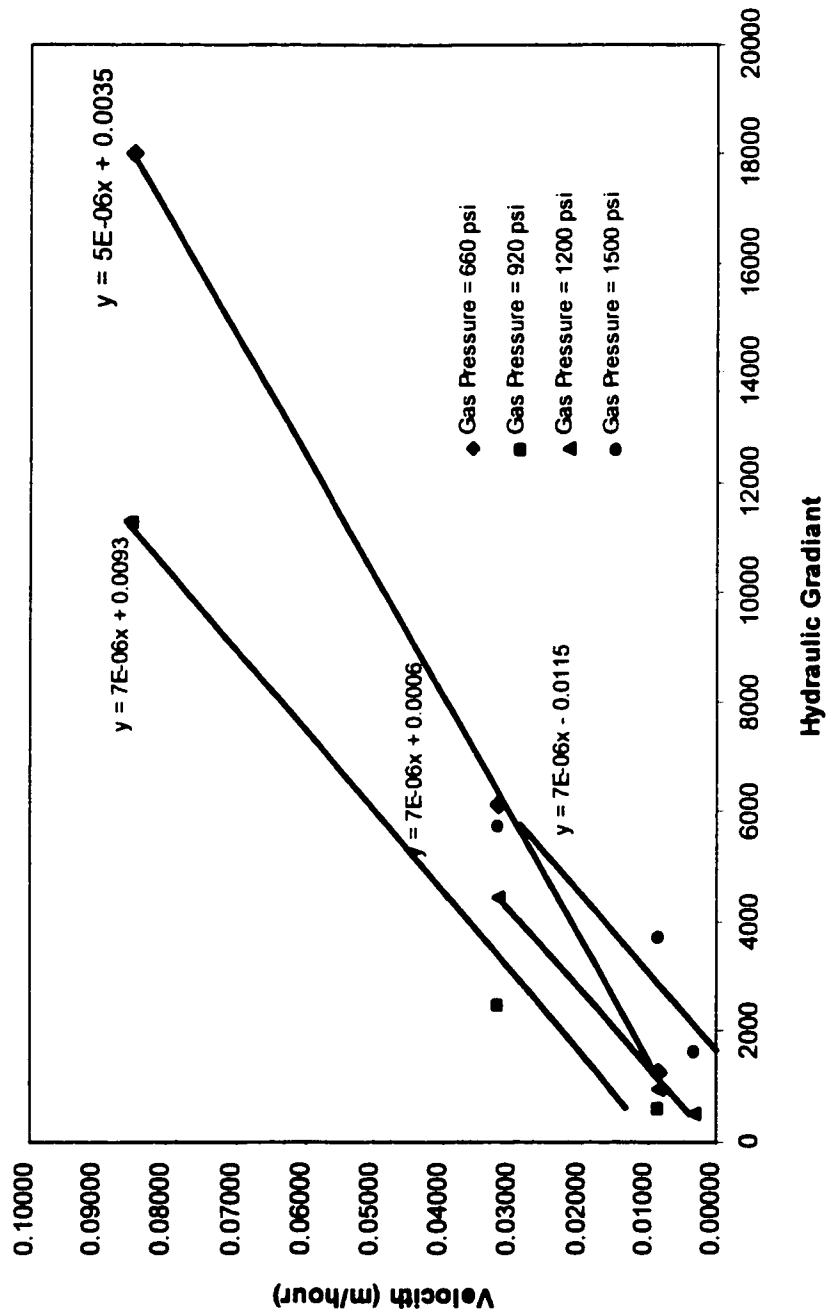Figure D-34 Permeability at 10 MPa Effective Stress Using CO2 as a Permeable, CR1.

Figure D-35 Permeability at 16 MPa Effective Stress Using CO2 as a Permeable, CR1.
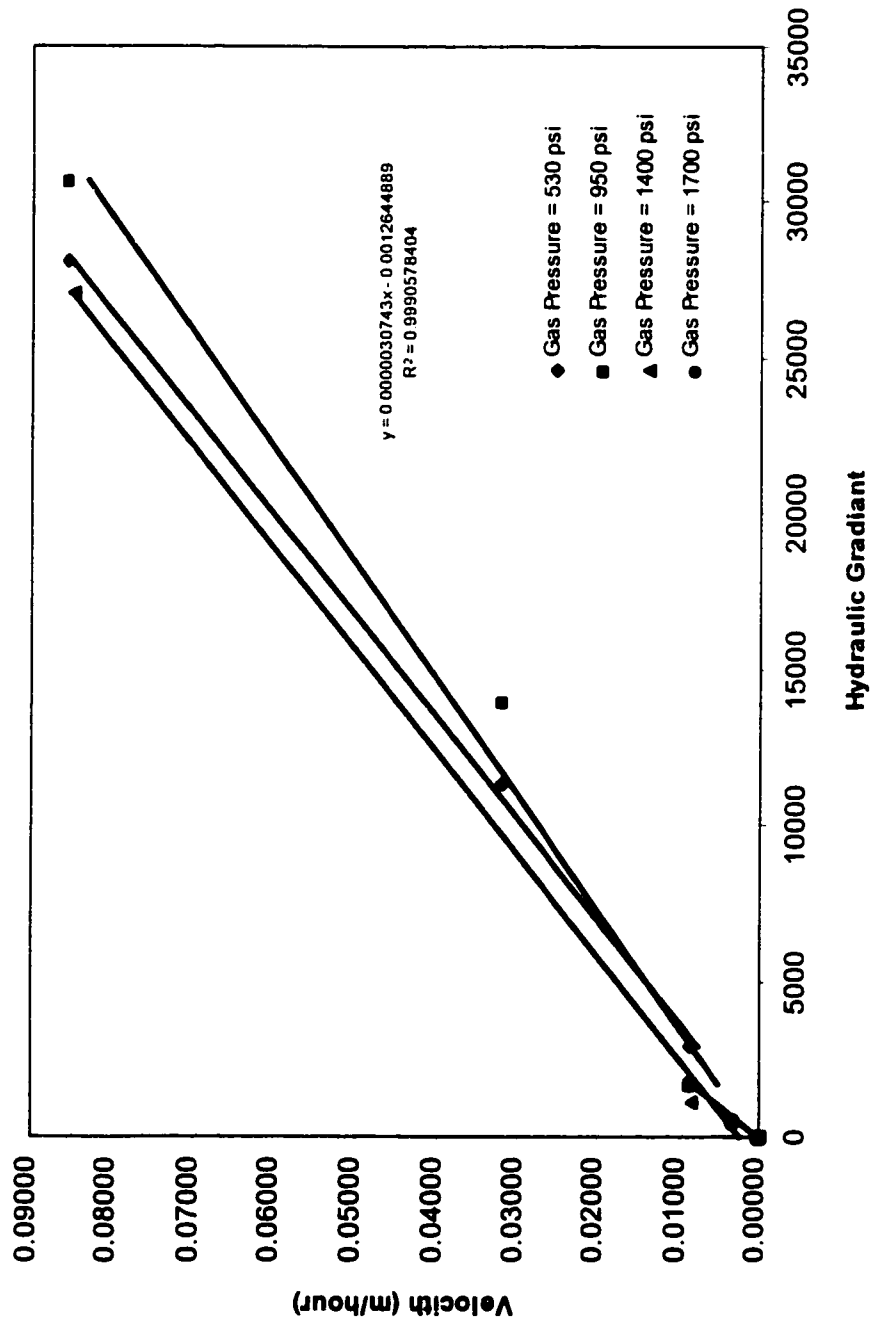
Velocity (m/hour) axis values: 0.09000, 0.08000, 0.07000, 0.06000, 0.05000, 0.04000, 0.03000, 0.02000, 0.01000, 0.00000

Hydraulic Gradiant axis values: 0, 5000, 10000, 15000, 20000, 25000, 30000, 35000

$y = 0.000030743x - 0.0012644889$
$R^2 = 0.9990578404$

- ◆ Gas Pressure = 530 psi
- ■ Gas Pressure = 950 psi
- ▲ Gas Pressure = 1400 psi
- ● Gas Pressure = 1700 psi

Figure D-36 Permeability at 6 MPa Effective Stress Using CO2 as a Permeable, CV1.

193

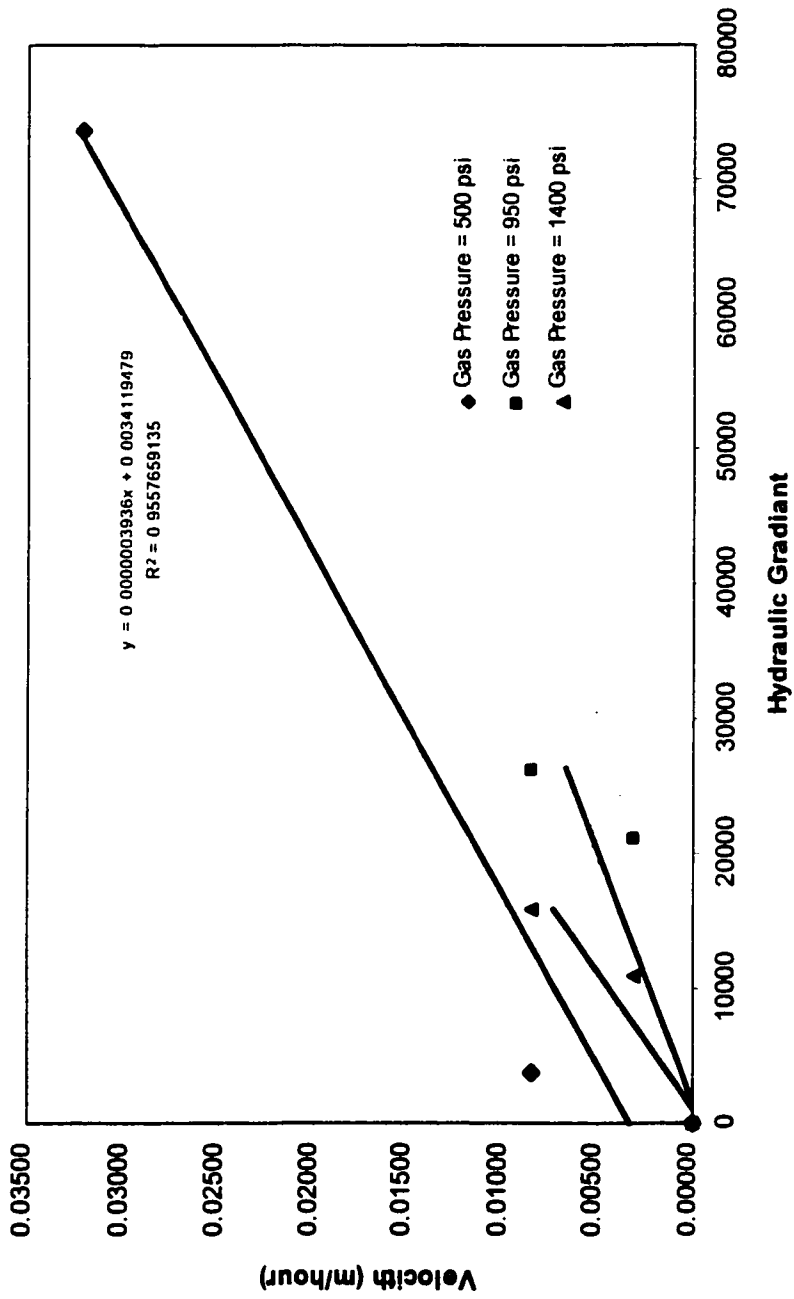Figure D-37 Permeability at 16 MPa Effective Stress Using CO2 as a Permeable, CV1.

Permeability At 6 Mpa Effective Stress

$y = 2E\text{-}06x - 0.0052$

$y = 2E\text{-}06x - 0.0277$

$y = 2E\text{-}06x - 0.0186$

- ◆ Gas Pressure = 550 psi
- ■ Gas Pressure =930 psi
- ▲ Gas Pressure = 1400 psi
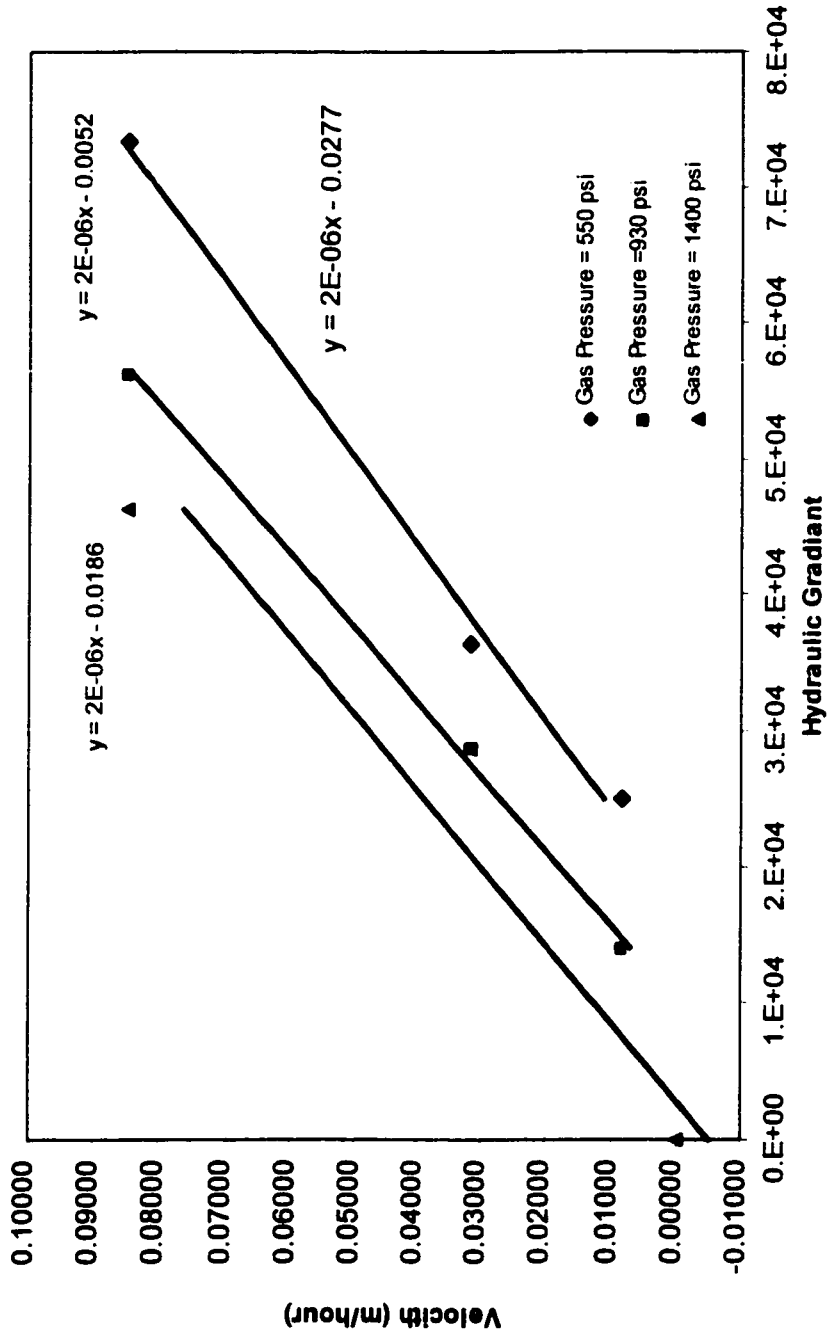
Hydraulic Gradiant

Velocith (m/hour)

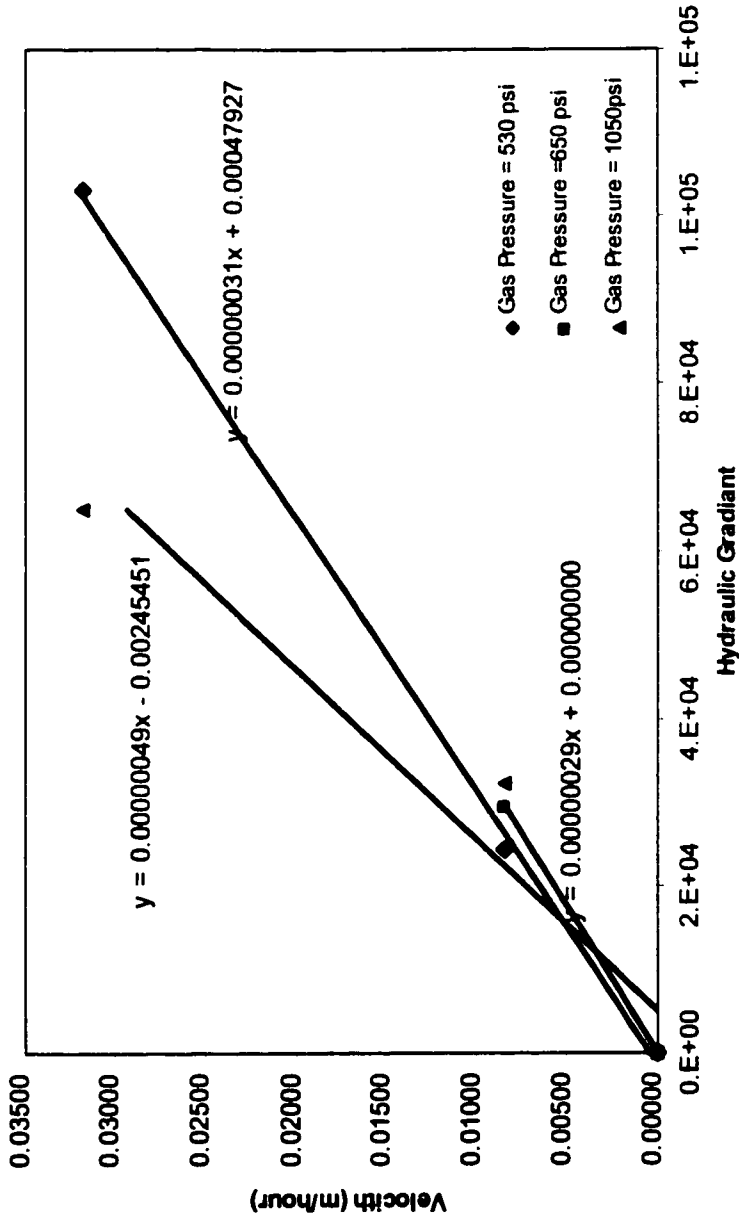Figure D-38 Permeability at 6 MPa Effective Stress Using CH₄ as a Permeable, CR2

195

Figure D-39 Permeability at 6 MPa Effective Stress Using CH4 as a Permeable, CV2

196